

1:1 ADDUCTS OF SELENIUM TETRAFLUORIDE

THE STRUCTURES OF SOME 1:1 ADDUCTS
OF
SELENIUM TETRAFLUORIDE

By
WILLIAM ALEXANDER WHITLA, B.Sc.

A Thesis
Submitted to the Faculty of Graduate Studies
in Partial Fulfillment of the Requirements
for the Degree
Doctor of Philosophy

McMaster University

October 1964

DOCTOR OF PHILOSOPHY (1964)
(Chemistry)

McMaster University
Hamilton, Ontario

TITLE: The Structures of Some 1:1 Adducts of Selenium Tetrafluoride.

AUTHOR: William Alexander Whitla, B.Sc. (McMaster University)

SUPERVISOR: Dr. R. J. Gillespie

NUMBER OF PAGES: ix, 208

SCOPE AND CONTENTS:

The addition compounds of selenium tetrafluoride with sulfur trioxide, boron trifluoride, and arsenic, antimony, bismuth, vanadium, niobium and tantalum pentafluorides have been prepared. These compounds have been studied in the solid state using X-ray powder diffraction, and infra-red and Raman spectroscopy; in the molten state using Raman spectroscopy, nuclear magnetic resonance spectroscopy, and conductimetric and viscosity measurements; and in solution using Raman spectroscopy, cryoscopy, conductivity and nuclear magnetic resonance spectroscopy.

The compound SeF_4SO_3 has a fluorosulfate-bridged polymeric structure. The remaining compounds have fluorine-bridged structures, this interaction being the strongest in SeF_4BF_3 and SeF_4VF_5 and decreasing in the order $\text{SeF}_4\text{NbF}_5 > \text{SeF}_4\text{TaF}_5 > \text{SeF}_4\text{AsF}_5 > \text{SeF}_4\text{SbF}_5 \sim \text{SeF}_4\text{BiF}_5$.

The characteristics of the SeF_3^+ group are discussed. The properties of fluorine bridging and various methods of detecting such interactions are also considered.

Acknowledgements

The author wishes to express his gratitude to Dr. R. J. Gillespie who suggested this problem, and under whose direction this work was done.

Also, he would like to express his thanks to his colleagues whose friendship and advice has been appreciated.

Thanks are due to Mr. R. Palme for construction of much of the glass apparatus.

Finally, the author would like to thank the National Research Council and the International Nickel Company of Canada for their financial support.

TABLE OF CONTENTS

CHAPTER I

Introduction	1
Purpose of this work	9

CHAPTER II. Infra-red and Raman Spectroscopy

Theory	10
Previous Spectroscopic Work	25
Possible Structural Models	27
Infra-red and Raman Spectra of SeF_4 Adducts	29
Discussion - SeF_4SO_3	40
SeF_4BF_3	48
SeF_4SbF_5	52
SeF_4AsF_5	58
SeF_4NbF_5	62
SeF_4TaF_5	65
SeF_4VF_5	68
SeF_4BiF_5	70
Raman Spectra of Solutions of SeF_4SO_3 and SeF_4BF_3	71

CHAPTER III. Nuclear Magnetic Resonance

Theory	73
N.M.R. Spectra of Selenium Tetrafluoride Adducts	80

CHAPTER IV. Cryoscopy in Nitrobenzene

Theory	87
Cryoscopic Measurements in Nitrobenzene	88
Conclusions	90

TABLE OF CONTENTS (cont'd)

CHAPTER V. Conductivity

Theory and Introduction	94
Conductivity of Molten Complexes	100
Conductivity in Nitrobenzene	107
Conductivity in Fluorosulfuric Acid	116

CHAPTER VI. X-ray Powder Diffraction

Theory	123
X-ray Powder Diffraction Data	127

CHAPTER VII. Conclusions

SeF_4SO_3	130
The Fluorosulfate Bridge	132
SeF_4SbF_5	133
The Fluorine Bridge	134
SeF_4AsF_5	138
SeF_4BiF_5	139
SeF_4BF_3	139
The Group Va Pentafluoride Adducts	141
General Observations	142
Properties of Fluorine Bridging	145
Summary	148
Suggestions for Extension of This Work	149

CHAPTER VIII Preparation and Purification of Materials

a) General Procedures	151
b) Purification of Materials	152
c) Preparation of Compounds	154
Analyses of Compounds	166

TABLE OF CONTENTS (cont'd)

CHAPTER IX. Experimental Techniques

1) Raman Spectroscopy	177
2) Infra-red Spectroscopy	184
3) Nuclear Magnetic Resonance Spectroscopy	190
4) Conductivity Measurements	191
5) Viscosity	198
6) Cryoscopy in Nitrobenzene	200
7) X-ray Powder Diffraction	204
References	205

LIST OF FIGURES

Figure	Description	Page
2.1	Infra-red and Raman Spectra of SeF_4SO_3	39
2.2	Infra-red and Raman Spectra of SeF_4PF_3	47
2.3	Infra-red and Raman Spectra of SeF_4SbF_5	51
2.4	Infra-red and Raman Spectra of SeF_4AsF_5	57
2.5	Infra-red and Raman Spectra of SeF_4NbF_5	61
2.6	Infra-red and Raman Spectra of SeF_4TaF_5	64
2.7	Infra-red and Raman Spectra of SeF_4VF_5 and Raman Spectrum of SeF_4BiF_5	67
2.8	SeF_4SO_3 : Fluorosulfate-bridged Structure	44
2.9	SeF_4SbF_5 : Linear Polymeric Structure	56
3.1	Equilibria of Solvated SeF_3^+	80
4.1	Cryoscopy in Nitrobenzene: ΔT vs. m	91
4.2	SeF_4SO_3 : Fluorosulfate-bridged Dimer	90
5.1	Conductivity of Molten Complexes: K vs. T	104
5.2	Conductivity in Nitrobenzene: Λ_m vs. \sqrt{m}	112
5.3	Conductivity in Nitrobenzene: K vs. m	113
5.4	Conductivity in Fluorosulfuric Acid: K vs. m	121
5.5	Structure of Dimeric SeF_3^+ Ion.	117
8.1	Apparatus for Preparation of Selenium Tetrafluoride	169
8.2	Fluorine Line	170
8.3	Preparative Apparatus	171
8.4	Preparative Apparatus	172
8.5	Sublimation Apparatus	173

List of Figures (cont'd.)

8.6	Preparative Line for SeF_4NbF_5 and SeF_4TaF_5	174
8.7	Preparative Line for SeF_4BF_5	175
8.8	Preparative Line for SeF_4VF_5	176
9.1	Raman Filter Jacket and Raman Tube	181
9.2	Air Heater	182
9.3	Solution and Low Temperature Raman Tubes	183
9.4	Infra-red Cell and Cold Finger	188
9.5	Infra-red Cell with Clamp	189
9.6	Conductivity Cell for Melts	195
9.7	Conductivity Cells	196
9.8	Weight Burettes	197
9.9	Viscometer	199
9.10	Cryoscope	205

LIST OF TABLES

TABLE	Description	Page
1.1	Addition Compounds of Selenium Tetrafluoride	4
2.1	Vibrational Frequencies for Fluorosulfate Ion	30
2.2	Vibrational Frequencies for Fluoroborate Ion	31
2.3	Vibrational Frequencies for Hexafluoroantimonate and Hexafluoroarsenate Ions.	32
2.4	Vibrational Frequencies of the Group Va Hexafluoride Anions	32
2.5	Raman Frequencies for Molten Complexes	33
2.6	Raman Frequencies for Solid Complexes	34
2.7	Infra-red Frequencies of Addition Compounds	35
2.8	Correlation Tables for T_d and O_h Point Groups	37
2.9	S-F Stretching Frequencies	45
2.10	Vibrational Spectrum of Selenium Tetrafluoride, Arsenic Trifluoride, and Antimony Pentafluoride	38
3.1	N.M.R. Spectrum of SeF_4SO_3 in Fluorosulfuric Acid	78
3.2	N.M.R. Spectra of Molten Complexes	78
3.3	N.M.R. Chemical Shifts of Some Fluoroanions and Fluoride Compounds	79
4.1	Cryoscopic Measurements in Nitrobenzene	92
5.1	Conductivity of Molten Complexes	105
5.2	Conductivity Measurements in Nitrobenzene	114
5.3	Conductivity Measurements in Fluorosulfuric Acid	122
5.4	Extent of Polymerization of SeF_4SO_3 in Fluorosulfuric Acid	118
6.1	Symmetry Requirements of the Crystal Systems	126
6.2	X-ray Powder Diffraction Data of Complexes	128

CHAPTER I

Introduction:

Selenium tetrafluoride was prepared first by Lebeau⁽¹⁾ by the direct fluorination of selenium metal. Later, Prideaux and Cox⁽²⁾ found that the tetrafluoride could be prepared by the reaction of selenium tetrachloride with silver (II) fluoride. However, the compound was not properly characterized until Aynsley, Peacock and Robinson⁽³⁾ obtained the compound pure by the direct fluorination of selenium metal at 0°C. This is the best method of preparation for selenium tetrafluoride, and the one used for this work.

Selenium tetrafluoride, SeF_4 , is a clear, colourless liquid which attacks pyrex glass slowly at room temperature. It can be handled easily in glass apparatus. It has a liquid range from -9.5°C to $+108^\circ\text{C}$; density, 2.733 g./ml.; and viscosity, 34.3 dynes/cm. (i.e., 3.50 centipoise).⁽⁴⁾

The structure of SeF_4 has been investigated by Raman and infra-red spectroscopy and by electron diffraction. Both methods show the molecule to have C_{2v} symmetry.

From the electron diffraction data⁽⁵⁾ the following molecular parameters were obtained:

Se-F	1.76 Å
F-F	3.0 Å
Two opposing $\angle \text{F-Se-F}$	$120^\circ \pm 10^\circ$
Remaining four $\angle \text{F-Se-F}$	$104.5^\circ \pm 10^\circ$

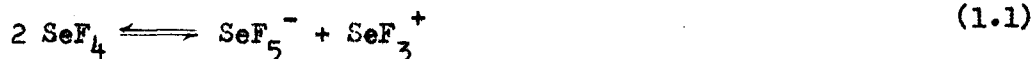
The structure of the molecule is best described as a distorted tetrahedron. There is some discrepancy between these molecular parameters for SeF_4 and those recently obtained from the microwave spectrum of SF_4 .⁽⁶⁾

Axial S-F	1.646 Å
Equatorial S-F	1.545 Å
\angle F-S-F	101°33'
Opposite \angle F-S-F	186°56'

The structure of SF_4 can be described as a trigonal bipyramid with one equatorial position occupied by a lone-pair of electrons. A related structure might be expected for SeF_4 ⁽⁷⁾, and a reevaluation of the electron diffraction data, using a model distorted in the same manner as SF_4 , would prove informative.

One would expect five fundamental frequencies in the vibrational spectrum for a molecule with five atoms and regular tetrahedral symmetry, T_d . Rolfe, Woodward and Long⁽⁸⁾ observed seven frequencies in the Raman spectrum of SeF_4 , which is sufficient to exclude T_d symmetry for SeF_4 . However, if the molecule had C_{2v} symmetry, nine fundamental frequencies would be expected. Thus the Raman spectrum is consistent with C_{2v} symmetry for SeF_4 .

The behaviour of SeF_4 as a solvent has been interpreted^(9,10,19) assuming the self-dissociation



Then the reactions



and



can be interpreted as neutralization reactions in SeF_4 . The compounds, SeF_3RuF_6 and SeF_3OsF_6 , are acids in this system, and TlSeF_5 and CsSeF_5 are bases. The small conductivity of liquid SeF_4 has been attributed to a small equilibrium concentration of the self-dissociation ions.^(9,10,12,13)

Selenium tetrafluoride is a non-oxidizing solvent, but it can behave as a reducing medium, in which case it is oxidized by fluorination to selenium hexafluoride. An example of such behaviour is the reaction of osmium hexafluoride with SeF_4 to give the SeF_4 adduct of osmium (V) and selenium hexafluoride.⁽¹⁰⁾

Selenium tetrafluoride might be expected to exhibit both acceptor and donor properties in its reactions with other compounds. The lone pair of electrons on SeF_4 , under suitable conditions, might be able to donate electrons, and, as molecules with five electron pairs in the valency shells (e.g., PF_5 and SbF_5) often show a tendency to acquire an extra pair to give an octahedral arrangement of six pairs, selenium tetrafluoride might be expected to show the same tendency and thus to exhibit acceptor properties. The acceptor properties for SeF_4 are clearly demonstrated by its reactions with a number of metal fluorides to give the salts, MSeF_5 ($\text{M} = \text{Li}, \text{Na}, \text{K}, \text{Cs}$ and Tl).⁽³⁾

There are also a large number of compounds of SeF_4 with metal fluorides for which the behaviour of the SeF_4 is less clear. These compounds are listed in Table 1.1.

TABLE 1.1

ADDITION COMPOUNDS OF SELENIUM TETRAFLUORIDE

<u>Complex</u>	<u>M.P. (°C)</u>	<u>Colour</u>	<u>Reference</u>
SeF_4SO_3	70	white	(11)
SeF_4BF_3	-46	white	(12)
SeF_4AsF_5	120	white	(12)
SeF_4SbF_5	122	white	(12)
SeF_4NbF_5	80	white	(80)
SeF_4TaF_5	120	white	(80)
SeF_4OsF_5	158	pale blue	(10)
$(\text{SeF}_4)_{0.4}\text{OsF}_5$	distils 200, 10^{-2}mm		(10)
SeF_4IrF_5	130 - 133	buff	(10)
$(\text{SeF}_4)_{0.4}\text{IrF}_5$	distils 200, 10^{-2}mm		(10)
SeF_4RuF_5	in solution in SeF_4 only		(10, 19)
SeF_4AuF_3	210 (dec.)	yellow	(19)
$(\text{SeF}_4)_2\text{GeF}_4$	subl. 100	white	(14)
$(\text{SeF}_4)_2\text{PtF}_4$	300 (dec.)	lt. orange	(17, 19)
$(\text{SeF}_4)_2\text{PdF}_4$	155 (dec.)	yellow	(18)
$(\text{SeF}_4)_2\text{VOF}_3$	dec. > 60	cream	(11)
$\text{SeF}_4\text{MoO}_2\text{F}_2$	71 - 72	cream	(20)
SeF_4WOF_4	60 - 63	yellow	(20)
SeF_4VF_4	---	lt. brown	(15)
SeF_4CrF_2	non-volatile	pink	(16)
SeF_4CrF_3	subl. 80 - 90	buff	(16)

Peacock⁽¹¹⁾ discovered the first of these addition compounds by reacting sulfur trioxide with SeF_4 . He isolated a white solid, SeF_4SO_3 , which he suggested might have the structure $\text{SeF}_3^+\text{SO}_3^-\text{F}^-$. He also prepared the compounds HgSeF_5 , by reaction of SeF_4 with mercury, and $\text{VOF}_3(\text{SeF}_4)_2$, by reaction of vanadium pentoxide with SeF_4 . He suggested that the latter compound had the constitution $(\text{SeF}_3)_2\text{VOF}_5$.

Bartlett and Robinson⁽¹²⁾ reported the preparation of the adducts of SeF_4 with boron trifluoride, arsenic pentafluoride and antimony pentafluoride. They made no statement concerning the structure of these compounds.

The adducts SeF_4OsF_5 and SeF_4IrF_5 were reported by Hepworth, Robinson and Westland.⁽¹⁰⁾ They carried out acid-base neutralization reactions in SeF_4 between these compounds and CsSeF_5 in order to prepare hexafluoroiridate (V) and hexafluoroosmate (V) salts. Their behaviour as acids in SeF_4 , as well as the fact that with water the compounds gave clear solutions containing selenious and hydrofluoric acids together with either hexafluoro-osmic or -iridic acid, indicated that the compounds could be formulated as $\text{SeF}_3\cdot\text{OsF}_6$ and $\text{SeF}_3\cdot\text{IrF}_6$.

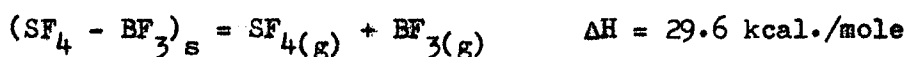
Peacock⁽¹³⁾, in a review article on transition metal fluorides, discussed the adducts of SeF_4 with niobium pentafluoride, tantalum pentafluoride, platinum tetrafluoride, gold trifluoride, palladium trifluoride, and molybdenum (VI) oxydifluoride. In the text of the article, the ionic character of SeF_4 adducts was again affirmed.

Not all the adducts mentioned by Peacock above have been properly characterized. No information on the niobium and tantalum pentafluoride adducts has been published elsewhere.⁽⁸⁰⁾ Bartlett and Robinson⁽²⁰⁾ have described the preparation of $\text{SeF}_4\text{MoO}_2\text{F}_2$ and SeF_4WOF_4 by the fluorination of molybdenum and tungsten trioxide in SeF_4 . They made no suggestion for their possible structures. The adducts $(\text{SeF}_4)_2\text{PdF}_4$ and SeF_4AuF_3 were described further by Bartlett and Robinson.⁽¹⁹⁾ The platinum (IV) adduct is isomorphous with the palladium (IV) and germanium (IV) adducts. They also reported that they were unable to isolate an adduct between ruthenium pentafluoride and SeF_4 although the two are miscible. Bartlett and Quail⁽¹⁸⁾ have reported the properties of the adduct $(\text{SeF}_4)_2\text{PdF}_4$. The palladium (III) adduct, SeF_4PdF_3 , reported earlier⁽⁶⁸⁾, was said to be a mixture of palladium difluoride and the palladium (IV) adduct. Bartlett and Yu⁽¹⁴⁾ described the preparation of the adduct $(\text{SeF}_4)_2\text{GeF}_4$.

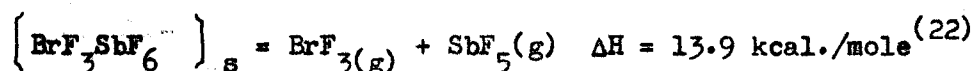
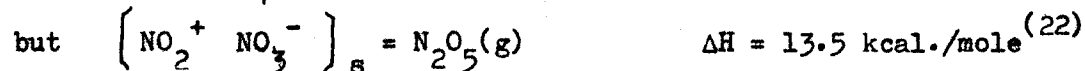
Although there is no structural evidence available for any of the SeF_4 adducts, there is some structural information concerning addition compounds related to those of SeF_4 . Bartlett and Robinson⁽¹⁹⁾ have reported indexing the X-ray powder pattern of SF_4SbF_5 as a simple cubic cell. Although they had not completed the structure determination, they said the symmetry was suggestive of an ionic formulation $\text{SF}_3^+\text{SbF}_6^-$.

Cotton and George⁽²¹⁾ have discussed the chemical and physical evidence concerning the constitution of the adduct of SF_4 with BF_3 . They discussed the donor ability of SF_4 relative to other molecules, e.g., PF_3 , and concluded that it is unlikely that compound formation was by donation

of electrons from SF_4 . Although BF_3 can act both as a general Lewis acid and as a strong F^- acceptor, they pointed out that for AsF_5 and SbF_5 , known to be strong F^- acceptors, there was little evidence that they were also good general Lewis acids. From this the authors postulated that the AsF_5 and SbF_5 adducts must be $\text{SF}_3^+ \text{AsF}_6^-$ and $\text{SF}_3^+ \text{SbF}_6^-$, implying the ability of SF_4 to form ionic adducts containing the SF_3^+ ion. The infra-red spectrum showed $\text{SF}_4 \text{BF}_3$ to be at least 95% dissociated in the vapour, and from vapour pressure measurements they calculated the enthalpy for the dissociation



Bartlett and Robinson⁽¹⁹⁾ and Seel and Detmar⁽²²⁾ have also obtained similar data and calculated values for $\Delta H = 24.8 \pm 0.2$ and 25.5 kcal./mole respectively. All these workers concluded that their ΔH values were consistent with dissociation of an ionic solid.



Bartlett and Robinson pointed out that a fluorine-bridged structure would also be consistent with the above data, but that fluorine bridging was unlikely in the SF_4 adducts since SF_4 was a poor acceptor. They

suggested that fluorine bridging may be more significant in the SeF_4 adducts since SeF_4 is a better acceptor than SF_4 (e.g., reacts with NOF , and forms MSeF_5 compounds).

As shown in the preceding discussion, many of the addition compounds of SeF_4 have been postulated to be ionic compounds on the basis of their chemical properties. However, the majority of these compounds are low-melting solids, a somewhat unusual property for ionic compounds. Also, these complexes have some vapour pressure at room temperature, and most of them can be sublimed under vacuum at temperatures below 100°C . Indeed, the adducts $\text{OsF}_5(\text{SeF}_4)_{0.4}$ and $\text{IrF}_5(\text{SeF}_4)_{0.4}$ can be distilled unchanged.⁽¹⁰⁾ Thus there is some question concerning the best description of the nature of the bonding in these compounds of selenium tetrafluoride.

Purpose of This Work

The purpose of this study has been to obtain some definite information concerning the structures of some of these addition complexes of selenium tetrafluoride, in particular some of the 1:1 adducts. The adducts with sulfur trioxide, boron trifluoride, and antimony, arsenic, bismuth, vanadium, niobium and tantalum pentafluorides were prepared. Of these, the bismuth and vanadium pentafluoride adducts are new compounds.

The compounds have been studied in the solid state using X-ray powder diffraction, and infra-red and Raman spectroscopy; in the molten state using Raman spectroscopy, nuclear magnetic resonance spectroscopy, and conductivity and viscosity measurements; and in solution using Raman spectroscopy, cryoscopy, nuclear magnetic resonance spectroscopy, and conductivity measurements.

CHAPTER II

Infra-red and Raman Spectroscopy

Theory

Infra-red spectra arise from transitions between rotational and vibrational levels of the ground electronic state of the molecule. The frequencies of the bands in the spectrum are determined by the mechanical motion of the molecule; their intensities, however, are connected with the electrical properties of the molecule. To a first approximation the mechanical and electrical effects can be discussed separately.

Vibrational transitions can be discussed most simply in terms of the harmonic oscillator model, for which the restoring force is proportional to the first order of the displacement, and the potential energy is proportional to the square of the displacement. This model accounts satisfactorily for frequencies corresponding to transitions in which only one quantum of vibration is excited. However, it is necessary to use a potential function with terms higher than the square of the potential to explain observed overtones and combination frequencies. If the potential energy, V , is expanded for small displacements, q_k , of the mass points k in a Taylor series about the equilibrium position of the mass points, one obtains:

$$\begin{aligned}
 V = V_0 + \sum_k \left(\frac{\partial V}{\partial q_k} \right)_0 q_k + \frac{1}{2} \sum_{k,l} \left(\frac{\partial^2 V}{\partial q_k \partial q_l} \right)_0 q_k q_l \\
 + \frac{1}{3} \sum_{k,l,m} \left(\frac{\partial^3 V}{\partial q_k \partial q_l \partial q_m} \right)_0 q_k q_l q_m + \dots
 \end{aligned}
 \quad (2.1)$$

where $q = x, y, z$. The subscript zero means that the derivatives are evaluated at the equilibrium position of the mass point. Thus the first two terms equal zero since the potential energy must be zero for zero displacement, and since at equilibrium no forces will be acting on the mass points. The third term is the same potential as the harmonic oscillator. The subsequent terms introduce mechanical anharmonicity into the potential energy. Although it is not possible to solve the Schrödinger equation exactly using this potential, solutions which are obtained by perturbation methods yield energy levels which account for the observed overtones and combination frequencies.

The intensities of transition between two energy states (i and j) of a molecule are determined theoretically by an integral of the form:

$$P_{ij} = \int \psi_i P \psi_j d\tau \quad (2.2)$$

The functions ψ_i and ψ_j are time dependent wave-functions of spatial coordinates, and must have the properties:

$$\int \psi_i \psi_j d\tau = 0 \quad \int \psi_i \psi_i d\tau = \int \psi_j \psi_j d\tau = 1 \quad (2.3)$$

P is a vector operator whose form is governed largely by the type of transition under consideration.

For infra-red transitions, P is the dipole moment, M , of the molecule.

$$M = \sum_k e_k r_k \quad (2.4)$$

where e_k is the charge on the mass point k , and r_k is the vector distance in some suitable coordinate system. Thus in a Cartesian system:

$$M^2 = M_x^2 + M_y^2 + M_z^2 \quad (2.5)$$

$$M_x = \sum_k e_k r_{kx} \quad M_y = \sum_k e_k r_{ky} \quad M_z = \sum_k e_k r_{kz} \quad (2.6)$$

For vibrational transitions, the coordinate r_k must change during a vibration, and consequently the dipole moment may be changing. If the mass points are not displaced greatly from their equilibrium positions, the dipole moment, M , can be expanded by a Taylor series in the small displacement, q_k , or in the normal coordinate, ξ_1 , to give:

$$\begin{aligned} M = M_0 + \sum_l \frac{\partial M}{\partial \xi_l} \bigg|_0 \xi_l + \frac{1}{2} \sum_{l,m} \frac{\partial^2 M}{\partial \xi_l \partial \xi_m} \bigg|_0 \xi_l \xi_m \\ + \frac{1}{3} \sum_{l,m,n} \frac{\partial^3 M}{\partial \xi_l \partial \xi_m \partial \xi_n} \bigg|_0 \xi_l \xi_m \xi_n + \dots \end{aligned} \quad (2.7)$$

This expansion is used for P in equation (2.2) to determine the intensity of infra-red transitions. The first term is zero since the two wave functions, ψ_i and ψ_j , must be orthogonal. Thus the second term must determine the intensity, and it follows that there must be a change in dipole moment during the vibration for an infra-red frequency to be observed.

The higher terms in the expansion result in electrical anharmonicity which permits the appearance of overtones and combination frequencies with

measurable intensity. This effect is similar to that produced by mechanical anharmonicity.

Raman spectroscopy is a result of an effect observed in the scattering of light by molecules. The majority of the scattered light from a monochromatic source is scattered without change in wavelength, but a small part of the scattered light is observed at wavelengths different from the incident light, and this phenomenon is known as the Raman effect.

The scattering occurs by an interaction between the light and the molecule which, in most cases, results only in a change in direction of the light (Rayleigh scattering). There is no absorption of the light energy by the molecule. However, in a small number of cases, changes in vibrational and rotational energy of the molecule take place during the interaction between the light and the molecule; the light is then scattered at a frequency changed from the incident frequency (Raman scattering). Some of the scattered light occurs at a smaller absolute frequency, $(\nu_0 - \Delta\nu)$, than the exciting frequency, ν_0 ; these lines are known as Stokes frequencies, and correspond to absorption of energy by the molecule during the scattering interaction. There are also frequencies at higher absolute frequency, $(\nu_0 + \Delta\nu)$, which are called anti-Stokes frequencies, and which correspond to a loss of energy by the molecule during the interaction with the light. The observed frequency shifts, $\Delta\nu$, are independent of ν_0 , the exciting frequency, provided ν_0 is not too close to an electronic absorption band of the molecule.

The shift in frequency from the exciting light, $\Delta\nu$, corresponds to the energy change which takes place when the light is scattered, and thus corresponds to the energy of the rotational and vibrational levels of the molecule which changed during the interaction with the light. According to classical theory, no difference in intensity of the Stokes and anti-Stokes frequencies is expected, but from a quantum mechanical approach, it is easily shown that the Stokes frequencies will appear much more strongly than the anti-Stokes frequencies. This is a result of the much larger population of molecules in the ground state than in the excited states. The Stokes frequencies are caused by changes from the ground state of the molecule; thus the Stokes frequencies are much stronger than the anti-Stokes frequencies which are a result of interaction with molecules in the excited state. Only when the Raman frequency is small enough that thermal energy allows a population of the excited state comparable with that of the ground state does the intensity of the anti-Stokes frequencies approach that of the Stokes frequencies. The Raman frequencies for a compound are generally obtained using the Stokes region of the Raman spectrum.

In the scattering process, the incident light wave, represented by an electric field, \vec{E} , induces a dipole moment in the molecule. This induced moment, \vec{p} , is related to \vec{E} by:

$$\vec{p} = \alpha \vec{E} \quad (2.8)$$

where α is the polarizability. If the vectors \vec{p} and \vec{E} are resolved into three components, p_x, p_y, p_z , and E_x, E_y, E_z , then α is the matrix or tensor

$$\alpha = \begin{pmatrix} \alpha_{xx} & \alpha_{xy} & \alpha_{xz} \\ \alpha_{yx} & \alpha_{yy} & \alpha_{yz} \\ \alpha_{zx} & \alpha_{zy} & \alpha_{zz} \end{pmatrix} \quad (2.9)$$

where $\alpha_{ij} = \alpha_{ji}$.

For light scattering to occur, there must be variation of the induced moment with time. The intensity of scattering depends on the magnitude of matrix elements of the type

$$\int \psi_{1v} \alpha_{ij} \psi_{2v} d\tau \quad (2.10)$$

where the ψ_{1v} are vibrational wave functions of the molecule. From classical considerations, the intensity of the scattered light can be shown to be given by:

$$\frac{16\pi^4 \nu^4 E_0^2 |\alpha|^2}{3c^2} \quad (2.11)$$

where E_0 is the magnitude of the electric field vector, and c , the velocity of light. From this relationship, it is evident that the intensity of the scattering varies as the fourth power of the frequency of the incident light.

If the nuclei remain in fixed positions, only scattering of light of the same frequency as the incident light would be observed. However, if the nuclei are allowed to move, the polarizability can be represented by:

$$\alpha = \alpha_0 + \Delta\alpha \quad (2.12)$$

where α_0 is the value of α for fixed nuclei and $\Delta\alpha$, the change in α resulting from the motion of the nuclei. In terms of the normal coordinates, q_1 , of the molecule, $\Delta\alpha$ is of the form:

$$\Delta\alpha = \sum_1 \left(\frac{\partial \alpha}{\partial q_1} \right)_0 q_1 \quad (2.13)$$

If the molecule has a normal vibration of frequency ν , it can be shown by classical methods that the scattered light will contain frequencies $\nu_0 \pm \nu$ for the incident light of frequency ν_0 .

In a quantum mechanical treatment, the polarizability is given by:

$$\alpha = \frac{2}{3hc} \sum_e \frac{\nu_{oe} M_{oe}^2}{\nu_{oe}^2 - \nu^2} \quad (2.14)$$

where ν is the frequency of the incident light in cm^{-1} , ν_{oe} is the wave number of an electronic level e above the normal level, and M_{oe} is the average dipole moment $\int \psi_0(r) \psi_e dr$ between the normal and the electronic level. Although the summation is made over all excited states of the molecule, the principal contribution to α will come from the lower excited electronic states. The components of α are given by a similar expression, e.g.,

$$\alpha_{xy} = \frac{1}{hc} \sum_e \frac{\nu_{oe} M_{oe}^x M_{oe}^y}{\nu_{oe}^2 - \nu^2}$$

$$M_{oe}^x = \int \psi_0 x \psi_e dr \quad M_{oe}^y = \int \psi_0 y \psi_e dr \quad (2.15)$$

For a vibrating molecule, equation (2.12) must be applied, and the components of α_0 are the same form as (2.15) above. The components of $\Delta\alpha$ can be shown to have the form:

$$(\Delta\alpha_{xy})_{ov} = \frac{1}{hc} \sum_e \left(\frac{M_{oe}^y M_{ev}^x}{\nu_{oe} - \nu} + \frac{M_{oe}^x M_{ev}^y}{\nu_{oe} - \nu_{ov} + \nu} \right) \quad (2.16)$$

where ν_{ov} is the wave number of a vibrational state. Since in general $\nu_{ov} \ll \nu_{oe} + \nu$, and since $M_{ev}^i \cong M_{oe}^i$, then (2.16) simplifies to:

$$(\Delta\alpha_{xy})_{ov} \cong \frac{1}{hc} \sum_e \frac{\nu_{oe} M_{oe}^x M_{oe}^y}{\nu_{oe}^2 - \nu^2} \quad (2.17)$$

Then every component of $\Delta\alpha$ will be equal to zero unless there exists at least one excited state e for which the transition probabilities M_{oe}^i and M_{oe}^j are simultaneously different from zero. For the Raman effect to occur, there must exist one excited electronic state which is capable of combining optically with two vibrational levels of the ground state.

The intensity of a Raman line will depend on the magnitude of integrals of the form:

$$\int \psi_{00} (\Delta\alpha_{ij}) \psi_{ov} d\tau \quad (2.18)$$

which must be summed over all excited states of the molecule. It is not possible to handle this quantity to calculate intensities. However, as will be shown later, it is possible to set up selection rules based on the

transformation properties of the wave function and α_{ij} under the various symmetry operations for the molecule.

If the matrix multiplication of equation (2.8) for the components of \vec{p} and \vec{E} is carried out, the following equations are obtained:

$$\begin{aligned}\vec{p}_x &= \alpha_{xx} \vec{E}_x + \alpha_{xy} \vec{E}_y + \alpha_{xz} \vec{E}_z \\ \vec{p}_y &= \alpha_{yx} \vec{E}_x + \alpha_{yy} \vec{E}_y + \alpha_{yz} \vec{E}_z \\ \vec{p}_z &= \alpha_{zx} \vec{E}_x + \alpha_{zy} \vec{E}_y + \alpha_{zz} \vec{E}_z\end{aligned}\quad (2.19)$$

where x , y and z are the axes of a coordinate system fixed in the molecule. The polarizability tensor used to generate the above equation can be visualized by means of a polarizability ellipsoid, generated by a plot from a given point of all moments which are induced by unit vectors \vec{E} . The ellipsoid has a maximum or minimum only in the direction of the principal axes of the ellipsoid, and it is only when \vec{E} lies along one of these directions that \vec{p} can have the same direction as \vec{E} . In general, the direction of \vec{E} does not coincide with the fixed axes, \vec{x} , \vec{y} and \vec{z} , and the induced moment \vec{p} will not lie entirely in the direction \vec{E} because of the contribution from off-diagonal elements of the polarizability tensor. This fact can be used in conjunction with polarized light to obtain further information concerning the nature of the molecular vibration which is responsible for the observed Raman line.

If the polarizability ellipsoid of a molecule is a sphere, the direction of the induced moment \vec{p} for any orientation of the system coincides with the direction of the field vector \vec{E} producing it. Therefore,

if a substance containing such molecules is irradiated and the scattered light observed at right angles to the incident beam, then the scattered light will be completely polarized in the plane at right angles to the incident beam whether the incident light is polarized or not. However, if the polarization ellipsoid is not a sphere, the direction of \vec{p} coincides with \vec{E} only when \vec{E} coincides with one of the axes of the polarizability ellipsoid. Thus, if such molecules are irradiated, \vec{p} is no longer restricted to the plane at right angles to the incident beam.

When the polarizability ellipsoid is not a sphere, it can be resolved into the sum of a spherical part α^I and an anisotropic part β^2 .

It can be shown that:

$$\alpha^I = \frac{1}{3} (\alpha_{xx} + \alpha_{yy} + \alpha_{zz}) \quad (2.20)$$

$$\begin{aligned} \beta^2 = \frac{1}{2} & \left[(\alpha_{xx} - \alpha_{yy})^2 + (\alpha_{yy} - \alpha_{zz})^2 + (\alpha_{zz} - \alpha_{xx})^2 \right. \\ & \left. + 6(\alpha_{xy}^2 + \alpha_{yz}^2 + \alpha_{zx}^2) \right] \quad (2.21) \end{aligned}$$

These two quantities are called the invariants of the polarizability tensor since their value is independent of the orientation of the coordinate axes relative to the polarizability ellipsoid.

The degree of polarization ρ can be defined as the ratio of the intensity of the scattered light polarized perpendicular to the xy plane, I_{\perp} , to that polarized parallel to this plane, I_{\parallel} , where the z axis is taken as the direction of propagation of the incident light and observation is made perpendicular to this direction. It can be shown that for natural incident light

$$\rho_n = \frac{I_{\perp}}{I_{\parallel}} = \frac{6\beta^2}{45(\alpha^I)^2 + 7\beta^2} \quad (2.22)$$

The degree of polarization for linear polarized incident light is related to ρ_n by:

$$\rho_1 = \frac{\rho_n}{2 - \rho_n} = \frac{3\beta^2}{45(\alpha^I)^2 + 4\beta^2} \quad (2.23)$$

ρ_n can have a maximum value of $6/7$ and a minimum value of zero, and thus ρ_1 max. = $3/4$ and ρ_1 min. = 0 .

It is useful to have some method to determine conditions when a transition between two states will be zero or some finite value. Such a distinction constitutes a selection rule and can be determined by examining the molecular symmetry of the states involved in the transitions.

For a given molecule, a series of symmetry operations can be found for which the molecule is unchanged. The wave functions for the molecule will be affected in various ways by these symmetry operators, as will the components of M and α . However, the integrand $(\psi_i P \psi_j)$ must remain invariant or remain totally symmetric under all symmetry operations, since a symmetry operation, which exchanges coordinates of identical particles, leads only to a change in the order of integration. For a case where a symmetry operation leads to a change in sign of the above integrand, then the value of the integrand must be zero. Thus we can use molecular symmetry to determine the basic selection rules for infra-red and Raman spectroscopy.

As stated above, a series of symmetry operations can be determined for any given molecule. These symmetry operations are said to form a group. The product of any two operations must be equal to another operation of the group. In this manner, a group multiplication table can be set up from which the product of any two operations can immediately be determined. Operation multiplication need not be commutative, i.e. $AB \neq BA$.

Any set of elements, which may be numbers or matrices, etc., which can be substituted for the symmetry operations yet conform to the group multiplication table, are said to be representations of a group. The representations of a group which cannot be reduced by suitable transformations are said to be irreducible representations of the group, and for each group it can be shown that there is a limited set of irreducible representations equal to the number of symmetry classes in the group.

The product of two representations is obtained by multiplication of the appropriate elements of the two representations. The resulting product must itself be a representation of a group. It may be one of the irreducible representations or a reducible representation, which can be reduced by a set of orthogonal transformations to the sum of several irreducible representations. This is called the direct product of the two representations.

These basic theorems of group theory can be used to determine the selection rules for spectroscopic transitions. The group representations for the various vibrational modes of the molecule can be determined by

examining the effects of the various symmetry operations on the molecule during vibration. Similarly, the behaviour of the various components of the vector operator, P , governing the type of transition can be classified. Using this information it can be shown when the integrand $(\psi_i P \psi_j)$ will be totally symmetric and thus finite.

In infra-red spectroscopy, the integrand $(\psi_i M \psi_j)$ must be totally symmetric; for this to be true, the direct product of the representations for ψ_i and ψ_j must correspond to the representation of one of the components of M . The components of M , in Cartesian coordinates, transform exactly the same as the coordinates themselves. Thus a simple rule can be made to define when infra-red frequencies will be allowed: A fundamental will be infra-red active if the normal mode involved belongs to the same representation as any one or several of the Cartesian coordinates.

In Raman spectroscopy, for the integral (2.18) to be totally symmetric, the direct product of the representations of ψ_{00} and ψ_{0v} must be the same as or contain the representation of one of the components of $\Delta\alpha$; or since, generally, the ground state representation must be totally symmetric, the upper state and at least one component of $\Delta\alpha$ must have the same representation. This can be stated more generally: A fundamental transition will be Raman active if the normal mode involved belongs to the same representation as one or more of the components of the polarizability tensor of the molecule.

One further selection rule relating infra-red and Raman spectra arises in molecules possessing a centre of symmetry. Since the representations of the dipole moment transform the same as the Cartesian coordinates,

and the representation of the polarizability, as products of the Cartesian coordinates, the only case where a vibration can be both infra-red and Raman-active is if all the representations for the components of both intensity integrals are totally symmetric. This cannot arise in a centrosymmetric point group. Thus in a centrosymmetric molecule, no Raman-active vibration is infra-red active, and no infra-red active vibration is also Raman-active.

The degree of polarization in Raman spectroscopy is related to the symmetry of the two states involved in the transition. The polarizability components, α_{xx} , α_{yy} and α_{zz} , all have a totally symmetric representation in each of the possible point groups. Thus if $\psi_v' \psi_v''$ are totally symmetric as well, then α^I will be non-zero; but if $\psi_v' \psi_v''$ are non-totally symmetric, then α^I equals zero. Thus the degree of polarization, ρ_n , of totally symmetric Raman lines has a value between zero and $6/7$, while for a non-totally symmetric Raman line it is $6/7$. A totally symmetric Raman line is one for which $\psi_v' \psi_v''$ is totally symmetric. Thus, if the normal mode involved in the transition has a totally symmetric representation in the point group of the molecule, then the Raman frequency will have a degree of polarization between zero and $6/7$. In the cubic point groups (T_d , O_h , etc.) the polarizability ellipsoid must be a sphere, and consequently the anisotropy β equals zero. Thus, in the cubic point groups, totally symmetric Raman lines are completely polarized ($\rho_n = 0$, $\rho_1 = 0$). For all non-cubic point groups, the degree of polarization for totally symmetric vibrations is intermediate between zero and $6/7$.

One further use of group theory can be discussed here. The preceding discussion has considered a molecule as being completely isolated from other molecules. In practice, this may be a good approximation. However, in liquids and crystals, it is frequently the case that the symmetry about the species of interest is affected by interaction with neighbouring molecules. Such interactions can be treated by considering an environment of fixed symmetry about the molecule, and it will be the symmetry of this environment which will determine the observed frequencies. The effective symmetry governing the behaviour of the vibrational states is called the site symmetry.

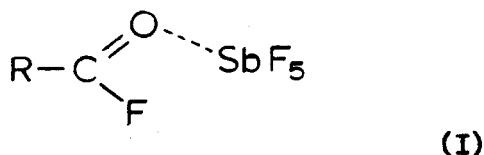
The site symmetry about a molecule cannot contain elements of symmetry not present in the molecule itself. However, it is frequently the case that symmetry elements present in the molecule are absent in the site symmetry. This lower site symmetry leads to changes in the selection rules and the splitting of degenerate states.

Previous Spectroscopic Work

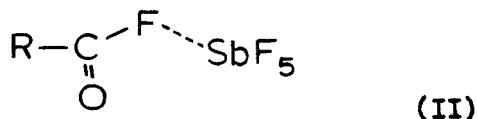
Since the discussion in the literature of the structure of the adducts of selenium tetrafluoride is mainly in terms of ionic models, a search has been made of the literature to obtain the infra-red and Raman frequencies characteristic of the anions encountered during this work. These are summarized in Tables 2.1, 2.2, 2.3, 2.4.

G. H. Olah and co-workers^(41,42) report studies on a series of acyl fluoride adducts with BF_3 , SbF_5 , AsF_5 and PF_5 . By studying the infra-red and n.m.r. spectra of these compounds, they conclude that the compounds are all ionic, forming the complex fluoro anion and an acyl carbonium ion. In the n.m.r. spectrum of the acetyl, propionyl and benzoyl fluoroborate adducts, one F^{19} resonance is observed both in HF solution and in SO_2 . However, in SO_2 the chemical shifts are shifted 63.3 - 64.8 p.p.m. from trifluoroacetic acid, whereas the chemical shifts are from 74.6 - 76.3 p.p.m. from CF_3COOH in liquid HF. This is stated as evidence for some complex formation in SO_2 solution.

The later paper reports the preparation and characterization of a series of acyl fluoride adducts of SbF_5 ⁽⁴²⁾. The infra-red spectra were interpreted on the basis of ionic hexafluoroantimonate. However, the proton n.m.r. spectra show more than one species present in solution, and they suggest a complex of the following type might also be present in solution:



The F^{19} n.m.r. spectra are interpreted on the basis of the SbF_6^- ion. However, several of the resonances are very broad, and they pointed out that the observed spectra would also be consistent with a fluorine-bridged structure, e.g.,



The data in these papers is poorly presented, and it is not possible to obtain all the observed spectroscopic frequencies and chemical shifts. The ionic structure of the compounds is based mainly on the observed carbonyl frequencies of the compounds, and no complete assignment is attempted. The frequencies for anionic species are tabulated without comment. It seems possible that the proton n.m.r. resonances which are consistent with a complex of type (I) would also be consistent with a complex of type (II) (i.e., both have two types of F in the ratio of 5:1). The absence of fluorine spin-spin coupling would be more consistent with (II) than with (I). Although coordination of the oxygen is observed in acetyl chloride complexes with aluminum trichloride⁽⁴³⁾ and titanium tetrachloride⁽⁴⁴⁾, the coordination through oxygen need not be the case with acetyl fluoride, and with strong fluoride acceptors coordination through fluorine is indeed likely. Thus, the nature of the complex observed is more likely to be of type (II) than of type (I).

Clark and O'Brien⁽²⁷⁾ have reported the preparation and characterization of the trimethyl tin compounds with tetrafluoroborate and hexafluorophosphate, -arsenate, and -antimonate. The infra-red spectra are all reproduced and are discussed fully. Strong interaction of the $(\text{CH}_3)_3\text{Sn}^+$ group with the anion is indicated from the spectra, and the frequencies for BF_4^- and SbF_6^- are reported for a site symmetry of C_{2v} due to strong ion interaction. The observed frequencies for AsF_6^- are interpreted on the basis of a site symmetry of D_{4h} . A site symmetry of C_{2v} corresponds to polymers formed by cis fluorine bridging. This paper gives the best data

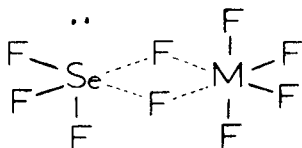
available in the literature pertaining to the behaviour of the anions BF_4^- , SbF_6^- and AsF_6^- under conditions of strong fluorine bridging.

Possible Structural Models

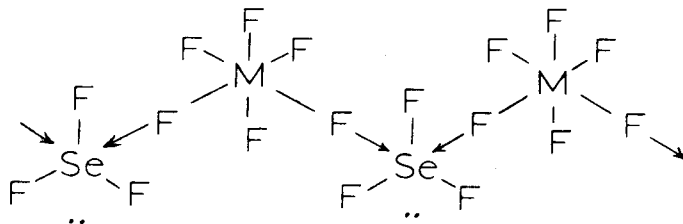
Model 1. The simple ionic model is the easiest possible structure to examine and, as shown in the preceding section, is the model which has been proposed most frequently for the structure of these compounds. With this model, all the compounds are expected to give the pyramidal SeF_3^+ ion. The anion is formed by fluoride ion donation to the other component of the adduct.

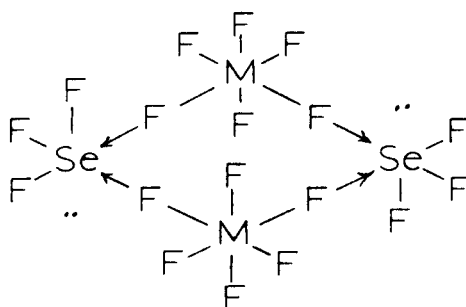
Model 2. This model is an extension of the first. The interaction of the ions in the solid and the melt is considered, and the observed data is examined taking into consideration a possible reduced site symmetry for the ions. This model is essentially ionic, but in the limit it approaches closely conditions for covalent bonding between groups.

Model 3. This model is essentially covalent in character. Fluorine bridging between the two groups is considered to give structures such as:



In such a structure, both the Se and the metal have six electron pairs associated with them. Fluorine bridging could also lead to linear or cyclic polymers.





This model is the opposite extreme to model 1. It is the consequence of strong interaction in model 2, and thus can be treated in much the same way as model 2, except that it must be extended to include characteristics associated with the bridging groups.

Model 4. The simple Lewis acid-base adduct must be mentioned for completeness. As for the SF_4 adducts, this structure is least likely for these compounds, and can be excluded on chemical grounds without the use of physical measurements. The stability of the fluoroanion to hydrolysis is the strongest chemical evidence against this model, and the n.m.r. data in Chapter III precludes any possibility of these adducts being Lewis acid-base adducts.

Infra-red and Raman Spectra of SeF_4 Adducts

The infra-red spectra are tabulated in Table 2.5, and the Raman spectra, in Tables 2.6 and 2.7. Table 2.10 contains the infra-red and Raman frequencies of SeF_4 , AsF_3 and the second component of each adduct where available.

In Figures 2.2 to 2.7 typical spectra for each of the compounds are reproduced.

In the following discussion, the abbreviations (IR), (R_1) and (R_s) are used to denote frequencies arising in the infra-red, the Raman of the liquid, and the Raman of the solid respectively.

TABLE 2.1

VIBRATIONAL FREQUENCIES FOR FLUOROSULFATE ION*

Infra-red							Assignment	Raman		
NaSO ₃ F (23)	KSO ₃ F (23)	RbSO ₃ F (23)	CsSO ₃ F (23)	NH ₄ SO ₃ F (23)	AgSO ₃ F (23)	Q ₃ CSO ₃ F (24)	(23,25)	KSO ₃ F in H ₂ O (25,26)	HSO ₃ F in H ₂ O (25)	H ₂ O in HSO ₃ F (25)
	565						ν_6 (SF wag)	409	408	408
	583						ν_3 (SO sym. bend)	566	562	562
							ν_5 (SO asym. bend)	592	600	608
740	732	729	728	737	767	710	ν_2 (SF str.)	786	782	808
785					785					
	970	973	971	970	975		$\left\{ \begin{array}{l} \nu_6 + \nu_3 \\ \nu_6 + \nu_5 \end{array} \right.$			
1095	1073	1072	1071	1072	1057	1070	ν_1 (SO sym. str.)	1082	1080	1083
1275	1277	1274	1258	1270	1235	1289	$\nu_2 + \nu_5$			
1295	1299	1294	1300	1304	1282	1336	ν_4 (SO asym. str.)	1250	1225	1235
	1656	1661	1662		1631	1643	$\nu_1 + \nu_5$			
2370	2349	2342	2353		2273	2320	$\nu_1 + \nu_4$			

* All Frequencies are in cm.⁻¹

The heading of each column contains the compound and the appropriate reference.

TABLE 2.2

VIBRATIONAL FREQUENCIES FOR FLUOROBORATE ION*

Infra-red											Raman			
(CH ₃) ₃ SnBF ₄ (27)	(28)	(29)	KBF ₄ (30)	(31)	NaBF ₄ (30)	NH ₄ BF ₄ (30)	NOBF ₄ (32)	Ca(BF ₄) ₂ (33)	CH ₃ COBF ₄ (34)	(35)	(36)	(37)	(38)	
												$\nu_2(E)$	369	353
446	447													
512	520 ^a	545	521	525	516	520			519					
525			535	536	527	533			537			$\nu_4(F_2)$	541	524
746	758		772	733	779	766				786	769	$\nu_1(A_1)$	786	769
930								928						
960		990												984
1070	1100 ^b		1030	1038	1036	1030	1035					$\nu_3(F_2)$		
1115			1059	1063	1078	1063		1060	1052	1100	1026		1100	
				1078							1064			
1170				1088										
1200				1107										
				1128										
			1290	1312		1289			1293					
			1305	1330	1305	1300		1310			1300			
				1623							1529			
				1644										
				1671										
				2340										
				2925							3509			

* All frequencies are in cm.⁻¹

The heading of each column contains the compound and the appropriate reference.

a This band was split into a doublet

b This band was split into a triplet

TABLE 2.3

VIBRATIONAL FREQUENCIES FOR HEXAFLUOROANTIMONATE AND HEXAFLUOROARSENATE IONS*

SbF ₆ ⁻ Infra-red				AsF ₆ ⁻ Infra-red				
(CH ₃) ₃ SnSbF ₆ (27)	SbF ₆ -HF (39)	(35)	NOSbF ₆ (32)	(CH ₃) ₃ SnAsF ₆ (27)	(35)	AgAsF ₆ (36)	RbAsF ₆ (36)	CsAsF ₆ (36)
454								
472					400			
640				675				
656	650	660	667	710	700	695	700	699
675							827	823
							972	970
870							1064	1068
990							1295	1300

TABLE 2.4

VIBRATIONAL FREQUENCIES OF THE GROUP Va HEXAFLUORIDE ANIONS*

VF ₆ ⁻ Infra-red (35)	Infra-red (35)	NbF ₆ ⁻ Raman (40)	TaF ₆ ⁻ Infra-red (35)
		ν ₅ 280	
		ν ₂ 562	
715	580	ν ₄	580
		ν ₁ 683	

* All Frequencies are in cm.⁻¹

The heading of each column contains the compound and the appropriate reference.

TABLE 2.5

RAMAN FREQUENCIES FOR MOLTEN COMPLEXES *

SeF_4SO_3	SeF_4BF_3	SeF_4SbF_5	SeF_4AsF_5	SeF_4VF_5	SeF_4NbF_5	SeF_4TaF_5
154 vw	163 vw		144 vw		155 w	
178 w	208 vw	235	239 w	215 vw	213 w	
269 vw	275 w	276 m				
321 v	300 w	309 sh m	311 m	260 w	256 sh s	
345 w	325 m	326 sh w	372 m		279 s	
381 w	357 m	373 m		335 vw	317 sh m	
	382 m	506 sh w	394 sh w		372 m	
			408 sh w			
416 w	420 vw	522 s	530 m br.			
567 w	525 m	537 s sh.	569 m		449 w	
587 w	657 m	561 s			469 w	
605 w	678 m sh	618 sh s	652 sh m		488 w	
670 sh w					500 w	
709 s br.	730 s br.	634 sh s	675 s		522 w	
753 s	763 vs	648 s		547 w	556 w	
			754 s br.			
	780 sh. s	663 s sh			579 w	643 w
805 w			784 vs		596 m	669 w
829 m	974 s br.	742 s			626 sh w	
1083 s		775 vs			650 sh m	715 sh s
	1050 w sh				724 s br.	721 s
1235 m br				719 m	769 vs	740 s
1290 m				753 s		774 s
				764 s		
				829 m		
				987 w		
				1036 s		

* Relative intensity of lines
s-strong, m-medium, w-weak, vw-very weak,
br-broad, sh-shoulder

TABLE 2.6

RAMAN FREQUENCIES FOR SOLID COMPLEXES *

SeF_4SO_3	SeF_4BF_3	SeF_4SbF_5	SeF_4AsF_5	SeF_4VF_5	SeF_4NbF_5	SeF_4TaF_5	SeF_4BiF_5
		144 vw		213 vw			149 vw
274 m	380			245 w	375 w	354 vw	216 vw
		264 vw	350 w	361 vw	390 vw	377 w	241 w
331 w	400	285 w	375 w				
363 m	449		398 w	400 w	450 m	400 vw	335 vw
	472	380 w	410 w		462 sh	472 w	355 w
408 vw		516 m br.	445 w				376 w
	530	560 m	465 w		577 m	565 w	400 vw
525 w	574		490 w				
596 vw	646	600 w	540 m		663 w	620 w	450 w
610 vw	665	645 vs	560 w				467 w
717 m br.	695	675 m	616 w		712 m	720 m	510 m
							530 sh.
753 s	726	690 sh w	660 s		738 m	742 m	582 s
819 m	759 s	746 s	690 w		769 s	773 s	596 s
1081 s		774 vs	721 m				615 sh
			753 m	760 s			727 m
1237 } m br.			778 s				742 m
1250 }				840 m			769 s
1290 m				1034 s			
							850 vw

* Relative intensity of lines

s-strong, m-medium, w-weak, vw-very weak

br-broad, sh-shoulder

TABLE 2.7

INFRA-RED FREQUENCIES OF ADDITION COMPOUNDS *

SeF_4SO_3		SeF_4BF_3		SeF_4SbF_5	
poly.	AgCl.	poly.	AgCl.	poly.	AgCl.
258w		260w		257s	
271w				269s	
285w		289w		284s	
292w				290sh	
317m		305w		304vw	
329sh		332sh.		330vvw	
338vw		343m			
346vw					
375m		379w		374m	
406w				451m	
426w		475shw		489m	486m
540sh		502shw		538} m	vw
		519s	514m	563} m	vw
561s	558m	533s		590sh	586sh
597m	{592} s	552shw	550shw	618s	
	{597} s				
	{697} s		652} m		641s
	{701} s		668} m		655s
	716sh				683s
	736m		725s		806shw
	752shw		746shs		738shw
	807m				765sh
	824m		831w		908w
	834sh				942w
	1076s		948sh		
			975} s		
	1167shw		1003} s		
	1224s		1030		
			1057s		
	1238s		1076} s		
			1089} s		
	1276s		1145shw		
	1422w		1195shw		
			1290w		
			284s		
			2915		

* Relative intensity of lines

s-strong, m-medium, w-weak, vw-very weak

sh-shoulder, shw-weak shoulder, shm-medium shoulder,

shs-strong shoulder, br-broad line

TABLE 2.7, cont'd

SeF_4AsF_5		SeF_4NbF_5		SeF_4TaF_5	
poly.	AgCl	poly.	AgCl	poly.	AgCl
285w		257shw		264shw	
305m		268sh		279sh	
		287shm		293	
366m		299sh		304	
383sh		307m		345	
398shw		321shw		357	
527}		370m		425shw	
538}		470			
558s(br)	547m	1 s(br)	472sbr,		
	568m	560	502 wsh	488s	493s
		583sh	571 s	512	511s
	653m		657}	530	
	697shw		670}	548	
	712s		715s		576m
	720}		766s		635s
	728}				
	743s		953w		668m
	760sh				728m
	781w				
	922m(br.)				769m
	953m(br.)				955mbr.
SeF_4VF_5					
poly.	AgCl				
278m					
305m					
326sh					
370m					
506sh					
534m					
549m					
560sh	570sh				
590m	603s				
	626s				
	655				
	668s				
	702s				
	754sh				
	962m.br.				
	1022m				

TABLE 2.8

CORRELATION TABLES* FOR T_d and O_h POINT GROUPS

(a)

T_d	C_{3v}	C_{2v}	C_3	C_2	C_s
A_1	A_1	A_1	A	A	A'
A_2	A_2	A_2	A	A	A''
E	E	$A_1 + A_2$	E	$2A$	$A' + A''$
T_1	$A_2 + E$	$A_2 + B_1 + B_2$	$A + E$	$A + 2B$	$A' + 2A''$
T_2	$A_1 + E$	$A_1 + B_1 + B_2$	$A + E$	$A + 2B$	$2A' + A''$

(b)

O_h	T_d	D_{4h}	C_{4v}	C_{2v}
A_{1g}	A_1	A_{1g}	A_1	A_1
A_{2g}	A_2	B_{1g}	B_1	A_2
E_g	E	$A_{1g} + B_{1g}$	$A_1 + B_1$	$A_1 + A_2$
T_{1g}	T_1	$A_{2g} + E_g$	$A_2 + E$	$A_2 + B_1 + B_2$
T_{2g}	T_2	$B_{2g} + E_g$	$B_2 + E$	$A_1 + B_1 + B_2$
A_{1u}	A_2	A_{1u}	A_2	A_2
A_{2u}	A_1	B_{1u}	B_2	A_1
E_u	E	$A_{1u} + B_{1u}$	$A_2 + B_2$	$A_1 + A_2$
T_{1u}	T_2	$A_{2u} + E_u$	$A_1 + E$	$A_1 + B_1 + B_2$
T_{2u}	T_1	$B_{2u} + E_u$	$B_1 + E$	$A_2 + B_1 + B_2$

*The correlation table for the group C_{3v} is a sub-group in the T_d correlation table.

(a) Ref. 66 - in part

(b) Ref. 67 - in part

TABLE 2.10 *

VIBRATIONAL SPECTRUM OF SELENIUM TETRAFLUORIDE, ARSENIC TRIFLUORIDE
and ANTIMONY PENTAFLUORIDE.

SeF ₄			AsF ₃			SbF ₅			
Infra-red		Raman	Infra-red		Raman	Infra-red		Raman	
solid	vapour	liquid	solid	vapour	liquid				
(70)	(70)	(8)	(70)	(70)	(69)	(39)	(64)	(64)	(39) (65)
		194			274			90	137
		360			341				150 188
		400						228	228 232
470					644			264	265 267
1		545					~300		300
570			660				326		
	622		690	701	707		335		345
720	736	713		738			439		
745	745	744					478		
						490	491		
		1009		1399			517		
				1439					585
									615
						655		667	668 673
						685	684		
						710	710	712	712 716
							727		
						745			749
							760		
							1140		
						1420			

* All frequencies are in cm.⁻¹

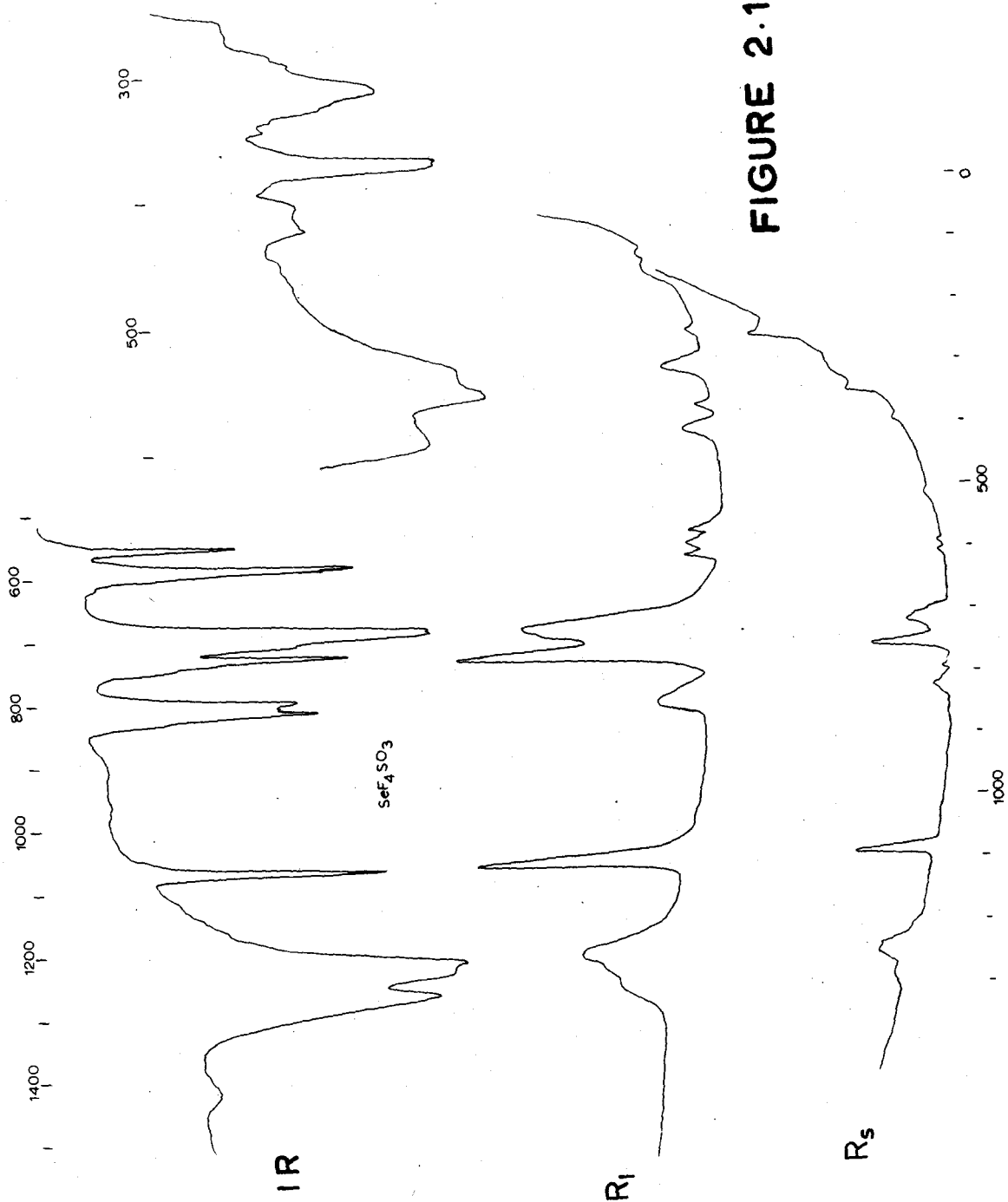


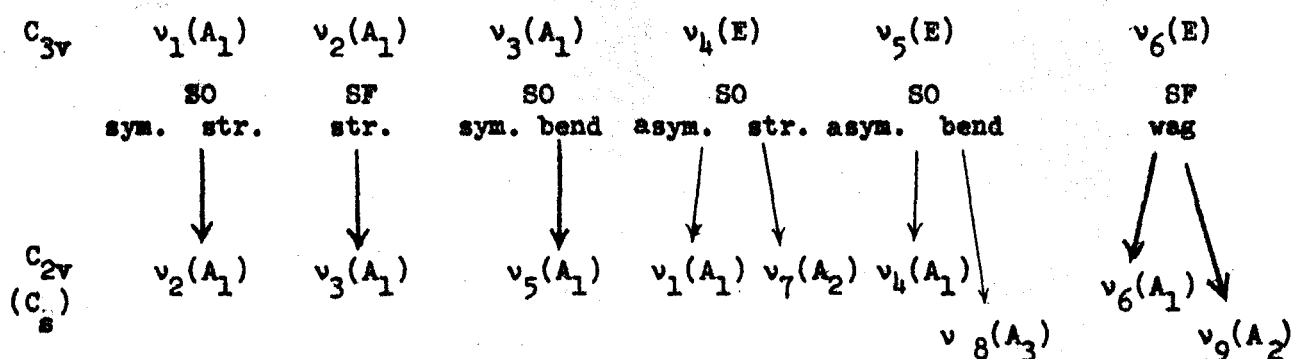
FIGURE 2.1

Discussion

SeF₄SO₃

It has been suggested that this compound is an ionic fluorosulfate. The observed fundamental frequencies for the fluorosulfate ion are given in Table 2.1. In SeF₄SO₃, the frequencies at 1238, 1076, 807, 597, 560 and 406 cm.⁻¹ in the infra-red and at 1235, 1083, 805, 605, 567 and 416 cm.⁻¹ in the Raman can be assigned to an ionic fluorosulfate. The remaining ion, SeF₃⁺, must have four lines in both the infra-red and Raman. However, even if suitable frequencies are selected for SeF₃⁺, almost as many lines remain unexplained as have been assigned. The strong frequencies at 1290 cm.⁻¹ in the Raman, and 1276 cm.⁻¹ in the infra-red, the band at 829 cm.⁻¹ in the Raman, and 824 cm.⁻¹ in the infra-red, and the many frequencies below 600 cm.⁻¹ in both infra-red and Raman are some of the more evident features unexplained by an ionic model.

An interpretation of the spectra on the basis of model 2 is more satisfactory. If the fluorosulfate ion interacts through one or two of the oxygen atoms, the site symmetry for the ion is C_{2v} or C_s. Reference to the correlation table (Table 2.8) for the C_{3v} point group shows that all degeneracies in the fluorosulfate ion will be removed by such a reduction in symmetry. Thus, the three E modes in the fluorosulfate group should be split into two frequencies. The expected correlation is shown below:



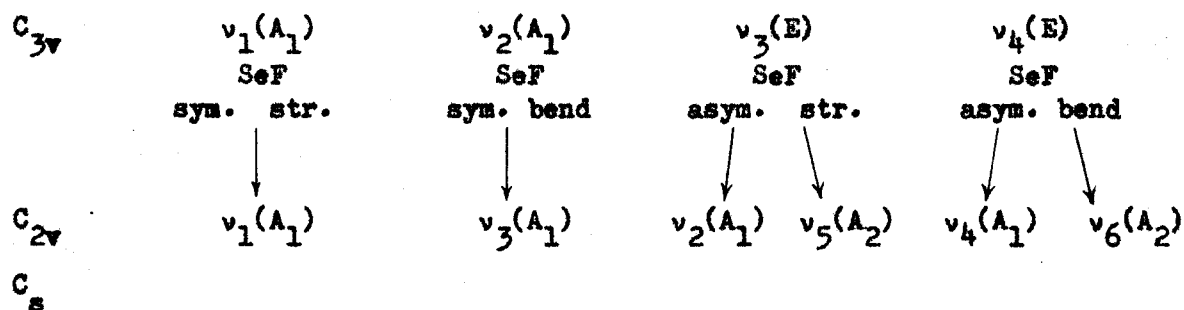
In the C_{2v} point group, the A_2 modes are forbidden in the infra-red. The expected splitting is observed in both the infra-red and Raman, and thus the SO_3F group must have C_s symmetry.

Thus the following assignments can be made:

$SO_3F^-(C_s)$	IR	$R_{liq.}$	R_{solid}
ν_1	1276	1290	1290
ν_2	1076	1083	1081
ν_3	824	829	819
ν_4	597	605	610
ν_5	560	567	525
ν_6	406	416	408
ν_7	1238	1235	1237
ν_8	592	587	596
ν_9	426	416	408

The symmetry of the SeF_3^+ ion must also be reduced in the process.

Its site symmetry may be C_{2v} or C_s ; in either case all degeneracies are removed. The expected changes are shown below:



All frequencies are Raman active, but under C_{2v} symmetry the A_2 modes are inactive in the infra-red.

The possible frequencies for SeF_3^+ can be selected by comparison with the observed frequencies for arsenic trifluoride which is isoelectronic with SeF_3^+ . The effect of the positive charge on the selenium will be to draw more electron density into the Se-F bonds of SeF_3^+ than that in the As-F bonds of AsF_3 . This will result in relatively stronger Se-F bonds and thus slightly higher vibrational frequencies in SeF_3^+ than in AsF_3 . Using this information, the following assignments can be made for SeF_3^+ :

$\text{SeF}_3^+ (C_s)$	IR	$R_{\text{liq.}}$	$R_{\text{g.}}$	$\text{AsF}_3^{(69)}$
ν_1	752	753	753	707
ν_2	736	709	717	341
ν_3	375	381	363	644
ν_4	317	321	331	274
ν_5	716	709	717	
ν_6	285	269	274	

This assignment satisfactorily explains the main features of the spectra. The lines at 1224 cm.^{-1} (IR) and 1250 cm.^{-1} ($R_{\text{g.}}$) can be assigned to the

combination band $\nu_3 + \nu_9(A'')$ of the fluorosulfate ion, which is increased in intensity by Fermi resonance with $\nu_7(A'')$. The shoulder on frequency $\nu_3(A')$ at 805 cm.^{-1} (R_1) and 807 cm.^{-1} (IR) may be the overtone $2\nu_6(A')$. The additional splitting of bands observed in the infra-red may be due to changes in the crystal at low temperatures.

An extension of the above interpretation must be made for model 3. There will be six additional frequencies as a result of the bridge, three associated with the bridge and three torsional type vibrations. The bridge asymmetric stretch essentially involves motion of the bridging atom only, and will occur at a reasonably high frequency. In SOS bridged compounds, this frequency has been assigned at $760\text{--}814 \text{ cm.}^{-1}$ (45) depending on the mass of the end groups. For the SeOS bridge in SeF_4SO_3 it might be expected to be about 800 cm.^{-1} . The frequency at 807 cm.^{-1} (IR) and 805 cm.^{-1} (R_1) can reasonably be assigned to this vibration. The remaining five additional frequencies will probably be less than 350 cm.^{-1} and can be assigned to the weak bands unassigned in that region. One difficulty arises with this interpretation. For a covalent fluorosulfate, the SO asymmetric stretch has always been observed above 1400 cm.^{-1} (46). Thus it is necessary to assign the SO asymmetric stretch in SeF_4SO_3 at 1422 cm.^{-1} and the SO symmetric stretch at 1224 cm.^{-1} . This leaves the strong line at 1080 cm.^{-1} in all spectra unexplained, and the lines at 1276 and 1234 cm.^{-1} would have to be assigned to overtones. Thus model 3, although solving certain difficulties, presents other difficulties which are difficult to rationalize.

One further possibility can be considered, that of a fluoro-sulfate-bridged polymer, i.e.

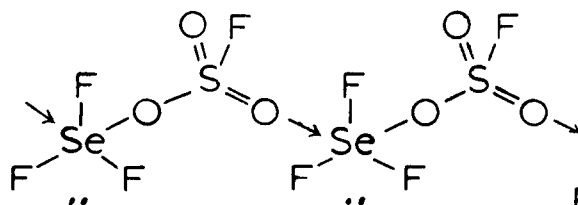


FIGURE 2.8

The compound $\text{SbF}_4\text{SO}_3\text{F}$ has a fluorosulfate-bridged structure as shown by its F^{19} n.m.r. spectrum. (47) The infra-red and Raman spectra of the compound are also reported. There are lines observed at 1430 and 1080 cm^{-1} in the Raman, and 1400 , 1216 and 1020 cm^{-1} in the infra-red. In SeF_4SO_3 , bands are observed in each of these regions, at 1422 , 1276 - 1224 and 1076 cm^{-1} in the infra-red, and at 1290 , 1250 , 1235 and 1082 cm^{-1} in the Raman. These frequencies appear to be typical of a bridged fluorosulfate group in the SO stretching region.

The S-F stretching frequency in $\text{SbF}_4\text{SO}_3\text{F}$ is observed at 890 cm^{-1} in the Raman, and 865 cm^{-1} in the infra-red. In SeF_4SO_3 , this frequency is assigned at 824 cm^{-1} (IR), 829 cm^{-1} (R_1) and 819 cm^{-1} (R_s). This assignment is intermediate between the value assigned for fluorosulfate ion which varies between 808 and 782 cm^{-1} in the Raman, and 740 and 729 cm^{-1} in the infra-red, and that assigned for $\text{SbF}_4\text{SO}_3\text{F}$. The S-F stretches of some covalent fluorosulfates in Table 2.9 give a basis for comparison.

TABLE 2.9

Compound	S-F Stretch(cm^{-1})	Reference
$\text{C}_2\text{F}_4(\text{SO}_3\text{F})_2$	906, 846	(48)
$\text{SF}_4(\text{SO}_3\text{F})_2$	887, 839	(48)
SO_2F_2	885, 848	(49)
$\text{S}_3\text{O}_8\text{F}_2$	876	(50,51)
$\text{S}_2\text{O}_5\text{F}_2$	872	(50,51)
$\text{C}_5\text{F}_8(\text{SO}_3\text{F})_2$	853	(48)
SO_3F_2	852	(52)
HSO_3F	850	(25)
$\text{S}_2\text{O}_6\text{F}_2$	848	(52)
$\text{SF}_5\text{SO}_3\text{F}$	842	(56)

These values vary between 906 and 839 cm^{-1} , and although the SF stretch in SeF_4SO_3 is not in this region, it is definitely higher than an ionic fluorosulfate, and the assigned frequency is consistent with fluorosulfate bridges of somewhat weaker strength than those in $\text{SbF}_4\text{SO}_3\text{F}$.

The remaining features of the spectrum will be essentially the same as for model 2. The symmetry of the SeF_3 units of the polymer is no higher than C_s and six frequencies can be expected as in model 2. The assignment of the SeF frequencies will be the same. Also, additional frequencies below 300 cm^{-1} will be expected in the polymer, and additional splitting at low temperatures can be expected as motion of adjacent units in the polymer becomes frozen in the crystal. Thus, the bridged polymeric structure for SeF_4SO_3 appears most likely since this is the only model capable of rationalizing all observed features of the spectra.

The Raman spectrum of SeF_4SO_3 in fluorosulfuric acid gives some information of the vibrational frequencies of the SeF_3^+ group. Lines were observed at 1088, 763, 729 and 321 cm^{-1} in addition to the lines from the solvent at 1436, 1233, 1205, 966, 847, 553 and 402 cm^{-1} . The line at 1088 cm^{-1} can be assigned to the fluorosulfate group, and the lines at 763, 729 and 321 cm^{-1} can be assigned to the SeF_3^+ group. These frequencies are in good agreement with those already assigned for SeF_4SO_3 itself.

As is shown in Chapter V, SeF_4SO_3 ionizes with appreciable polymerization in fluorosulfuric acid, and the n.m.r. spectrum indicated that the SeF_3^+ ion is strongly solvated in fluorosulfuric acid. Thus the vibration frequencies for the SeF_3^+ group are likely those for the solvated species. The broad appearance of the line at 721 cm^{-1} is consistent with this interpretation, and this line may actually be two unresolved frequencies as expected for C_s symmetry of the solvated ion.

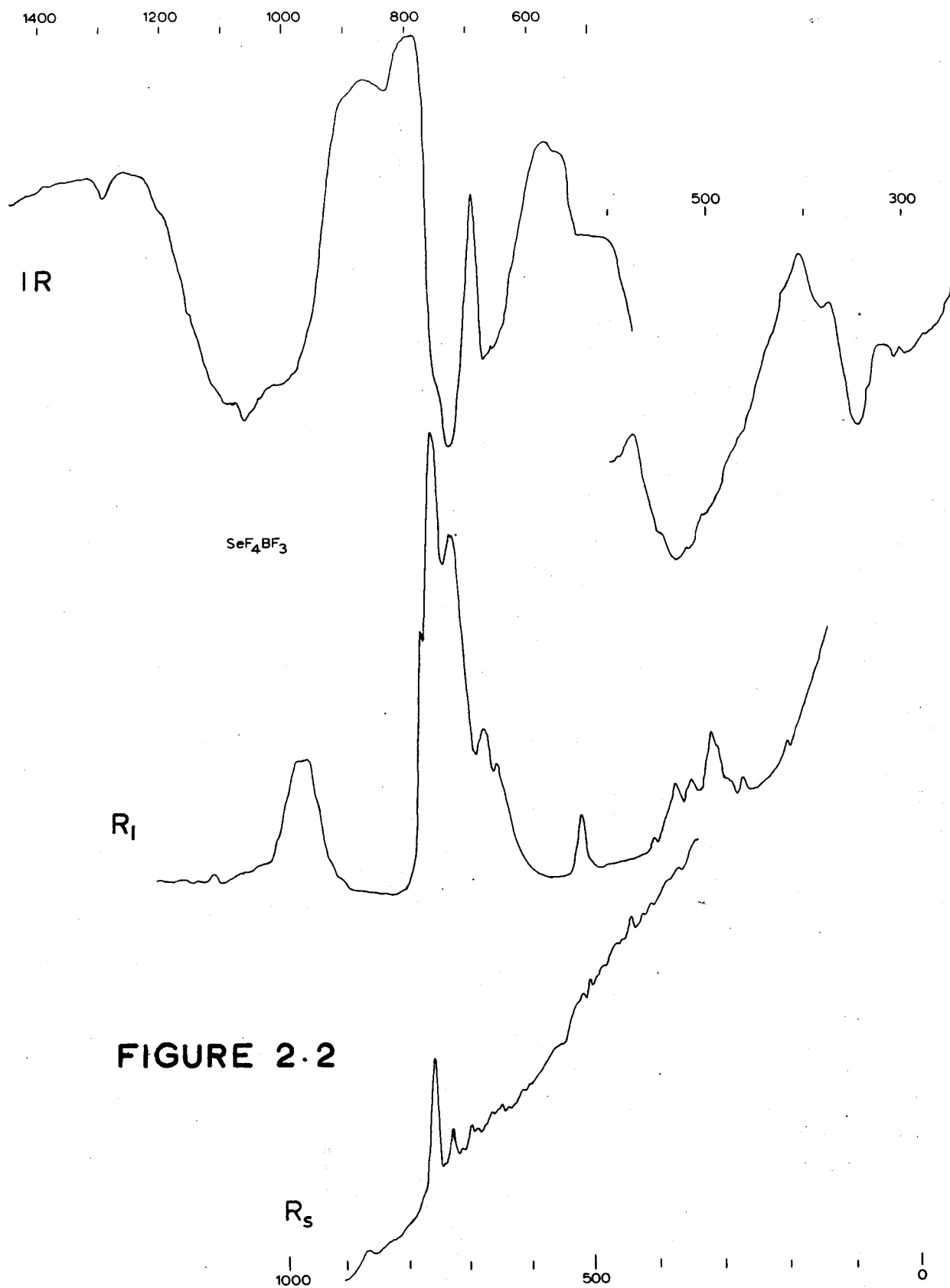


FIGURE 2.2

SeF₄BF₃

An assignment of the spectra for SeF₄BF₃ according to model 1 is somewhat unsatisfactory. In tetrahedral BF₄⁻, only ν_3 and ν_4 are infra-red active, and have been assigned previously (Table 2.2) at 1030 and 1060 cm.⁻¹, and 520 and 535 cm.⁻¹ respectively (the splitting being due to B¹⁰ and B¹¹ isotopes). All four fundamentals are allowed in the Raman, and the observed frequencies are given in Table 2.2. The ion SeF₃⁺ can have four fundamentals, all infra-red and Raman active. Thus the frequencies at 1050, 763, 525 and 357 cm.⁻¹ in the Raman of the liquid, at 759 and 530 cm.⁻¹ in the Raman of the solid, and at 1090, 1057, 533 and 519 cm.⁻¹ in the infra-red can be assigned to the BF₄⁻ ion, and the lines at 763, 730, 382 and 275 cm.⁻¹ in the Raman of the liquid, at 759, 726 and 380 cm.⁻¹ in the Raman of the solid, and at 746, 725, 379 and 289 cm.⁻¹ in the infra-red can be assigned to the SeF₃⁺ ion. However, many lines remain unassigned, and thus this model must be rejected.

Interaction between the ions can reduce the site symmetry of BF₄⁻ to C_{3v} (interaction at one fluorine) or to C_{2v} (interaction at two fluorines). The degeneracy is only partially removed in C_{3v} (Table 2.8) but is completely removed under C_{2v} symmetry. The strong band between 1200 and 950 cm.⁻¹ in the infra-red has three maxima at 1000, 1057 and 1080 cm.⁻¹ which is consistent only with the complete removal of the degeneracy of ν_3 . The further splitting observed is due to the isotopic

shift of B^{10} and B^{11} . This assignment is in good agreement with that of Clark and O'Brien for BF_4^- in $(CH_3)_3SnBF_4$ ⁽²⁷⁾ where C_{2v} site symmetry for the BF_4^- ion is also found. Thus the following correlation table shows the expected changes:

T_d	$\nu_1(A_1)$ sym. str.	$\nu_2(E_1)$ sym. bend	$\nu_3(T_2)$ asym. str.	$\nu_4(T_2)$ asym. bend
C_{2v}	$\nu_2(A_1)$	$\nu_4(A_1)$ $\nu_5(A_2)$	$\nu_1(A_1)$ $\nu_6(B_1)$ $\nu_8(B_2)$	$\nu_3(A_1)$ $\nu_7(B_1)$ $\nu_9(B_2)$
C_s				

The A_2 mode is infra-red inactive for C_{2v} symmetry.

Thus the three frequencies at 1050, 1080 and 1000 $cm.^{-1}$ (IR) can be assigned to ν_1 , ν_6 and ν_8 respectively, and similarly 1050 and 974 $cm.^{-1}$ (R_1) to ν_1 and ν_8 . ν_2 can be assigned at 746 $cm.^{-1}$ (IR), 780 $cm.^{-1}$ (R_1) and 759 $cm.^{-1}$ (R_g). ν_4 and ν_5 can be assigned at 343 and 305 $cm.^{-1}$ (IR), and 357 and 300 $cm.^{-1}$ (R_1) respectively (the symmetric bend being less than the asymmetric bend in CCl_4 ⁽⁵⁹⁾, and CF_4 ⁽⁶³⁾). The frequencies arising from ν_4 (T_d) can be assigned as ν_3 at 519 $cm.^{-1}$ (IR), 525 $cm.^{-1}$ (R_1), and 530 $cm.^{-1}$ (R_g), ν_7 at 652 $cm.^{-1}$ (IR), 657 $cm.^{-1}$ (R_1) and 646 $cm.^{-1}$ (R_g), and ν_9 at 475 $cm.^{-1}$ (IR), 420 $cm.^{-1}$ (R_1) and 472 $cm.^{-1}$ (R_g).

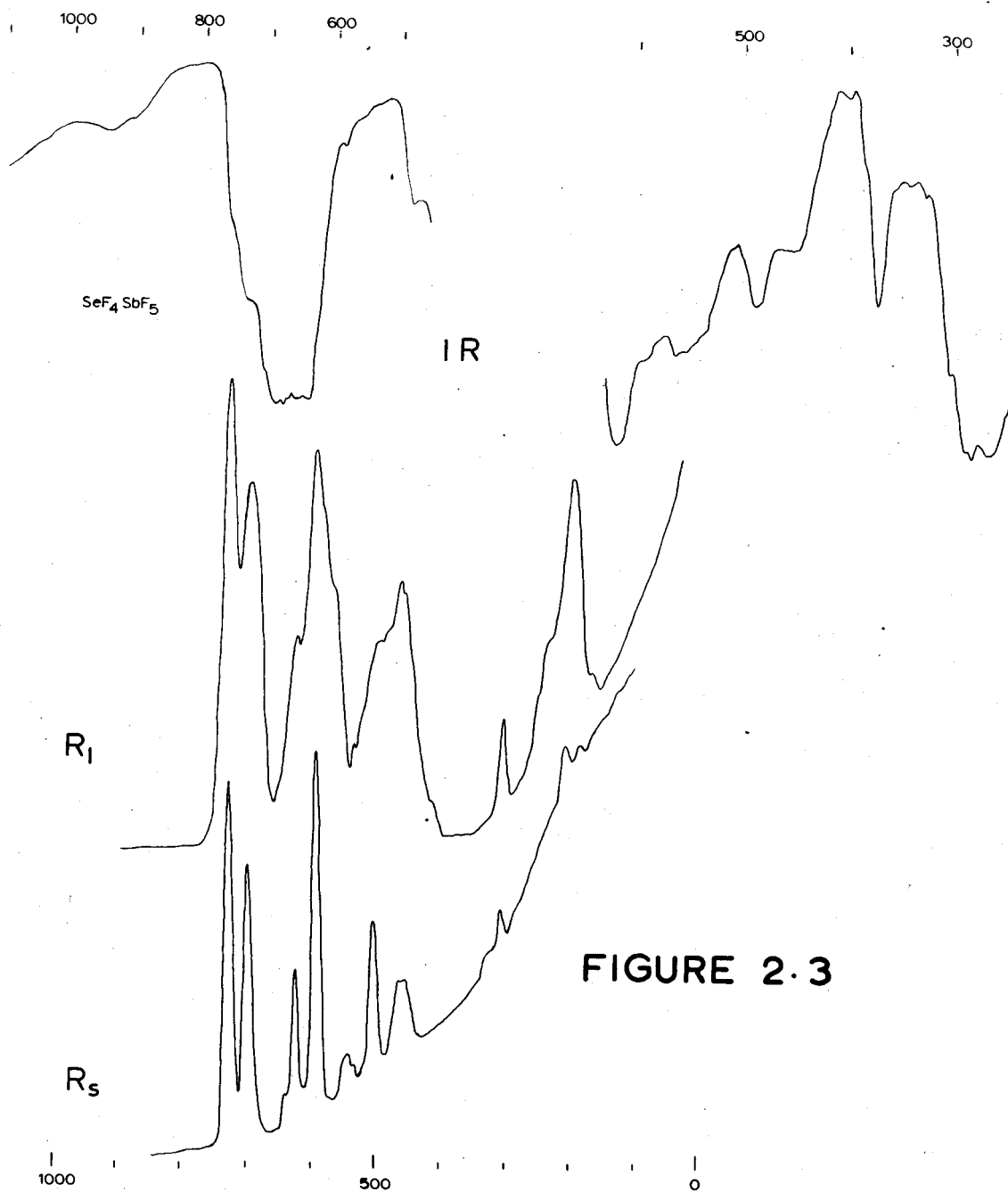
The following frequencies can be assigned to SeF_3^+ :

$SeF_3^+(C_s)$	IR	R_1	R_g
ν_1	746	763	759
ν_2	725	730	726
ν_3	379	382	380
ν_4	332	325	—
ν_5	668	678	695
ν_6	289	275	—

This assignment satisfactorily accounts for the observed spectra. Some of the shoulders will be due to B^{10} and B^{11} isotopic splitting, but this will be large only where the normal mode involves significant motion of the boron. This must be the case with the frequencies between 950-1200 cm^{-1} and around 650 cm^{-1} and 550 cm^{-1} , particularly in the infra-red.

The interpretation of the spectra on the basis of model 3 is essentially the same as for model 2, since fluorine bridging is only a type of strong interaction. The frequency at ~~831~~ cm^{-1} (IR) and 780 cm^{-1} (R_1) can well be assigned to the asymmetric stretch of the fluorine bridge. The other bridge frequencies are likely of much lower frequency and can be assigned, along with the skeletal frequencies, to the lines below 250 cm^{-1} . The remaining features of the spectrum can be assigned in much the same manner as for model 2.

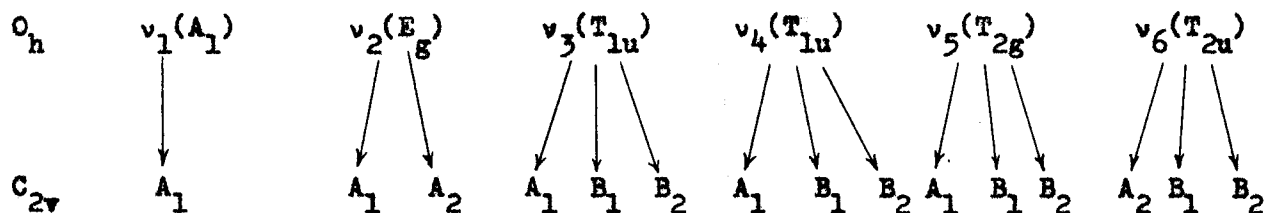
Thus it is difficult to distinguish between the structures based on models 2 and 3. However, the essential difference between these two structures is in the degree of interaction only. Model 3 is the same as model 2 except the interaction between ions is stronger and more directed. The large splittings observed in the spectra would seem to favour the fluorine-bridged structure.



SeF₄SbF₅

The vibrational frequencies for hexafluoroantimonate ion (Table 2.3) can be used to interpret the spectra for SeF₄SbF₅ according to model 1. For the free octahedral ion, there are only two infra-red active vibrations, ν_3 (T_{1u}) and ν_4 (T_{1u}). There are three active fundamentals in the Raman, ν_1 (A_{1g}), ν_2 (E_g), and ν_5 (T_{2g}), and the remaining fundamental, ν_6 (T_{2u}), is inactive in both infra-red and Raman. Thus, including the four possible frequencies for SeF₃⁺ ion, model 1 can give only six frequencies for SeF₄SbF₅ in the infra-red, and seven frequencies in the Raman. Since many more frequencies are observed, the simple ionic structure is not tenable.

Interaction between the ions involving essentially one fluorine in SbF₆⁻ produces a site symmetry of C_{4v}. Interaction through two fluorines reduces the symmetry further to C_{2v} or D_{4h} for cis and trans interaction respectively. If three fluorines were to interact, the symmetry would be either C_{3v} or C_{2v}. The degeneracies of the octahedral ion are only partially removed under the site symmetries D_{4h}, C_{4v} and C_{3v} (Table 2.8), but complete removal of the degeneracies is expected under C_{2v} symmetry. The frequency ν_3 in the octahedral ion has been assigned around 660 cm.⁻¹ (39,32). Frequencies in this region are observed in both the infra-red and the Raman spectra, and these bands can be described best as triplets at 641, 655 and 683 cm.⁻¹ (IR), at 634, 648 and 663 cm.⁻¹ (R₁) and at 645, 675 and 690 cm.⁻¹ (R₈). This observation is only consistent with complete removal of the degeneracy of ν_3 and is evidence for C_{2v} site symmetry for SbF₆⁻. Thus, the following changes are expected for the SbF₆⁻ frequencies:



The two A_2 modes are forbidden in the infra-red.

Clark and O'Brien have assigned frequencies for SbF_6^- on the basis of C_{2v} site symmetry in $(CH_3)_3 SnSbF_6$ (27). They observed three lines at 675, 656 and 640 cm^{-1} , which they assigned to $v_3(O_h)$ with the degeneracy removed. This is in excellent agreement with the frequencies observed in SeF_4SbF_5 . They also observed lines at 990, 870, 472 and 454 cm^{-1} ; corresponding lines are observed at 942, 908, 486 and 451 cm^{-1} in SeF_4SbF_5 . This gives further confirmation for C_{2v} symmetry of the SbF_6^- ion in SeF_4SbF_5 .

An interesting comparison can be made with the vibrational spectrum of SbF_5 . From the F^{19} n.m.r. spectrum, Hoffman et al (57) have shown that liquid SbF_5 consists of linear polymers formed by cis-fluorine bridging. Also the vapour is associated to the extent $(SbF_5)_3$ at 152°C and $(SbF_5)_2$ at 252°C (58). Thus the fluorine environment about each antimony in SbF_5 has the same symmetry as in an SbF_6^- ion of C_{2v} symmetry. In the Raman of SbF_5 (Table 2.10), there are two strong lines at 719 and 673 cm^{-1} and three weak lines at 749, 617 and 580 cm^{-1} which can be assigned to SbF stretching modes. In SeF_4SbF_5 , there are two strong bands at 663 and 648 cm^{-1} and shoulders at 634 and 618 cm^{-1} . A band with maxima at 522, 537 and 561 cm^{-1} occurs in SeF_4SbF_5 which has no equivalence in the spectrum of SbF_5 , but a band shifted to lower frequency at 491, 478 and 439 cm^{-1} .

is found in the infra-red of the vapour; these may well be of similar origin. Two lines in SeF_4SbF_5 at 308 and 235 cm^{-1} correspond to similar lines in SbF_5 at 302 and 232 cm^{-1} . The line at 269 cm^{-1} in SbF_5 is coincident with an SeF bend at 276 cm^{-1} in SeF_4SbF_5 . This frequency is stronger in SeF_4SbF_5 than in the other compounds, and thus two lines may be contributing to the band. The two remaining lines in SbF_5 at 188 and 137 cm^{-1} may have analogies in SeF_4SbF_5 , but the background of the spectrum is too high to observe the frequencies. In the infra-red, the SbF stretches are at 745, 710, 685 and 655 cm^{-1} in SbF_5 and at 683, 655 and 641 cm^{-1} in SeF_4SbF_5 . The bands at 517, 491, 478 and 439 cm^{-1} in SbF_5 are found at 489 and 451 cm^{-1} in SeF_4SbF_5 , and bands at 335, 326 and approximately 300 cm^{-1} in SbF_5 are found at 330 and 290 cm^{-1} in SeF_4SbF_5 . The apparent similarity between SbF_5 and SeF_4SbF_5 indicates some structural similarity and gives good support to assigning frequencies for SbF_6^- ion in SeF_4SbF_5 on the basis of C_{2v} symmetry for the ion. Thus the following assignment can be made for SbF_6^- in SeF_4SbF_5 :

R_L	R_S	IR	Assignment
663	675	683	SbF sym. str.
648	645	655	SbF asym. str.
634		641	
618	600	618	
561	560	590	SbF asym. bend
539		563	
522	516	538	
506			
		489	SbF sym. bend
		451	
326		330	

(cont'd)

R_1	R_s	IR	Assignment
309		304	
276		269	
		257	
235			

Fifteen frequencies are expected in the Raman, and thirteen in the infra-red, and the observed number of frequencies is consistent with these facts.

The frequencies for SeF_3^+ , given below, are consistent with C_s site symmetry for the ion:

$\text{SeF}_3^+(C_s)$	IR	R_1	R_s
ν_1	765	775	774
ν_2	738	742	746
ν_3	374	373	380
ν_4	330	326	-
ν_5	706	742	690
ν_6	284	276	285

The frequencies for ν_1 are rather high compared with the previous assignments for SeF_3^+ . This may be a result of less interaction between ions (i.e., a greater charge on SeF_3^+ relative to other compounds).

The assignment of the spectra according to model 2 is excellent, and little improvement can be expected for model 3. The high SeF stretching frequency may be coincident with the asymmetric stretching

frequency of a bridging fluorine atom. The other additional frequencies expected for model 3 are all likely below 300 cm.^{-1} and can easily be accommodated by the observed spectra. In any case, because of the grouping of frequencies in the spectra, it is difficult to distinguish between an interpretation of the spectra based on model 2 or on model 3, and either model can give a satisfactory explanation of the vibrational frequencies.

One further possibility can give additional Sb-F frequencies, but its importance is difficult to estimate. Trans interaction with the SbF_6^- group is possible, and such interaction is likely to give slightly different frequencies for the SbF_6^- group. The higher site symmetry of the ion and the unknown concentration of such species make it difficult to assign any frequencies to such interaction.

Thus the main features of the vibrational spectra of SeF_4SbF_5 can be explained by cis interaction between two fluorine atoms on the SbF_6^- group and the SeF_3^+ group giving a structural relationship between the SbF_6^- and SeF_3^+ ions as shown below:

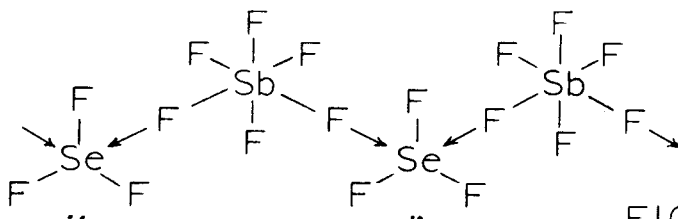
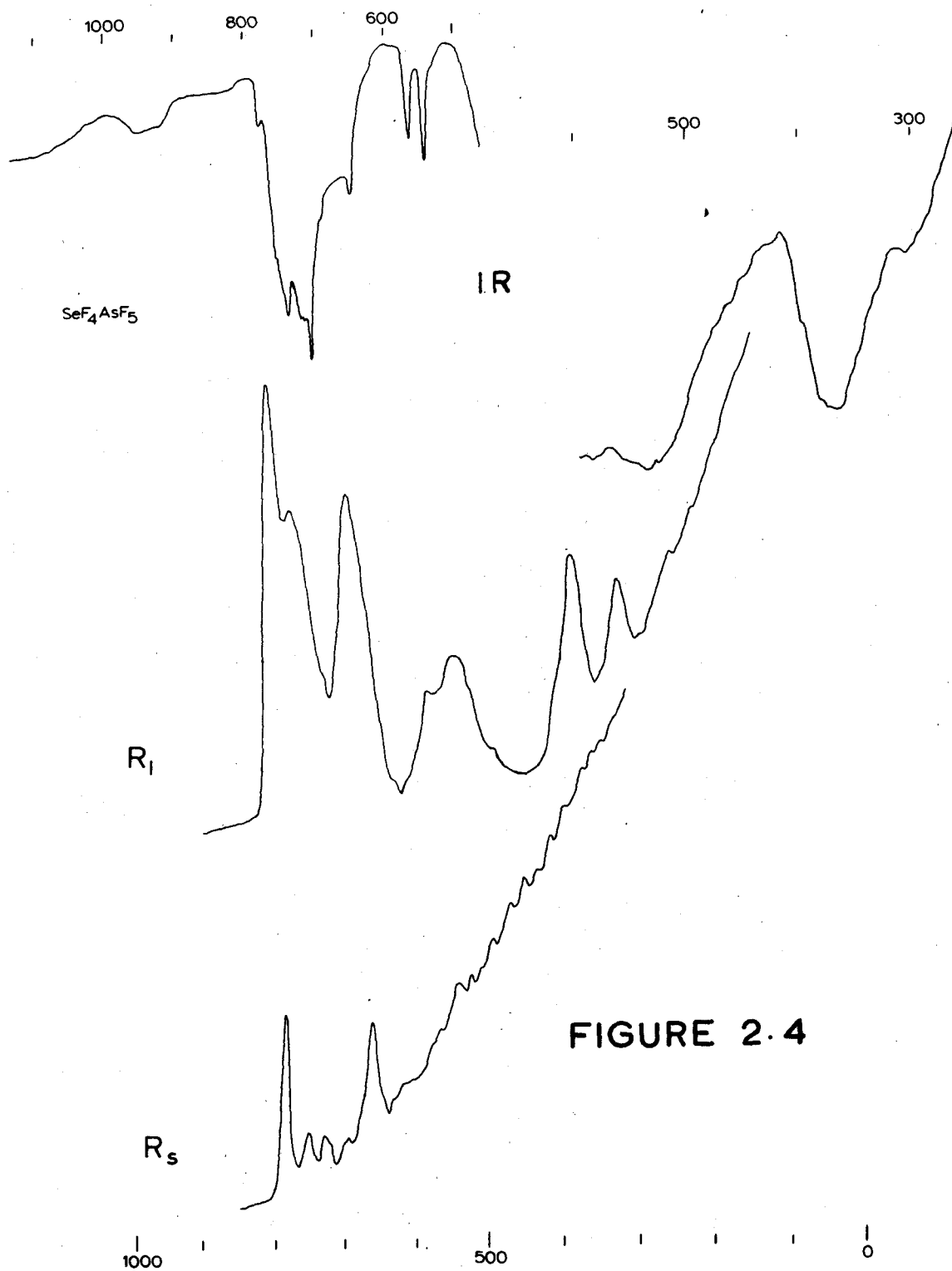


FIGURE 2.9

The importance of fluorine bridging in such interaction is difficult to estimate from the spectra alone, and the possibility of trans interaction of the SbF_6^- group may also make some contribution.



SeF₄AsF₅

The assignment of the vibrational spectra for SeF₄AsF₅ is complicated by the small difference in mass between arsenic and selenium, and thus many of the vibrational frequencies occur in the same regions. The bands between 785 and 650 cm.⁻¹ must contain all the SeF and AsF stretching frequencies. Thus some overlap is expected for any interpretation.

As for SeF₄SbF₅, in an ionic model, only six vibrational frequencies are expected in the infra-red, and seven in the Raman. Many more frequencies than this are observed, and thus such a structure is unlikely.

An assignment based on model 2 is a more satisfactory possibility. As in SeF₄SbF₅, the frequencies for SeF₃⁺ can be assigned for C_s symmetry for the ion, i.e.,

SeF ₃ ⁺ (C _s)	IR	R _L	R _S
ν ₁	781	784	778
ν ₂	760	754	753
ν ₃	366	372	375
ν ₄	305	311	-
ν ₅	720	754	721
ν ₆	285	-	-

The lower frequency lines are not observed in the solid Raman because of the high background.

A marked similarity can be seen between the spectra of SeF_4AsF_5 and SeF_4SbF_5 particularly in the Raman, although the resolution is not as good in SeF_4AsF_5 . In the Raman of the melt, the band at 675 cm^{-1} with a shoulder at 652 cm^{-1} corresponds to the band at 648 cm^{-1} with shoulders at 634 and 618 cm^{-1} in SeF_4SbF_5 . A shoulder at 714 cm^{-1} and the band at 663 cm^{-1} in SeF_4SbF_5 can be attributed to the respective symmetric stretching modes. The band at $569, 530$ and 480 cm^{-1} in SeF_4AsF_5 has the same contour as the band at $561, 537$ and 522 cm^{-1} in SeF_4SbF_6 . The lower frequency bands in SeF_4AsF_5 are shifted to higher frequency, and lines at $394, 311$ and 239 cm^{-1} correspond to the lines at $326, 308, 276$ and 233 cm^{-1} in SeF_4SbF_5 . In the infra-red, a similar comparison can be made. The AsF stretching frequencies, $712, 697$ and 653 cm^{-1} , are shifted, as in the Raman, to higher frequency from $706, 683, 655$ and 641 cm^{-1} in SeF_4SbF_5 . A band with maxima at $568, 558, 547, 538$ and 527 cm^{-1} is shifted very little from that in SeF_4SbF_5 at $586, 563$ and 538 cm^{-1} . The doublet at 489 and 451 cm^{-1} in SeF_4SbF_5 is absent in SeF_4AsF_5 , and must be shifted up into the region of the previous band where two additional frequencies are observed. The remaining bands at $398, 383$ and 305 cm^{-1} must correspond to the series of lines at $330, 304, 290, 269$ and 257 cm^{-1} in SeF_4SbF_5 . A comparison of the Raman frequencies of the solid is not warranted since the very high background on these spectra makes the position of the lines somewhat uncertain. The frequencies given are for lines which appear in more than one exposure.

The frequencies for AsF_6^- observed by Clark and O'Brien ⁽³⁾ were assigned to D_{4h} symmetry for the ion. Although similar frequencies are

observed in SeF_4AsF_5 , the number of frequencies observed in both the infra-red and Raman is not consistent with such an assignment in SeF_4AsF_5 . Also, the point group D_{4h} has a centre of symmetry, and duplication of frequencies in the infra-red and Raman, as observed in SeF_4AsF_5 , is not allowed for this point group.

Thus the structure of SeF_4AsF_5 appears to be closely related to that of SeF_4SbF_5 . The spectra are consistent with a SeF_3^+ ion of C_{3v} site symmetry and an AsF_6^- ion of C_{2v} site symmetry. The shift of the SeF stretching frequencies to higher wave number is another indication of related structure for these compounds and may well be an indication of increased fluorine bridging.

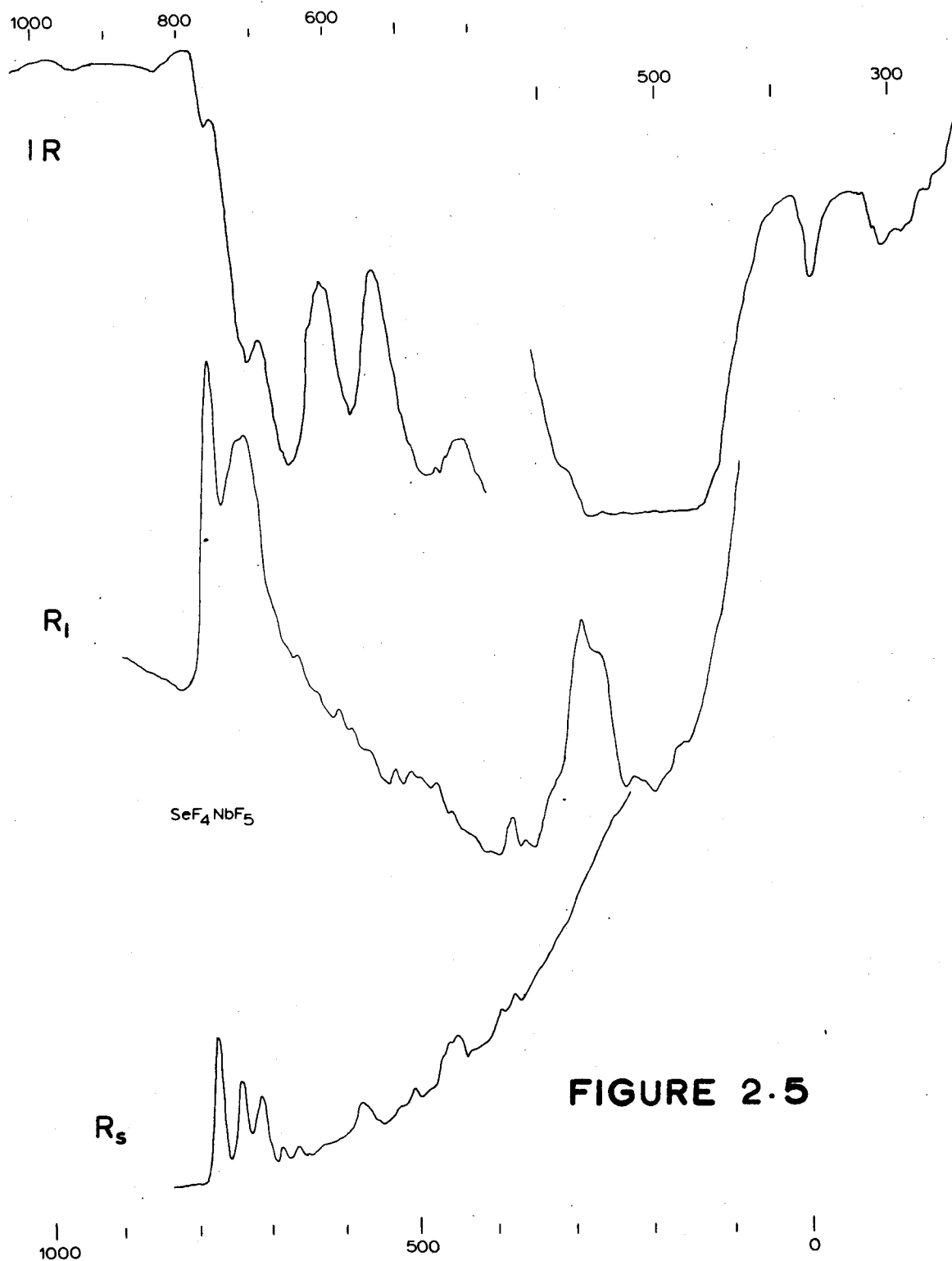


FIGURE 2.5

SeF₄NbF₅

The infra-red spectra for this compound all show broad, poorly resolved bands, and the niobium frequencies in the Raman are all very weak. These difficulties make a complete interpretation of the spectra difficult. As with the previous compounds, the number of frequencies eliminates immediately the possibility of a simple ionic structure.

The SeF stretch is again shifted to higher frequency as in SeF₄SbF₅ and SeF₄AsF₅. Thus the following assignment of SeF₃⁺ frequencies, assuming C_s symmetry, seems reasonable:

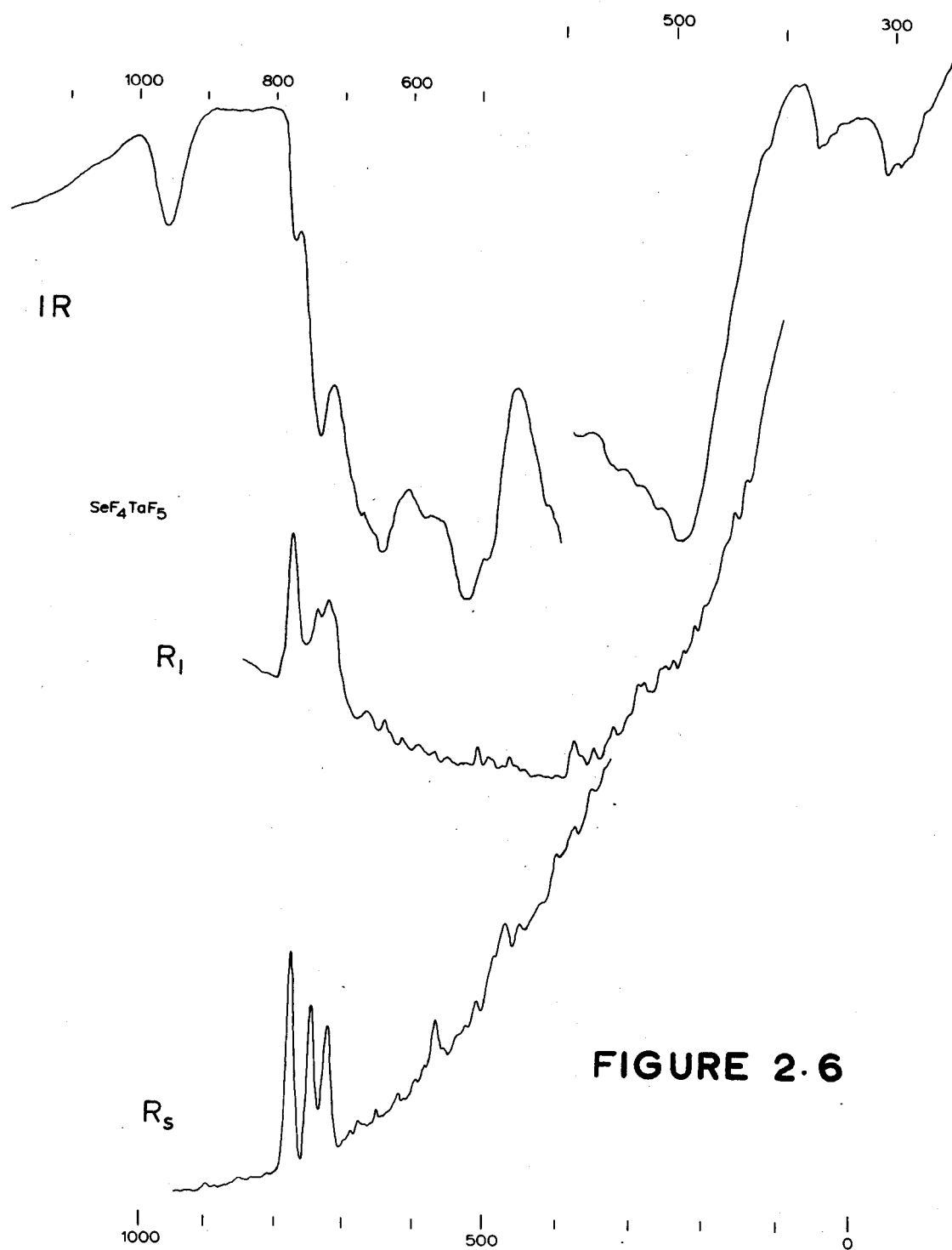
SeF ₃ ⁺ (C _s)	IR	R ₁	R _s
ν ₁	766	769	769
ν ₂	715	724	738
ν ₃	370	372	375
ν ₄	321	317	-
ν ₅	715	724	712
ν ₆	287	279	-

The high background in the solid spectra obscures any frequencies below 350 cm.⁻¹.

Raman frequencies for octahedral NbF₆⁻ have been observed and assigned as ν₁ at 683 cm.⁻¹, ν₂ at 562 cm.⁻¹ and ν₅ at 280 cm.⁻¹ (18). In SeF₄NbF₅, a band with many maxima is observed from 650 cm.⁻¹ to 450 cm.⁻¹ in the Raman of the liquid, and in the solid, lines are observed at 712, 663, 577, 462 and 450 cm.⁻¹ in the Raman and at 670, 657, 583, 560 and 470 cm.⁻¹ in the infra-red. Reduced symmetry is apparent, and

for C_{2v} site symmetry, ν_1 , ν_2 , ν_3 and ν_4 for the octahedral ion should give rise to eight lines in the infra-red, and nine lines in the Raman in this frequency range. The observed number of lines is consistent with this change, and the appearance in the infra-red of frequencies in the range of ν_1 and ν_2 of the octahedral ion is also good indication of such changes.

Thus the spectra for SeF_4NbF_5 can be interpreted in the same manner as those for SeF_4SbF_5 , and related structures are expected for the two compounds.



SeF₄TaF₅

The appearance of these spectra are almost identical to those of SeF₄NbF₅, and the same difficulties are encountered. Even with a colourless melt, the tantalum frequencies in the Raman are too weak and diffuse to be measured consistently. However, the number of frequencies which are present in all spectra eliminates any possibility of the compound having simple ionic character.

By analogy with SeF₄NbF₅, an assignment of the SeF₃⁺ frequencies can be made as follows:

SeF ₃ ⁺ (C _s)	IR	R _L	R _S
ν ₁	769	774	773
ν ₂	728	740	742
ν ₃	357	-	377
ν ₄	304	-	-
ν ₅	728	721	720
ν ₆	279	-	-

The variation in frequency is similar to that observed in SeF₄NbF₅, and this assignment is reasonable in view of the experimental difficulties in the Raman.

In the infra-red, frequencies at 668, 635, 576, 548, 530, 512, 488 and 425 cm.⁻¹ are observed in SeF₄TaF₅ and at 670, 657, 583, 571 and 560-470 cm.⁻¹ in SeF₄NbF₅. The similar appearance of these bands and the frequency relationship between them indicate related structures for the two

compounds. Thus vibration spectra for SeF_4TaF_5 can be assigned on the basis of model 2, SeF_4TaF_5 having a structure related to that of SeF_4SbF_5 .

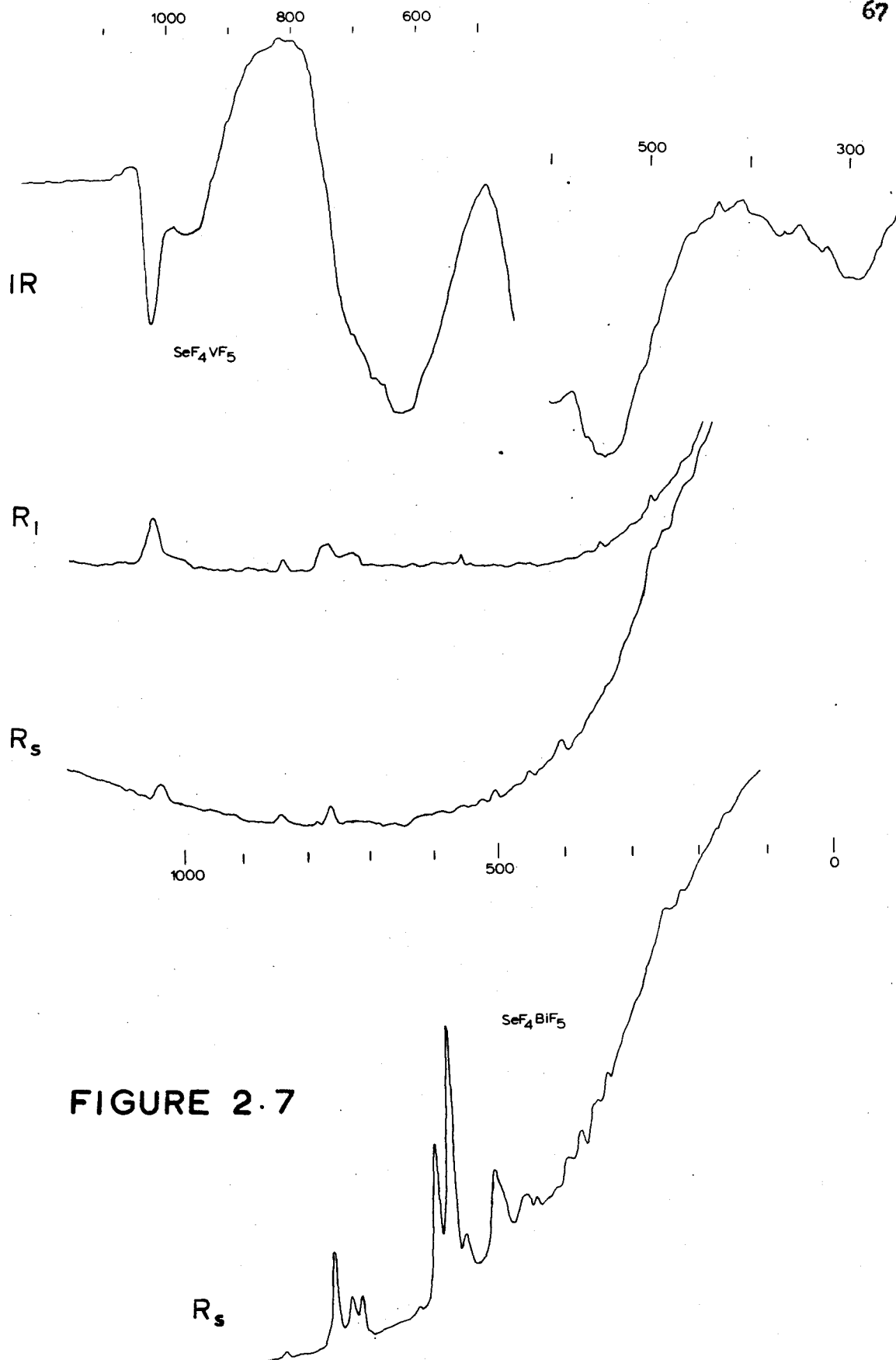


FIGURE 2.7

SeF₄VF₅

The Raman spectra of this compound are very weak because of the yellow colour of the melt; the solid spectra were obtained after solidification of the melt. Thus it is best to base an interpretation of the vibrational spectra of SeF₄VF₅ on the infra-red spectra.

The appearance of the infra-red spectrum of this compound is very similar to that of SeF₄SbF₅ and a similar interpretation of the spectra appears reasonable. The frequencies for the SeF₃⁺ group can be assigned on the basis of C_s symmetry as follows:

SeF ₃ ⁺ (C _s)	IR	R ₁	R _s
ν ₁	760	764	760
ν ₂	722	753	-
ν ₃	370	-	361
ν ₄	326	335	-
ν ₅	702	719	-
ν ₆	278	260	-

This is in good agreement with the frequencies assigned for this group in the other complexes.

The remaining frequencies in the spectra can be assigned to the VF₆⁻ group. The V-F stretching frequencies are observed at somewhat lower frequency than reported previously for VF₆⁻ (Table 2.4), but the splitting observed in these bands is consistent with lower site symmetry for the VF₆⁻ ion.

The one apparent difference between the spectra of SeF_4VF_5 and SeF_4SbF_5 is the marked increase in intensity of the lines at 962 and 1022 cm^{-1} in SeF_4VF_5 compared with the lines at 908 and 942 cm^{-1} in SeF_4SbF_5 . These bands must have their origin with the MF_6^- group and are possibly the frequency $\nu_2(\text{O}_h)$ which is inactive for the free octahedral ion. The increased intensity in SeF_4VF_5 may indicate stronger interaction between the SeF_3^+ and MF_6^- groups in SeF_4VF_5 than is present in SeF_4SbF_5 . Indeed, the intensity of these frequencies relative to the intensity of the stretching frequencies may be the best criterion of the degree to which the two ions interact and as such is a measure of the importance of fluorine bridging in these compounds. The compound SeF_4VF_5 is the only compound to show this pair of frequencies in both the infra-red and Raman spectra.

SeF₄BiF₅

An interpretation of the solid Raman spectrum of this compound can be made by comparison with that of SeF₄SbF₅. As with the latter compound, the number of frequencies excludes an interpretation based on a simple ionic model, and some ion interaction must be considered.

On the basis of C_s site symmetry, the following assignment can be made for the SeF₃⁺ ion:

SeF ₃ ⁺ (C _s)	R _s
ν ₁	769
ν ₂	742
ν ₃	376
ν ₄	335
ν ₅	727
ν ₆	241

The remaining lines are shifted to lower frequency than in SeF₄SbF₅. The lines at 615, 596, and 586 cm.⁻¹ are shifted from 690, 675 and 645 cm.⁻¹ in SeF₄SbF₅, and a doublet at 600 cm.⁻¹ is found at 530 and 510 cm.⁻¹ in SeF₄BiF₅. The lines at 467, 450 and 400 cm.⁻¹ in SeF₄BiF₅ can be related to those at 560 and 516 cm.⁻¹ in SeF₄SbF₅. The lower frequencies are more numerous in SeF₄BiF₅ than in SeF₄SbF₅ and may indicate somewhat greater interaction between ions. In any case, the structural relationship between the two compounds is apparent from this comparison.

Raman Spectra of Solutions of SeF_4SO_3 and SeF_4BF_3

Raman spectra of solutions of SeF_4SO_3 and SeF_4BF_3 in dimethylformamide, formamide and nitromethane have been obtained. The compounds are soluble in acetonitrile, but these solutions are not stable, darkening in two or three minutes even at -35°C , and thus the spectra in acetonitrile were not obtained. The observed changes in the spectra of these solutions compared with that of the solvent are almost the same for both compounds, the similarities in the spectra following the solvent rather than the compound.

In dimethylformamide, a solvent line at 661 cm^{-1} is surrounded by additional lines at 555, 580, 629 and 690 cm^{-1} for solutions of SeF_4SO_3 , and by lines at 598, 620, 639 and 691 cm^{-1} for solutions of SeF_4BF_3 . A band with maxima at 1012, 1096 and 1168 cm^{-1} is much more complex in both solutions, the solution of SeF_4SO_3 having maxima at 1010, 1070, 1099, 1127, 1153, 1170 and 1237 cm^{-1} , and for SeF_4BF_3 having maxima at 1018, 1055, 1099, 1123, 1177, 1233 and 1252 cm^{-1} . The remaining bands in the spectrum are essentially unchanged from the pure solvent. In formamide, for solutions of both SeF_4SO_3 and SeF_4BF_3 , a solvent line at 608 cm^{-1} is shifted to 586 cm^{-1} , and weak lines are observed at 408, 436, 453, 501, 763, 813, 856 and 1077 cm^{-1} for solutions of SeF_4SO_3 , and at 430, 450, 523, 769, 821 and 852 cm^{-1} for SeF_4BF_3 . The lines at 408 and 1077 cm^{-1} can be assigned to the fluorosulfate ion, and the line at 769 cm^{-1} to the tetrafluoroborate ion. The remaining lines must

correspond to species associated with the SeF_3^+ group. In nitromethane, lines are observed for solutions of SeF_4SO_3 at 264, 321, 382, 431, 557, 703, 731, 800 and 1062 cm^{-1} which are not present in the pure solvent, and for SeF_4BF_3 lines at 270, 324, 364, 381, 434, 543, 707 and 739 cm^{-1} are observed in addition to the solvent peaks. For the solutions of SeF_4SO_3 , the lines at 1062, 800 and 557 cm^{-1} can be assigned to the fluorosulfate ion, and for SeF_4BF_3 the lines at 543 and 364 cm^{-1} to the tetrafluoroborate ion. The remaining lines must belong to the SeF_3^+ group. The lines at 731, 703, 382, 321, and 264 for SeF_4SO_3 and at 739, 707, 381, 364, and 270 cm^{-1} for SeF_4BF_3 are in good agreement with previous assignments for SeF_3^+ of C_∞ symmetry. Thus it is likely that nitromethane is coordinating with the SeF_3^+ ion and removing the degeneracy of the SeF vibrational frequencies.

These Raman spectra indicate considerable interaction between the solvent and the SeF_3^+ group, particularly in dimethylformamide and formamide where the frequencies expected for the SeF_3^+ group are not observed. In nitromethane, the frequencies assigned to SeF_3^+ are the same for both compounds and are consistent with C_∞ symmetry for the group. Thus frequencies characteristic of a free SeF_3^+ ion are not observed. It is possible that the free SeF_3^+ ion is not stable, and it must be stabilized by coordination with the solvent or with a suitable anion.

CHAPTER III

Nuclear Magnetic Resonance

Theory

Certain atomic nuclei possess magnetic moments as well as the other properties characteristic of nuclei. In the presence of a magnetic field, the degeneracy of these nuclear levels is removed, and thermal distribution of the population of these levels will result. Although this change can only be observed directly in special cases, it is possible to induce transition between the various magnetic levels of the nucleus by irradiation with energy of appropriate frequency. Under these conditions energy is absorbed by the nucleus, and thus a resonance signal can be observed. It is this phenomenon which is the basis of nuclear magnetic resonance spectroscopy (NMR).

If the maximum observable component of the angular momentum of a nucleus is I , it is found that the nucleus will have $2I + 1$ spin states in which the components of angular momentum in any given direction will be $I, (I-1), \dots, (-I+1), -I$. These states are all degenerate in the absence of a magnetic field. When $I = 0$, the observed magnetic moment of the nucleus is zero, but when I is finite, a magnetic moment is observed which is always parallel to the magnetic moment vector. The complete set of observable values is given by $m\mu/I$ where μ is defined as the maximum observable component of the magnetic moment, and m is the magnetic quantum number having the possible values $I, (I-1), \dots, (-I+1), -I$. The magnitude of μ is given by:

$$\mu = \gamma I \hbar \quad (3.1)$$

where γ is the magnetogyric ratio. The magnetic moment can also be expressed in terms of the nuclear magneton, and it can be shown that the observed magnetic moment of a nucleus of spin I is given by:

$$\mu = g \frac{e \hbar}{2 M_p c} I \quad (3.2)$$

where e is the charge on the proton, M_p , the mass of the proton, c , the velocity of light, and g , the nuclear g factor.

If a nucleus with a magnetic moment is placed in a uniform magnetic field H_0 in the z direction, the change in energy is given by

$$-\mu_z H_0 \quad (3.3)$$

where μ_z is the component of the nuclear moment in that direction. For a nucleus of spin I , μ_z will have $2I + 1$ distinct values, and the energy for the various states will be $\mu_z H_0$. These levels will be equally spaced, their separation being $\mu_z H_0 / I$.

During an NMR experiment, transitions are induced between these various magnetic levels by radiation of the appropriate frequency. The frequency of radiation for transitions between neighbouring levels is given by

$$h\nu = \frac{\mu H_0}{I} \quad (3.4)$$

or in terms of the magnetogyric ratio

$$\nu = \frac{\gamma H_0}{2\pi} \quad (3.5)$$

The frequency is dependent on the magnetic field strength, and for applied fields around 10,000 gauss, the frequency is in the megacycle region. The intensity of the observed resonance is directly proportional to the number of magnetic nuclei involved.

With no other effects operating, the resonance frequency for a given nucleus would be the same regardless of the chemical environment. However, there are several effects of the environment which alter the situation. The magnetic moments of neighbouring nuclei produce a magnetic field at a given nucleus. When the neighbouring nuclei are in fixed position, as in a solid, different nuclei in a specimen will experience various fields because of this effect, and the observed resonance will occur over a range of frequencies. However, in liquids and gases, the thermal motion of the molecules averages out the magnetic field from this effect to zero. Thus the resonances observed for liquids and gases are sharp and well defined. This averaging of the fluctuating magnetic environment does not produce any change in the expected frequency of the resonance.

The electrons surrounding a nucleus give rise to a second effect. In the magnetic field, the induced orbital motion of the electrons produces a field at the nucleus in opposition to the applied field. This diamagnetic effect is proportional to the field H_0 ; thus the local magnetic field at the nucleus is given by

$$H = H_0(1 - \sigma) \quad (3.6)$$

where σ is the screening constant, and the separation between the nuclear spin states is reduced. If observations are made at constant frequency,

an increased field strength must be used in order to observe resonance. Since the effect of the electrons surrounding a nucleus varies with the chemical environment, the value of the screening constant is different for each chemically unique magnetic nucleus. Thus resonance will occur in a different part of the spectrum for each chemically distinct site, and their relative intensities are proportional to the numbers of magnetic nuclei at each site.

Separate resonances are observed for each type of nucleus in a compound as long as there is no mechanism which allows the magnetic nuclei to exchange positions. However, if such an exchange is sufficiently rapid, coalescence of the resonance signals is observed. This is a result of the uncertainty principle which can be expressed as:

$$\tau \Delta\nu \cong \frac{1}{2\pi} \quad (3.7)$$

where $\Delta\nu$ is the separation between the resonance lines, and τ the smallest time for which the two separate states can be distinguished. Thus if the rate of exchange is sufficiently rapid, the lifetimes of the states will become less than this critical value, and the signals cannot be separated. Under such conditions, a resonance is observed at a position between the two resonances determined by the weighted average of the number of magnetic nuclei at each of the exchanging sites.

An effect known as spin-spin coupling occurs when a magnetic nucleus has other magnetic nuclei as near neighbours. The nuclear spin of the one nucleus tends to orient the spins of the electrons nearby, which in turn

orient the spins of other electrons and thence the spins of neighbouring nuclei. For two types of neighbouring nuclei, n_A and n_B , with large chemical shifts, it can be shown that this electron-coupled spin interaction results in $2n_B I_A - 1$ lines for the A nuclei, and $2n_A I_B - 1$ lines for the B nuclei, where I_A and I_B are the nuclear spins of the respective nuclei. The separation between the observed lines, J , is called the coupling constant and is independent of the applied magnetic field. The simple spin-spin pattern described above is obtained only when the ratio of the chemical shift to the coupling constant, δ/J , is large. Mixing of spin states occurs when the coupling constant and the chemical shift are of the same order of magnitude, resulting in more complicated splitting.

Spin multiplets may be collapsed by rapid disturbance or relaxation of the second nucleus causing the splitting. When the second nucleus has a spin greater than $1/2$, the nucleus possesses a nuclear quadrupole moment which allows spin-lattice relaxation to occur from fluctuating electric field gradients. This quadrupole relaxation generally results in the complete collapse of any spin-spin multiplets which might be observed by coupling with nuclei with spins greater than $1/2$.

TABLE 3.1*

	δ (ppm. rel. CF_3COOH)		J(c/s)	T($^{\circ}\text{C}$)
SeF_4SO_3 in HSO_3F	-119.4(15)	-86.6(9)	-	28
	-119.4(10)	-84.9(23)	-	-35
	-119.4(24)	-84.8(23)	-	-45
	-119.4(10)	-84.8(37)	-	-54
	-119.4(13)	-83.8(48)	1088	-85

TABLE 3.2*

Compound	δ (ppm. rel. CF_3COOH)		Relative area	T($^{\circ}\text{C}$)
SeF_4SO_3	-119 (14)	-84.2(61)	0.33	87
SeF_4BF_3	-41.4(690)			75
SeF_4SbF_5	+27.0(360)	-95.7(27)	2.0	158
SeF_4AsF_5	-52.5(310)			176
SeF_4NbF_5	-170 (260)			150
SeF_4TaF_5	-56.4(200)			158

*figure in brackets following chemical shift gives line width in c/s.

TABLE 3.3

Compound or Ion	δ (ppm-rel. CF_3COOH)	Conditions	Reference
HSO_3F	-119.4	pure	
BF_4^-	+71.0	NaBF_4 in H_2O	72
AsF_6^-	-18.1	AgAsF_6 in H_2O	72
SbF_6^-	+32.3	KSbF_6 in H_2O	72
NbF_6^-	-110	NbF_5 in 48% HF	
	-178	NbF_5 + DMF in acetonitrile	73
TaF_6^-	+3.7	TaF_5 in 48% HF	
SeF_4	-141	pure	72
BF_3	+54.2	pure	72
AsF_5	-11.3	pure	72
SbF_5	+6.83, +26.2, + 52.0	pure	72
NbF_5	-257	melt at 117°C	
TaF_5	-177	melt at 124°C	

N.M.R. Spectra of Selenium Tetrafluoride Adducts

Table 3.1 gives the observed n.m.r. data for a solution of SeF_4SO_3 in fluorosulfuric acid. The doublet due to Se^{77} ($I = 1/2$, 7.5% abundance) coupling with fluorine is only observed at the lowest temperature, although a careful search was made at each temperature. An exchange process can result in the collapse of such spin-spin coupling; the gradual broadening of the fluorine on selenium resonance as the temperature is lowered indicates that the rate of some exchange process is being reduced, thereby supporting this explanation for the observed absence of $\text{Se}^{77}\text{-F}$ coupling at higher temperatures.

No intramolecular exchange process is possible in the SeF_3^+ ion since all three fluorines are equivalent. Thus some intermolecular exchange process must be involved, and exchange involving some solvated species appears most reasonable. The successive addition of a solvent molecule (X) can be represented by the equilibria below:

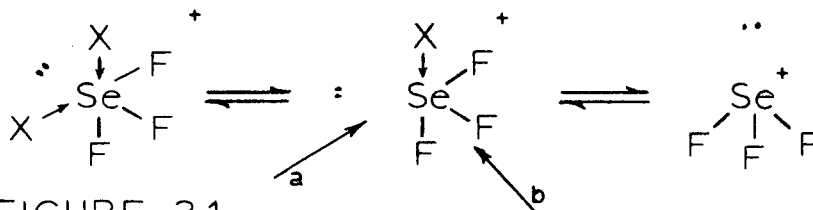


FIGURE 3.1

Either equilibrium alone can account for the observed exchange, and a contribution from both equilibria would lead to even more rapid exchange. In both solvated ions there are two types of fluorine atoms; the gain or loss of a solvent molecule can result in exchange between two different fluorine atoms on re-formation of the original solvated species. For example,

addition of a solvent molecule at 'a' to the monosolvated ion can give the illustrated isomer of the disolvated ion, but addition at 'b' gives an isomer of the disolvated ion with the solvent molecules trans to each other. In the subsequent loss of a solvent molecule from the disolvated ion, the original monosolvated ion is formed if the same solvent molecule leaves as entered. If the other molecule leaves, then a different monosolvated ion results with the axial and equatorial atoms interchanged. A similar exchange can be described with respect to the disolvated ion. The disolvated ion is possibly the more stable ion because of the favourable presence of six electron pairs about the selenium atom (i.e., pseudo-six coordination).

The two peaks in the observed spectrum are assigned to the fluorosulfuric acid solvent exchanging with fluorosulfate ion, and to a solvated SeF_3^+ ion.

Table 3.2 contains the n.m.r. data for the molten complexes at temperatures just above their melting points. The recorded temperature is high (approximately 20° high at 100°C), the error being greater the higher the temperature; this is due to the position of the thermocouple in the variable temperature probe. The temperature reported (uncorrected) is that which was just sufficient to melt the sample completely.

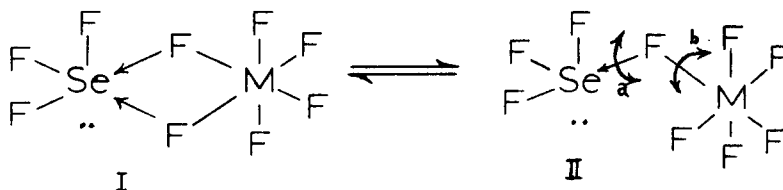
The spectrum of SeF_4SO_3 has two peaks, one with a chemical shift the same as fluorosulfuric acid and the other the same as the fluorine on selenium resonance in the solution of SeF_4SO_3 in fluorosulfuric acid. The ratio of the areas of the two peaks is consistent with the formula $\text{SeF}_3\text{SO}_3\text{F}$. No fine structure was observed in either resonance.

As indicated above, it is likely that the SeF_3^+ ion is solvated in solution. The close relationship between the spectra of SeF_4SO_3 in solution and in the melt must indicate almost identical environments under both conditions. The infra-red spectra have been interpreted on the basis of a fluorosulfate-bridged polymer (Fig. 2.8). Such a structure provides a covalent fluorosulfate group, and an environment for the SeF_3 group almost identical to the disolvated ion. Thus the observed chemical shift for the fluorosulfate group is close to fluorosulfuric acid, and the observed fluorine on selenium resonance must correspond to that of an SeF_3 group with six electron pairs around the selenium. This suggests that the disolvated ion must be the predominant species in solution.

Two peaks are also observed in the spectrum of SeF_4SbF_5 . The low field resonance is shifted to slightly lower field than the fluorine on selenium peak in SeF_4SO_3 , and can be assigned to fluorine on selenium as well; the high field resonance is in the fluorine on antimony region (cf. SbF_5 , SbF_6^- . Table 3.3). The relative areas of the two resonances are consistent with the formula SeF_3SbF_6 . No fine structure was observed in either signal.

The observed shift of the fluorine on selenium resonance to lower field can be explained by the change in environment between SeF_4SO_3 and SeF_4SbF_5 . In SeF_4SO_3 , there are two fluorosulfate groups attached to the SeF_3 group to give six electron pairs about selenium. In SeF_4SbF_5 , the SeF_3 group can only coordinate through fluorine bridges with fluorine atoms on antimony. This change from coordination by oxygen to coordination by fluorine must be accompanied by a shift to lower field.

The spectrum of each of the remaining compounds contains only one broad line. No other resonance could be located. The only possible explanation for these observations is that all the fluorine atoms are undergoing exchange, and an average signal over all possible types of fluorine in the compound is being observed. Such exchange can occur in a fluorine-bridged system through the breaking and reforming of the fluorine bridges.



A monomer structure, such as I above, is converted to II by the breaking of a fluorine bridge. From II, structure I may be reformed after rotation about either the Se-F bond (a) or the F-M bond (b), resulting in the exchange of the fluorine atoms on the selenium and on the other metal. The possibility of either side of the bridge breaking allows exchange between a fluorine atom on selenium and a fluorine atom on the metal, and thus this type of structure allows complete exchange between all fluorine atoms. A linear or cyclic polymeric fluorine-bridged system would also be capable of such total exchange. It is difficult to devise any other exchange scheme which would give complete and rapid exchange of fluorine atoms in these compounds. Muetterties and Phillips⁽⁷¹⁾ have proposed an analogous fluorine-bridged structure to explain the observation of a single F^{19} resonance from the compound AsF_3SbF_5 .

Of the compounds capable of forming fluorine bridged structures, SeF_4SbF_5 is the only one to show more than one fluorine resonance. This can be explained by the large chemical shift between fluorine on selenium and fluorine on antimony and by the more ionic nature of the bonding in SeF_4SbF_5 than in the other complexes. The ionic character describes the degree of asymmetry of the fluorine bridge, and in SeF_4SbF_5 the fluorine atoms in such bridges are displaced toward the antimony atom. Such bridges have a greater tendency to break leaving the fluorine atom on the antimony rather than on the selenium, and this makes exchange of fluorine atoms between selenium and antimony more difficult and thus slower. Although SeF_4BF_3 has a larger chemical shift between fluorine on selenium and fluorine on boron, the greater covalent character of SeF_4BF_3 leads to more rapid exchange. Also the fact that there are fewer fluorine atoms to exchange in SeF_4BF_3 makes some contribution to the more rapid exchange rate.

An attempt can be made to calculate the expected chemical shift of the compounds exhibiting complete collapse from the known chemical shifts of the starting compounds. A formula such as

$$\begin{aligned}\delta\text{Se}_{x\text{M}_y} &= \delta\text{M}_y - \frac{x}{x+y} (\delta\text{M}_y - \delta\text{Se}_x) \\ &= \delta\text{Se}_x + \frac{y}{x+y} (\delta\text{M}_y - \delta\text{Se}_x)\end{aligned}\quad (3.8)$$

may be used, where Se_x is the selenium fluoride with x fluorine atoms, and M_y is the second component with y fluorine atoms. Using the chemical shift data in Table 3.3, the following values relative to CF_3COOH are obtained from SeF_4 and MF_y :

SeF_4BF_3	-29 ppm.
SeF_4AsF_5	-67 ppm.
SeF_4NbF_5	-207 ppm.
SeF_4TaF_5	-162 ppm.

These values correspond to the chemical shift of a 1:1 mixture of SeF_4 and MF_y which is undergoing complete exchange to give one signal, and may be valid for the covalent compound SeF_4MF_y . Except for SeF_4BF_3 , these values are all to lower field than the observed chemical shift.

A value for SeF_3^+ can be taken from SeF_4SbF_5 as -95 ppm. relative to trifluoroacetic acid. Using this value and the chemical shift of the appropriate anion, the following chemical shifts relative to trifluoroacetic acid are calculated using equation (3.8):

SeF_3BF_4	0 ppm.
SeF_3AsF_6	-44 ppm.
SeF_3NbF_6	-105 ppm. (based on NbF_6^- -110 ppm.)
	-153 ppm. (based on NbF_6^- -178 ppm.)
SeF_3TaF_6	-29 ppm.

These values are all to higher field than the observed chemical shift.

It appears that the first method for calculating the chemical shift overestimates the covalent character, and the second, the ionic character of the complexes. Except for SeF_4BF_3 , the observed chemical shift lies between the two calculated values. If no other effects are considered, the position of the observed resonance between the two calculated values gives the relative importance of ionic and covalent

structures. Then SeF_4AsF_6 is approximately 50% ionic, SeF_4NbF_5 about 30% ionic, and SeF_4TaF_5 70 - 80% ionic. The compound SeF_4BF_3 must be essentially covalent.

CHAPTER IV

Cryoscopy in Nitrobenzene

Theory

The depression of the freezing point of a solvent by the addition of a solute is well known and is a result of changes in the phase equilibria due to the lowering of the vapour pressure. Assuming linear changes in vapour pressure with temperature near the freezing point, for dilute solutions which obey Raoult's Law the freezing point depression, ΔT , is given by

$$\Delta T = \frac{RT_o^2}{1000 l_f} \cdot m \quad (4.1)$$

where T_o is the freezing point of the solvent, l_f , the heat of fusion per gram for the solvent, and m , the molality of the solute. The molal freezing point constant is defined by

$$K_f = \frac{RT_o^2}{1000 l_f} \quad (4.2)$$

and thus

$$\Delta T = K_f \cdot m \quad (4.3)$$

This equation applies, within the limits of the assumptions made in the derivation, for any solute as long as no dissociation takes place. However,

in cases where the solute dissociates to form more than one particle, a more general expression can be used, i.e.,

$$\Delta T = K_f v m \quad (4.4)$$

where v is equal to the number of particles formed from each molecule of solute.

Assuming $v = 1$, the freezing point depression in a solvent where K_f is known can be used to determine the molecular weight of the solute. From equation (4.1) the following relation is obtained:

$$M_2 = K_f \frac{1000 w_2}{\Delta T \cdot w_1} \quad (4.5)$$

where w_1 and w_2 are the weight of solvent and solute respectively.

Cryoscopic Measurements in Nitrobenzene

The experimental data for each of the complexes is given in Table 4.1. The solutions are not stable and darken slowly during the time for each experimental run. The solutions of SeF_4SO_3 and SeF_4BF_3 are the most stable, and the stability increases in the order $\text{SeF}_4\text{SbF}_5 \sim \text{SeF}_4\text{AsF}_5 < \text{SeF}_4\text{NbF}_5 \sim \text{SeF}_4\text{TaF}_5$. The decomposition increases the observed freezing point depression. The total time for each experiment varied between three and four hours, and the decomposition during this time, although noticeable, is small enough to be neglected. The compounds SeF_4BiF_5 and SeF_4VF_5 were not obtained in sufficient quantity to study by this technique.

The slope of a plot of C vs. ΔT for each compound can be used to obtain the molecular weight. However, such a plot does not give a linear

change with increasing ΔT , and thus the molecular weight must be changing with concentration.

More information can be obtained from a plot of m vs. ΔT , as shown in Fig. 4.1. The straight lines, A, drawn from the origin for each compound correspond to the formation of two molecules for each solute (i.e., $v = 2$); this corresponds to complete ionization of the compound. The slope, $v = 1$, is represented by the trinitrobenzene curve, and by the line, B, at the origin of the SeF_4SO_3 curve. The tangent, C, to the curve for SeF_4SO_3 at higher concentration is the theoretical slope for $v = 0.5$.

For SeF_4BF_3 , SeF_4AsF_5 , SeF_4NbF_5 and SeF_4TaF_5 an initial slope of 2.0 is observed. The initial slope of SeF_4SbF_5 is slightly greater than 2.0. This may be due to some decomposition of the first addition which was made to the nitrobenzene at room temperature or to trace amounts of water which reacted with the first addition.

As the concentration of the compound increases, the observed slope decreases, and in the case of SeF_4BF_3 approaches unity. This observation can be explained either by association as ion pairs or by the presence of molecular units which are incompletely dissociated into ions. The relatively high dielectric constant of nitrobenzene (37.6 at 10°C ⁽⁵³⁾) reduces the likelihood of ion pair formation. Although the formation of ion pairs cannot be disregarded, it is likely that the observed association is by fluorine bridging between the ions. Thus SeF_4AsF_5 and SeF_4SbF_5 appear to be associated to the smallest extent, with SeF_4NbF_5 and SeF_4TaF_5 showing somewhat greater association. The compound SeF_4BF_3 shows strong

association, and around the concentration of 0.08 m. it is almost completely associated.

The behaviour of SeF_4SO_3 is very different from the other compounds. The initial slope of the curve is much less than 2.0 and close to 1.0. The slope of the curve decreases rapidly and at higher concentrations approaches a slope of 0.5. These facts can be explained by the formation of a fluorosulfate-bridged dimer in solution, i.e.,

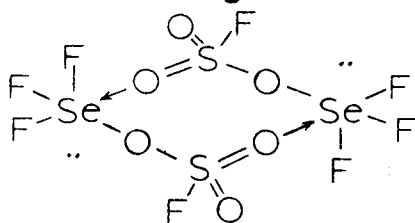


Figure 4.2

The presence of monomer, dimer and higher polymers in solution would also explain the observed behaviour. However, even at the highest concentrations studied, the slope approaches 0.5, and this is more consistent with the predominant formation of dimers.

Conclusions

In nitrobenzene, the compounds capable of forming octahedral anions are completely ionized in dilute solution, and show some degree of association as the concentration increases. The compound SeF_4BF_3 shows similar behaviour initially, but is more highly associated as the concentration increases. The association may be explained by fluorine bridging between the ions.

The compound SeF_4SO_3 is associated into fluorosulfate-bridged polymers and is only slightly dissociated into ions at lower concentrations. The observed behaviour is consistent with the predominant formation of dimers in solution.

CRYOSCOPY in NITROBENZENE

FIGURE 4.1

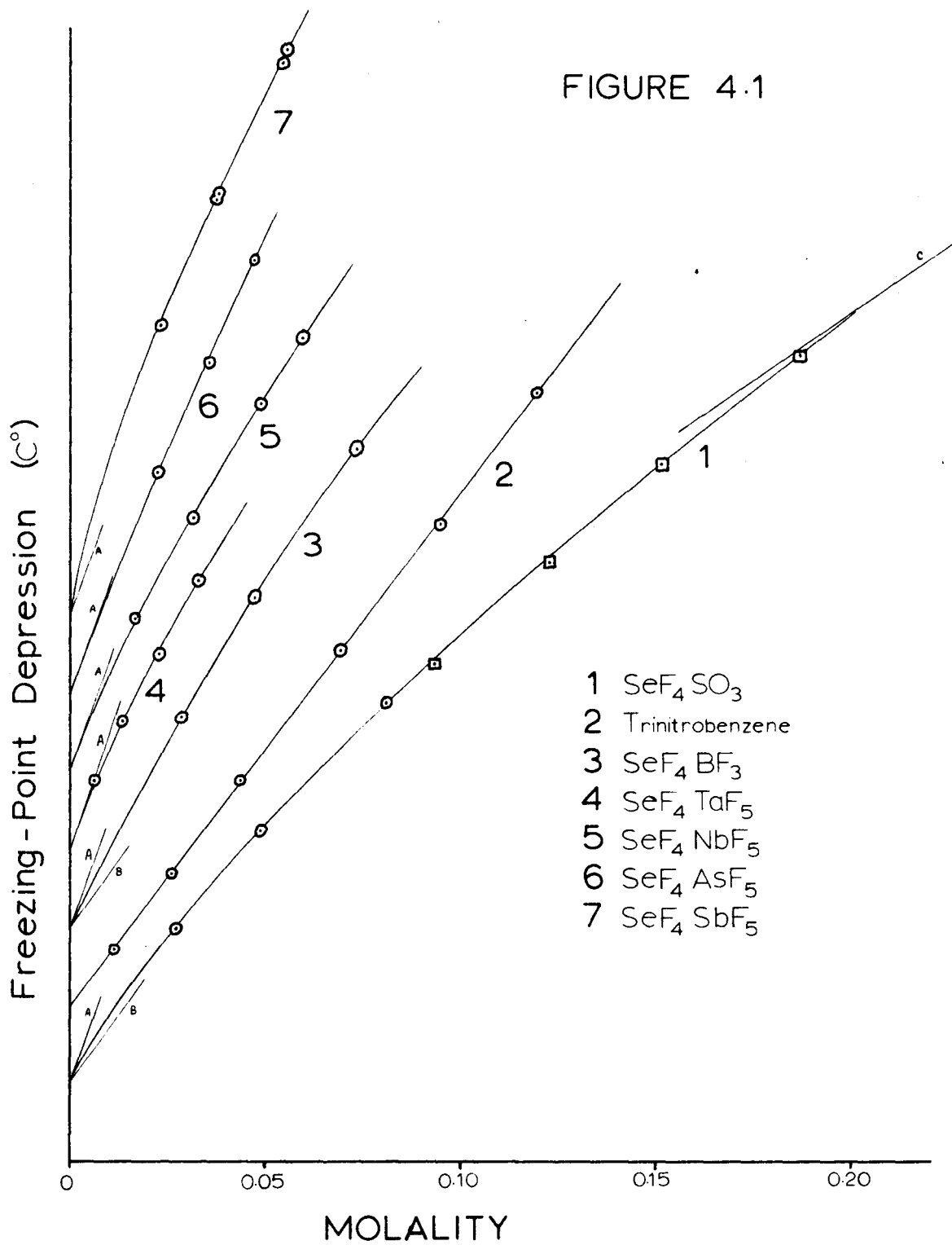


TABLE 4.1

CRYOSCOPIC MEASUREMENTS IN NITROBENZENE

Trinitrobenzene		F.W. = 213.108		
Expt. 125	w(g)	C(g/kg.)	molality	$\Delta T(^{\circ}\text{C})$
$T_o = 5.564^{\circ}\text{C}$	0.2246	2.418	0.01135	0.071
	0.5189	5.559	0.02608	0.169
	0.8595	9.299	0.04363	0.289
	1.3772	14.71	0.06902	0.455
	1.9050	20.19	0.09474	0.618
	2.3941	25.51	0.1197	0.786
<u>SeF₄SO₃</u>		F.W. = 235.03		
Expt. 131	w(g)	C(g/kg)	molality	$\Delta T(^{\circ}\text{C})$
$T_o = 5.704^{\circ}\text{C}$	0.6400	6.462	0.02749	0.199
	1.1319	11.46	0.04876	0.324
	1.8609	19.00	0.08084	0.488
Expt. 143				
$T_o = 5.698^{\circ}\text{C}$	2.1528	22.01	0.09367	0.538
	2.8280	28.84	0.1227	0.668
	3.4923	35.60	0.1515	0.792
	4.3395	44.02	0.1873	0.936
<u>SeF₄BF₃</u>		F. W. = 222.78		
Expt. 135	w(g)	C(g/kg)	molality	$\Delta T(^{\circ}\text{C})$
$T_o = 5.689^{\circ}\text{C}$	0.6080	6.360	0.02855	0.270
	1.0031	10.52	0.04722	0.423
	1.5545	16.34	0.07335	0.613
<u>SeF₄SbF₅</u>		F.W. = 371.72		
Expt. 126	w(g)	C(g/kg)	molality	$\Delta T(^{\circ}\text{C})$
$T_o = 5.573^{\circ}\text{C}$	0.8338	8.663	0.02331	0.371
	1.3383	13.98	0.03761	0.533
		14.15	0.03807	0.538
	1.9808	20.19	0.05432	0.708
		20.63	0.05550	0.726

<u>SeF₄AsF₅</u>		F.W. = 324.87		
Expt. 129	w(g)	C(g/kg.)	molality	ΔT(C°)
T _o = 5.678°C	0.7028	7.264	0.02236	0.282
	1.0993	11.49	0.03537	0.425
	1.4743	15.35	0.04725	0.556

<u>SeF₄NbF₅</u>		F.W. = 342.87		
Expt. 128	w(g)	C(g/kg)	molality	ΔT(C°)
T _o = 5.671°C	0.5437	5.717	0.01667	0.196
	1.0318	10.81	0.03153	0.324
	1.5947	16.77	0.04891	0.471
	1.9214	20.22	0.05896	0.556

<u>SeF₄TaF₅</u>		F.W. = 430.91		
Expt. 130	w(g)	C(g/kg)	molality	ΔT(C°)
T _o = 5.702°C	0.2622	2.759	0.006403	0.089
	0.5698	5.971	0.01386	0.164
	0.9522	9.981	0.02316	0.251
	1.3515	14.16	0.03286	0.343

CHAPTER V

Conductivity

Theory and Introduction

The electrical conductivity of solutions obeys Ohm's Law, and thus the specific resistance of a solution may be defined as the resistance in ohms of a specimen 1 cm. in length and 1 sq. cm. in cross section by analogy with the resistivity in conductors. The specific conductance, K , of a solution is defined as the reciprocal of the specific resistance.

In solvents highly associated by hydrogen bonding, ionic conduction can take place by a proton transfer mechanism, in which case ions capable of conduction by this method show abnormally high mobilities. This is observed with such solvents as water, sulfuric acid and fluorosulfuric acid. Conductivities in such solvents can be interpreted simply by assuming conduction to be due only to these highly conducting ions.

In fluorosulfuric acid, the self-dissociation ions, SO_3F^- and $\text{H}_2\text{SO}_3\text{F}^+$, conduct by the proton transfer mechanism through the hydrogen bonded structures in the liquid. The conductivity of a solute can be interpreted to show the number of SO_3F^- or $\text{H}_2\text{SO}_3\text{F}^+$ ions formed per molecule of solute by comparison with the conduction of a compound whose ionization is known, e.g., KSO_3F . From this information the mode of ionization of the solute in fluorosulfuric acid can often be determined.

For solutions where conduction occurs by proton transfer, it is sufficient to use the specific conductance at various concentrations to

interpret the behaviour in solution, since the auto-protolysis ions are essentially responsible for the observed conductivity. However, in electrolyte solutions where such conduction does not occur or is not possible, it is more convenient to define a quantity called the equivalent conductance, Λ , as

$$\Lambda = 1000 \frac{K}{C} \quad (5.1)$$

where C is the concentration in gram equivalents per litre.

The theoretical variation of Λ with concentration is expressed by the Debye-Hückel-Onsager equation,

$$\Lambda = \Lambda_0 - \left[\frac{82.4}{(DT)^{1/2} \eta} + \frac{8.20 \times 10^5}{(DT)^{3/2}} \Lambda_0 \right] \sqrt{C} \quad (5.2)$$

where D is the dielectric constant, η , the viscosity, T , the absolute temperature, and Λ_0 , the equivalent conductance at infinite dilution.

For electrolytes which are only partially ionized in solution, a modified form of the above equation is used. The degree of dissociation can be defined as the fraction of the solute which is dissociated into ions that are free to carry current. The form of the relation is

$$\Lambda = \alpha \left[\Lambda_0 - (A + B\Lambda_0) \sqrt{\alpha C} \right] \quad (5.3)$$

where A and B represent the constants in equation (5.2), and α is the degree of dissociation. For weak electrolytes, the term $\sqrt{\alpha C}$ is small, and thus the correction term, $(A + B\Lambda_0) \sqrt{\alpha C}$, can be neglected relative to Λ_0 . Thus equation (5.3) can be simplified, and an approximate value for the degree of dissociation can be obtained readily from the conductance ratio, i.e.,

$$\alpha = \frac{\lambda}{\lambda_0} \quad (5.4)$$

Greenwood and Martin^(54,55) have developed a method of estimating the degree of ionic dissociation of molten salts by considering conduction to be due to the normal independent migration of ions whose mobility is controlled by their size and charge and by the viscosity of the medium. A distinction is made between ionization, an appreciable charge separation within a molecule, and ionic dissociation, a separation of the molecule into cations and anions which are free to migrate under an applied field. Thus they estimate the extent to which kinetically free ions are formed; the structure of the undissociated form of the complex is not involved, and it may or may not be ionized.

The following derivation applies only when conduction is due to an ionic transport mechanism. In general, the specific conductance, K , and molar conductance, $\mu = MKd^{-1}$, vary exponentially with temperature, i.e.,

$$K = K_0 e^{\frac{-E_K}{RT}} \quad (5.5)$$

$$\mu = \mu_0 e^{\frac{-E_\mu}{RT}} \quad (5.6)$$

where M is the molecular weight, d , the density, and E_K and E_μ the activation energies of ionic migration for the substance, calculated on the basis of 1 ml. and 1 mole respectively.

The viscosity can also be represented by an exponential relation

$$\eta = \eta_0 e^{\frac{E_\eta}{RT}} \quad (5.7)$$

where E_η is the activation energy for viscous flow. Eliminating T from equations (5.5) and (5.7) gives

$$K^m \eta = \text{constant} \quad (5.8)$$

where $m = E_\eta/E_K$. Similarly, from equations (5.6) and (5.7)

$$\mu^{m'} \eta = \text{constant} \quad (5.9)$$

where $m' = E_\eta/E_\mu$.

The following derivation for the degree of dissociation was shown experimentally to be applicable only where m or m' was approximately unity⁽⁵³⁾, and thus

$$\mu \eta = \text{constant} \quad (5.10)$$

This implies that similar processes must be involved in both viscous flow and ionic mobility.

The specific conductivity depends on the number of cations and anions (n_+ , n_-), their mobilities (v_+ , v_-) and the electronic charge, i.e.,

$$K = n_+ e v_+ + n_- e v_- \quad (5.11)$$

For 1:1 electrolyte, the number of cations and anions are equal, and in terms of an average mobility, $v = 1/2(v_+ + v_-)$,

$$K = 2nev \quad (5.12)$$

where n is the number of current carriers of one sign. The number of molecules per ml. is d/M , so that the number of molecules, n_0 , is

$$n_o = \frac{Nd}{M} \quad (5.13)$$

where N is Avogadro's number. From equations (5.12) and (5.13) the ratio of the number of ions of one sign to the total original number of molecules is

$$\frac{n}{n_o} = \frac{MK}{2Ndev} \quad (5.14)$$

For a system which follows equation (5.10), the average mobility in a medium of viscosity η can be related to a standard reference mobility v_o in a medium of unit viscosity (1 cp.) by the relation

$$v = v_o \eta^{-1} \quad (5.15)$$

In a 1:1 electrolyte, the number of ions of one sign equals the number of dissociating molecules, and thus the percent ionic dissociation can be obtained from equations (5.14) and (5.15) as

$$\alpha\% = \frac{100}{n_o} \cdot \frac{n}{v} = \frac{MK\eta}{d} \cdot \frac{100}{2Nev_o} \quad (5.16)$$

In general, values of v_o in any solvent are found to lie in a narrow range. In water, ionic mobilities, except for hydroxyl and hydronium ion, fall in the range 2.5×10^{-4} to 10×10^{-4} cm.² sec.⁻¹ volt⁻¹; thus if the value 5×10^{-4} cm.² sec.⁻¹ volt⁻¹ is used in equation (5.16) for v_o , all mobilities should lie within a factor of 2. Substituting this value for v_o and the values for the other constants in (5.16) gives

$$\alpha\% \approx \mu\eta \quad (5.17)$$

This expression can be used to estimate the degree of ionic dissociation for melts where conduction is due to an ionic transport mechanism.

If only the kinematic viscosity (η_k) is available, then the variation of the density of the compound with temperature is not necessary, and the degree of ionic dissociation can be calculated from

$$\alpha\% = MK\eta_k \quad (5.18)$$

For molten electrolytes where equation (5.10) does not hold, the authors have shown⁽⁵³⁾ that an estimate of the degree of dissociation can be made using the constant in equation (5.9) and the observed value of m' ; thus

$$\alpha\% = \mu^{m'} \eta \quad (5.19)$$

Conductivity of Molten Complexes

The data for the conductivity of the melt for each of the complexes except SeF_4VF_5 and SeF_4BiF_5 is given in Table 5.1. The compound SeF_4VF_5 was not obtained in sufficient quantity, and SeF_4BiF_5 attacks pyrex glass at its melting point.

Fig. 5.1 gives a graphical representation of the data for each compound. From individual graphs of K vs. T , the following values for the specific conductance at the melting point of each compound were obtained:

<u>Compound</u>	<u>M.P. ($^{\circ}\text{C}$)</u>	<u>K ($\text{ohm}^{-1} \text{ cm}^{-1}$)</u>	<u>Expt.</u>
SeF_4SO_3	70.0	6.30×10^{-4}	105
		5.86×10^{-4}	107
SeF_4BF_3	55.2	1.93×10^{-2}	123
		1.46×10^{-2}	134
SeF_4SbF_5	121.5	2.24×10^{-2}	108
		2.18×10^{-2}	110
SeF_4AsF_5	135.0	3.13×10^{-2}	111
		3.25×10^{-2}	117
SeF_4NbF_5	104.0	1.60×10^{-2}	113
		1.58×10^{-2}	115
SeF_4TaF_5	122.0	1.62×10^{-2}	118
		1.61×10^{-2}	120

The variation in the values obtained is probably due to the method of measuring the temperature rather than to any significant difference in the conductivity. The temperature was measured in the air bath, and a

variation of one or two centigrade degrees was observed depending on the position of the thermocouple relative to the cell. Such a variation is sufficient to explain most of the observed change. The larger change observed for SeF_4BF_3 must be significant. The second experiment (Expt. 134) is the more reliable as this experiment used freshly prepared compound. The earlier experiment used a sample of the compound which had been sitting in a Raman tube for several months.

An inspection of the values for $K_{m.p.}$ immediately shows a similarity between the latter five complexes, and an apparent difference for SeF_4SO_3 . This observation is consistent with the nature of these compounds as determined by other techniques.

An attempt can be made to calculate the degree of ionic dissociation using the method of Greenwood and Martin^(54,55). As the available quantity of most of the compounds was limited, viscosity measurements were made only for SeF_4SbF_5 , and these are given below:

<u>Expt. 122</u>	<u>T (°K)</u>	<u>η/d (cp.ml.g.⁻¹)</u>	<u>$K \times 10^2$ (ohm⁻¹ cm.⁻¹)</u>
	413.7	3.288	2.77
	405.2	3.757	2.51
	399.2	3.989	2.32

A plot of $\log \eta/d$ vs. $1/T$ gives a value for $E_{\eta/d} = 1.85$ kcal./mole.

Plotting the conductivity data, $\log K$ vs. $1/T$, gives the value for $E_K = 1.79$ kcal./mole. Hence, the ratio $E_{\eta/d}/E_K = 1.04$ for SeF_4SbF_5 . This is the condition which must hold for the application of equation (5.17) or (5.18).

Using the values of K in the above table (interpolated from Expt. 110) and the molecular weight 371.72 for SeF_4SbF_5 , the degree of dissociation for SeF_4SbF_5 was found from equation (5.18) to vary from 34 - 35% between 126 and 140°C.

As viscosity data for the other complexes is not available, it is necessary to make some assumptions in order to interpret the conductivity data. For the pentafluoride adducts, the sizes of the molecules and their shapes will be essentially the same from one compound to another, and thus only small changes in the viscosity would be expected. Also, for these complexes, the packing of the molecules in the liquid should be essentially the same; hence, the assumption $M = d$ seems reasonable. On the basis of these two assumptions, a value for μ can be obtained for the other complexes from the value known for SeF_4SbF_5 .

$$\text{i.e., Since } \eta_1 \approx \eta_2 \quad (5.19)$$

$$\text{and } \frac{M_1}{d_1} \approx \frac{M_2}{d_2} \quad (5.20)$$

$$\text{then } \mu_1 \approx \mu_2 \quad (5.21)$$

From SeF_4SbF_5 , $\mu = M\eta_k = 1.5 \times 10^3$. Using this value for μ , the following degrees of dissociation are found from the conductivity at the melting point:

SeF_4AsF_5	48%
SeF_4NbF_5	24%
SeF_4TaF_5	24%
SeF_4BF_3	22%
SeF_4SO_3	0.9%

The many approximations necessary to obtain these values raise the question of what meaning they may have. On their own, these values must be considered dubious, but as one piece of evidence in an argument they may have more meaning. This interpretation of the conductivity data shows clearly the close relationship between the pentafluoride adducts and the boron trifluoride adduct, and singles out the SeF_4SO_3 complex as unique in the series. This is in complete accord with the interpretation of the results of other physical measurements.

An interesting calculation can be made for the degree of dissociation in SeF_4 itself. From equation (5.17),

$$\alpha\% = \frac{(154.96)(3.50)}{(2.733)} \times 8.28 \times 10^{-5}$$

$$= 0.0164 \%$$

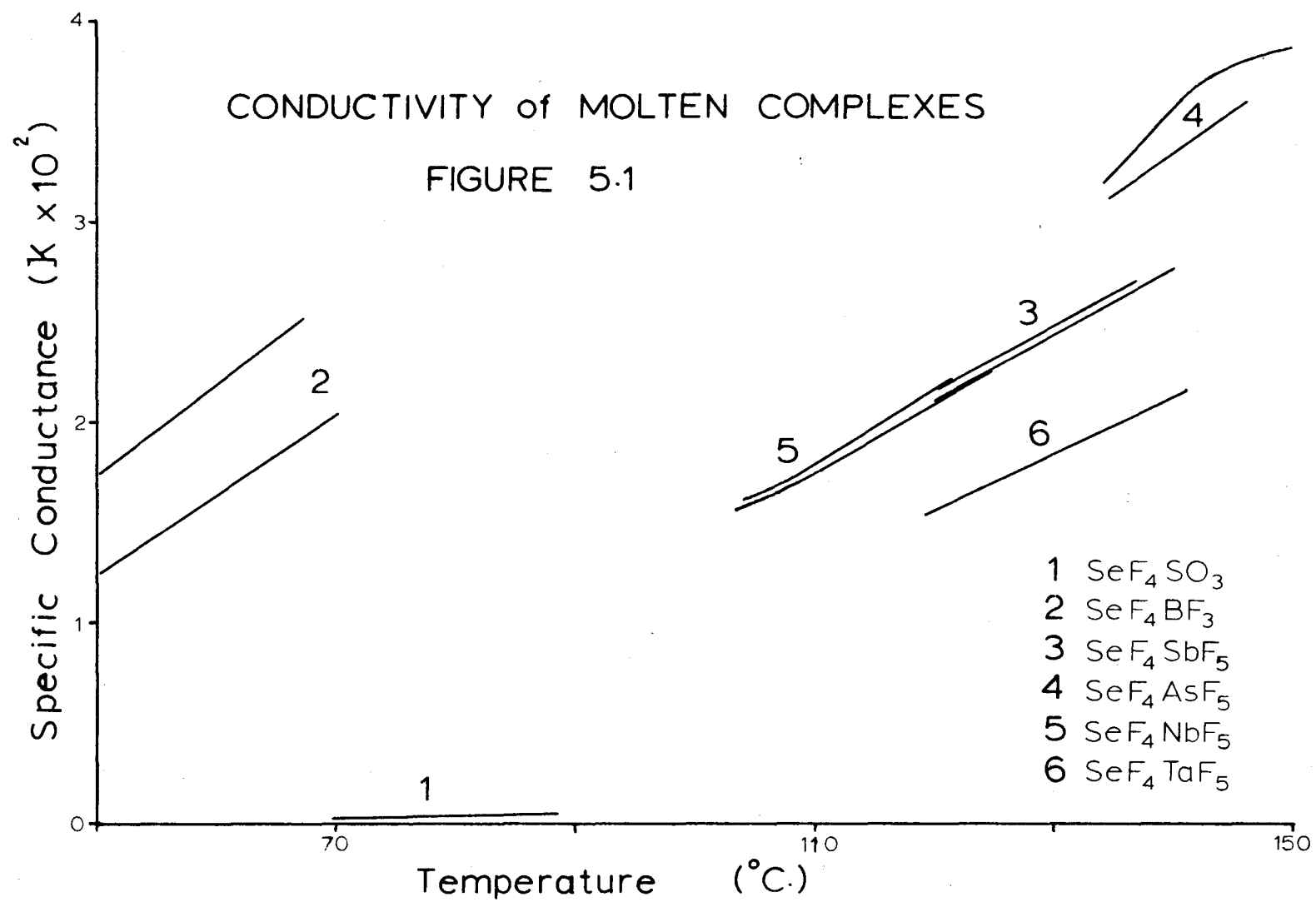


TABLE 5.1

CONDUCTIVITY OF MOLTEN COMPLEXES



	T(°C)	Kx10 ³ (ohm ⁻¹ cm ⁻¹)		T(°C)	Kx10 ³ (ohm ⁻¹ cm ⁻¹)
Expt. 105	88.0	1.23	Expt. 107	81.3	0.946
	85.6	1.17		80.3	0.906
	84.9	1.15		77.0	0.816
	82.3	1.05		72.9	0.675
	79.7	0.950		70.7	0.607
	75.9	0.814			
	74.2	0.765			
	73.3	0.739			
	70.9	0.666			



	T(°C)	Kx10 ² (ohm ⁻¹ cm ⁻¹)		T(°C)	Kx10 ² (ohm ⁻¹ cm ⁻¹)
Expt. 123	68.3	2.40	Expt. 134	69.5	1.997
	67.0	2.525		65.8	1.880
	62.8	2.296		63.2	1.774
	59.3	2.130		59.9	1.638
	57.9	2.055		57.9	1.569
	56.2	1.979		55.4	1.483
	54.9	1.907		53.1	1.380
	53.2	1.834		61.0	1.654
	52.0	1.776			
	49.3	1.658			



	T(°C)	Kx10 ² (ohm ⁻¹ cm ⁻¹)		T(°C)	Kx10 ² (ohm ⁻¹ cm ⁻¹)
Expt. 108	146.5	3.00	Expt. 110	142.0	2.819
	144.3	2.898		138.8	2.719
	136.1	2.675		137.0	2.654
	133.2	2.580		134.5	2.582
	128.6	2.447		132.3	2.518
	125.4	2.355		130.5	2.459
	122.1	2.257		127.5	2.370
	121.4	2.229		123.6	2.247
	119.1	2.163		120.6	2.166
				119.8	2.135

TABLE 5.1, cont'd

SeF₄AsF₅

	T(°C)	Kx10 ² (ohm ⁻¹ cm ⁻¹)		T(°C)	Kx10 ² (ohm ⁻¹ cm ⁻¹)
Expt. 111	146.6	3.618	Expt. 117	149.7	3.856
	145.5	3.567		144.1	3.740
	142.6	3.431		140.7	3.601
	139.6	3.334		137.8	3.452
	134.4	3.109		135.4	3.315
	133.5	2.717		134.0	3.255
	136.3	3.092			

SeF₄NbF₅

	T(°C)	Kx10 ² (ohm ⁻¹ cm ⁻¹)		T(°C)	Kx10 ² (ohm ⁻¹ cm ⁻¹)
Expt. 113	129.8	2.419	Expt. 115	132.8	2.52
	130.7	2.463		127.3	2.347
	122.6	2.257		122.0	2.161
	118.8	2.114		117.3	2.006
	116.1	2.015		115.0	1.919
	112.3	1.880		111.2	1.790
	110.1	1.797		108.3	1.704
	108.0	1.734		106.0	1.635
	105.2	1.640		102.8	1.539

SeF₄TaF₅

	T(°C)	Kx10 ² (ohm ⁻¹ cm ⁻¹)		T(°C)	Kx10 ² (ohm ⁻¹ cm ⁻¹)
Expt. 118	135.2	1.981	Expt. 120	138.3	2.089
	132.9	1.956		136.2	2.032
	130.6	1.884		133.6	1.942
	125.0	1.706		130.1	1.844
	122.7	1.647		126.3	1.733
	119.3	1.551		124.3	1.677
	124.0	1.660		122.8	1.633
	128.6	1.806		120.8	1.579
	140.0	2.143			

SeF₄

Expt. 119	K = 8.28 x 10 ⁻⁵ ohm ⁻¹ cm ⁻¹
-----------	--

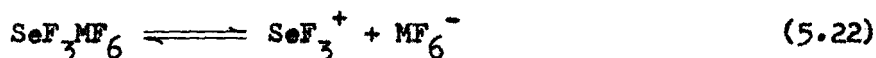
Conductivity Measurements in Nitrobenzene

The conductivity data for each compound in nitrobenzene is given in Table 5.2. Since the density of the solutions is not known, the equivalent conductance, Λ_m , was calculated using the concentration in molal units, rather than the customary molar units. A plot of Λ_m vs. \sqrt{m} is given in Fig. 5.2. An attempt was made to fit the conductivity curves to the modified Onsager equation (equation 5.3) by the method of Fuoss (74), and by successive approximation according to Fuoss and Kraus (75). However, such methods require data at lower concentrations than was available from this work, and thus did not yield reliable values for Λ_0 .

An interpretation of the conductivity data is more readily obtained from a plot of K vs. m as found in Fig. 5.3. For comparison, the data of Van Dyke and Cramford (76) for aluminum chloride in nitrobenzene has also been plotted in Fig. 5.3. From this plot it is apparent that the behaviour of SeF_4SbF_5 , SeF_4AsF_5 , SeF_4TaF_5 and SeF_4NbF_5 differs significantly from that of SeF_4VF_5 , SeF_4BF_3 and SeF_4SO_3 .

The conductance of SeF_4VF_5 and SeF_4BF_3 show approximately the same behaviour as aluminum chloride and must be weak electrolytes in nitrobenzene. The conductance of SeF_4SO_3 lies below that of aluminum chloride at all concentrations, and this compound is essentially unionized in nitrobenzene.

The compounds SeF_4SbF_5 , SeF_4AsF_5 , SeF_4NbF_5 and SeF_4TaF_5 show appreciable ionization in nitrobenzene, and an approximate value of the dissociation constant for each compound can be obtained by assuming that the compounds are completely ionized in dilute solution. The initial slope gives the curve for the completely ionized compound, and this curve can be extrapolated to give the conductance of the ions at a given concentration. If the compound ionizes according to the relation



then

$$K_1 = \frac{[\text{SeF}_3^+][\text{MF}_6^-]}{[\text{SeF}_3\text{MF}_6]} \quad (5.23)$$

It is possible to obtain the concentration of each species in equation (5.23) from the conductivity curves. The concentration of ions is given by the concentration, m_1 , of the theoretical, completely dissociated complex having the same conductance as a concentration, m_s , of the compound itself. The concentration of each ion is then m_1 , and $[\text{SeF}_3\text{MF}_6]$ is $m_s - m_1$, and thus

$$K_1 = \frac{(m_1)^2}{m_s - m_1} \quad (5.24)$$

Using the equation (5.24), the following values for K_1 were obtained:

	at 0.06 m.	at 0.045 m.	at 0.03 m.	α %(0.045 m.)
SeF_4SbF_5	0.083	0.063	0.059	67%
SeF_4AsF_5	0.049	0.045	0.040	62%
SeF_4TaF_5	0.025	0.023	0.021	51%
SeF_4NbF_5	0.011	0.010	0.0099	38%
SeF_4VF_5	11×10^{-4}	8.3×10^{-4}	4.0×10^{-4}	13%
SeF_4BF_3	5.3×10^{-4}	4.3×10^{-4}	2.7×10^{-4}	9%
SeF_4SO_3	9.2×10^{-5}	5.9×10^{-5}	4.5×10^{-5}	4%

The degree of dissociation, α , is given by the ratio m_1/m_s , and by substituting $m_1 = \alpha m_s$ in equation (5.24) the usual expression for K_1 in terms of α is obtained, i.e.,

$$K_1 = \frac{m_s \alpha^2}{1 - \alpha} \quad (5.25)$$

Values of α at 0.045 m. are given in the right-hand column above, and these values for the degree of dissociation verify the qualitative interpretation of the conductivity data. The variation in the dissociation constants with concentration can be attributed to non-ideality in these solutions and to uncertainty in determining the initial slope of the conductivity curves.

The observed differences in the conductimetric behaviour of these compounds in nitrobenzene can be related to the relative ability of the solvent and the accompanying anion to stabilize the SeF_3^+ group. The anions SbF_6^- and AsF_6^- appear least effective for stabilizing the SeF_3^+

group, and stabilization mainly by solvation results in appreciable ionization. The anions NbF_6^- and TaF_6^- must stabilize the SeF_3^+ groups more effectively and can compete with the solvent in this role; thus these compounds are less ionized in nitrobenzene. The compound SeF_4VF_5 is only slightly dissociated in nitrobenzene, and thus the VF_6^- ion must stabilize the SeF_3^+ group more effectively than either NbF_6^- or TaF_6^- . The conductivity behaviour of SeF_4BF_3 is almost that of a weak electrolyte, and thus BF_4^- must be more effective for stabilizing the SeF_3^+ group than the solvent.

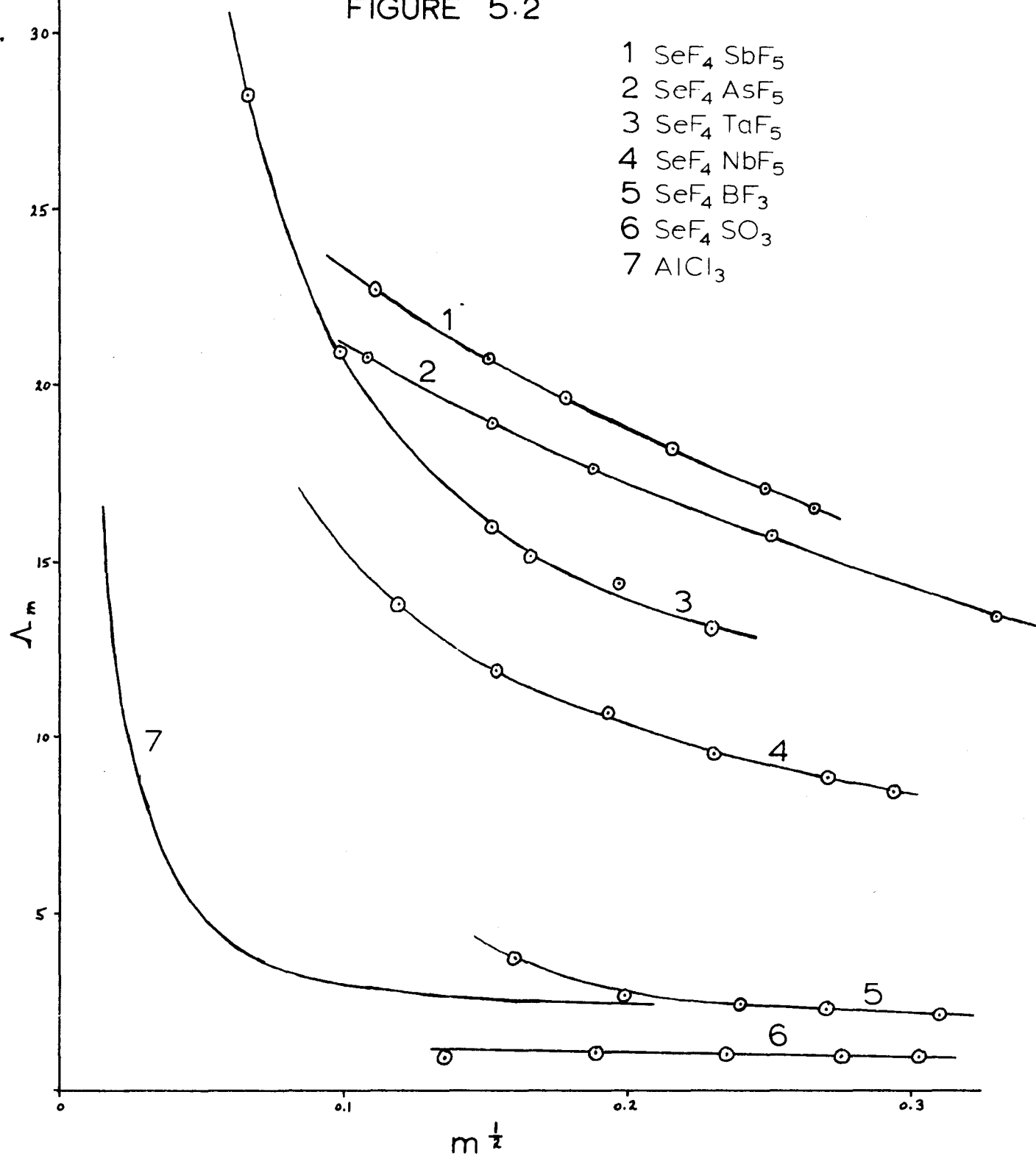
The behaviour of SeF_4SO_3 as a weak electrolyte indicates that the fluorosulfate group is almost entirely associated with the SeF_3^+ group, and only a small fraction of the compound is dissociated into ions.

This interpretation of the conductivity behaviour is supported by the relative stability of the solutions as indicated by the degree of darkening of these solutions. The stability of the solutions decreases in the order $\text{SeF}_4\text{VF}_5 \sim \text{SeF}_4\text{SO}_3 > \text{SeF}_4\text{BF}_3 > \text{SeF}_4\text{NbF}_5 > \text{SeF}_4\text{TaF}_5 > \text{SeF}_4\text{AsF}_5 \sim \text{SeF}_4\text{SbF}_5$, and this order corresponds to the order of decreasing anion stabilization of the SeF_3^+ group as interpreted above. This indicates that the darkening of these solutions is due to some interaction between SeF_3^+ and the solvent, and that the initial decomposition takes place via species formed through such interactions.

Thus the degree of ionization of the compounds depends on the ability of the solvent to compete with the anion to stabilize the SeF_3^+ group. The hexafluoride anions are the least effective in this role and show the greatest ionic behaviour, increasing in the order $\text{WF}_6^- \ll \text{NbF}_6^- < \text{TaF}_6^- < \text{AsF}_6^- < \text{SbF}_6^-$. The tetrafluoroborate ion is a much better stabilizing ion, and the compound is highly associated in solution. These anions probably stabilize the SeF_3^+ group through a fluorine-bridged interaction. The conductivity behaviour of SeF_4SO_3 is consistent with a covalent compound which is only ionized to a small extent in solution.

CONDUCTIVITY in NITROBENZENE

FIGURE 5.2



CONDUCTIVITY in NITROBENZENE

FIGURE 5.3

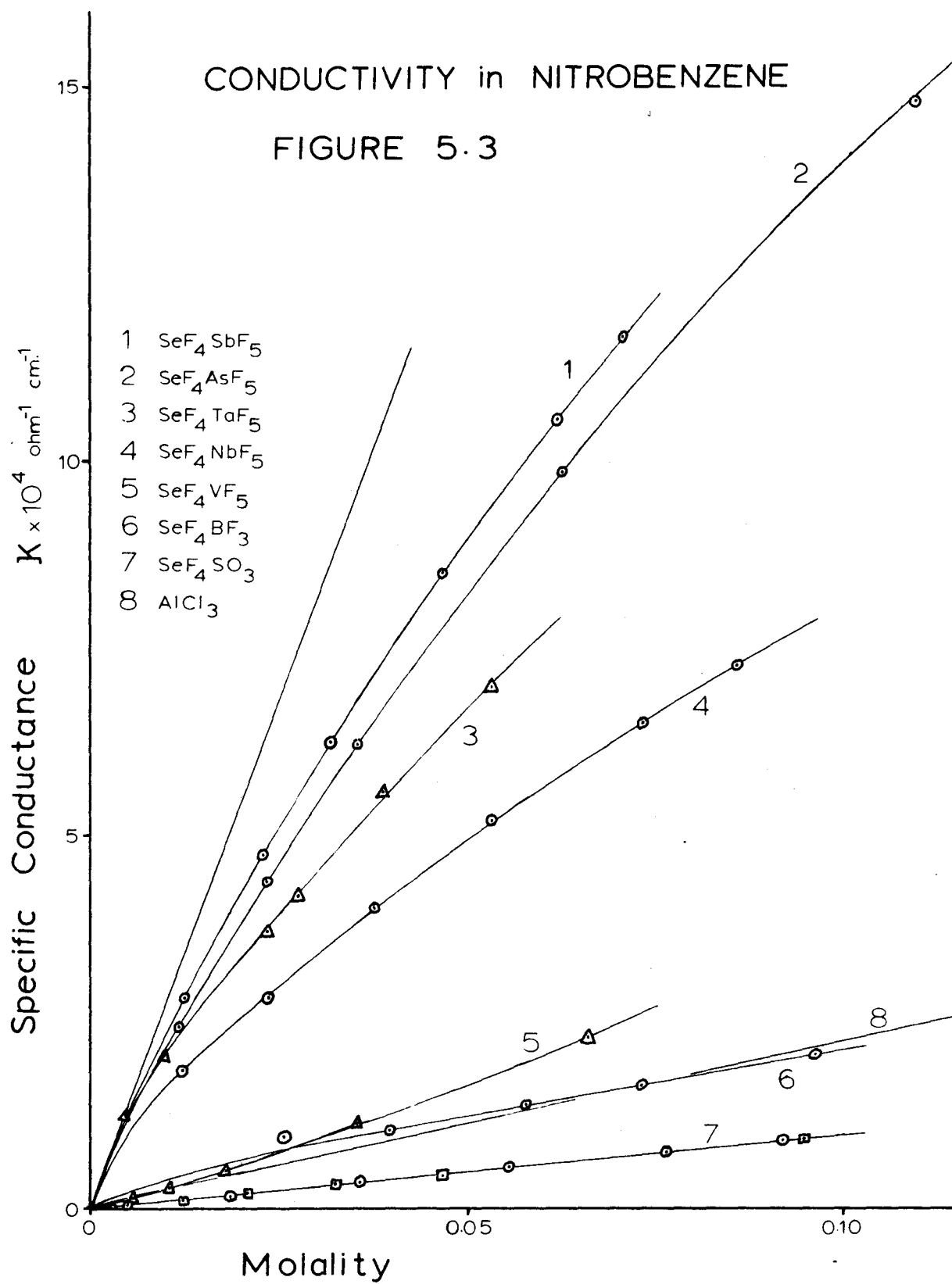


TABLE 5.2

CONDUCTIVITY MEASUREMENTS IN NITROBENZENE

<u>SeF₄SO₃</u>					
$K_o = 8 \times 10^{-8} \text{ ohm}^{-1} \text{ cm}^{-1}$					
Expt. 138	w(g)	m	\sqrt{m}	$K \times 10^5 (\text{ohm}^{-1} \text{ cm}^{-1})$	$\Lambda \text{ m}$
	0.2673	0.01837	0.1355	1.68	0.915
	0.5187	0.03565	0.1888	3.624	1.017
	0.8041	0.05527	0.2351	5.542	1.003
	1.1126	0.07648	0.2765	7.569	0.9897
	1.3376	0.09194	0.3032	9.065	0.9860
Expt. 145		0.09480	0.3079	9.224	0.9720
		0.04672	0.2161	4.587	0.9819
		0.03227	0.1796	3.244	1.006
		0.02066	0.1437	2.164	1.047
		0.01214	0.1102	1.048	0.8634
		0.004888	0.06991	0.522	1.06
		0.002663	0.05161	0.002	0.009
<u>SeF₄BF₃</u>					
$K_o = 2 \times 10^{-7} \text{ ohm}^{-1} \text{ cm}^{-1}$					
Expt. 140	w(g)	m	\sqrt{m}	$K \times 10^4 (\text{ohm}^{-1} \text{ cm}^{-1})$	$\Lambda \text{ m}$
	0.3481	0.02564	0.1601	0.9665	3.770
	0.5379	0.03962	0.1990	1.043	2.633
	0.7852	0.05784	0.2405	1.395	2.412
	0.9930	0.07314	0.2704	1.663	2.274
	1.3087	0.09640	0.3105	2.038	2.114
<u>SeF₄SbF₅</u>					
$K_o = 3 \times 10^{-7} \text{ ohm}^{-1} \text{ cm}^{-1}$					
Expt. 139	w(g)	m	\sqrt{m}	$K \times 10^4 (\text{ohm}^{-1} \text{ cm}^{-1})$	$\Lambda \text{ m}$
	0.2370	0.01236	0.1112	2.814	22.77
	0.4365	0.02277	0.1509	4.722	20.74
	0.6095	0.03180	0.1783	6.233	19.60
	0.8968	0.04678	0.2163	8.500	18.17
	1.1897	0.06206	0.2491	10.57	17.03
	1.3570	0.07079	0.2661	11.66	16.47

TABLE 5.2, cont'd

SeF₄AsF₅

	m	\sqrt{m}	$K \times 10^4 (\text{ohm}^{-1} \text{cm}^{-1})$	Λ_m
Expt. 144	0.1688	0.4108	19.47	11.53
	0.1098	0.3314	14.80	13.48
	0.06276	0.2505	9.864	15.72
	0.03527	0.1878	6.210	17.61
	0.02317	0.1522	4.387	18.93
	0.01162	0.1078	2.421	20.83

SeF₄VF₅

	m	\sqrt{m}	$K \times 10^{-5} (\text{ohm}^{-1} \text{cm}^{-1})$	Λ_m
Expt. 146	0.06594	0.2568	22.96	3.481
	0.03520	0.1876	11.62	3.302
	0.01774	0.1332	5.161	2.909
	0.01030	0.1015	2.984	2.897
	0.005403	0.07351	1.518	2.809
	0.002739	0.05234	0.7428	2.712

SeF₄NbF₅

$$K_o = 3 \times 10^{-7} \text{ ohm}^{-1} \text{cm}^{-1}$$

Expt. 136	w(g)	m	\sqrt{m}	$K \times 10^4 (\text{ohm}^{-1} \text{cm}^{-1})$	Λ_m
	0.2337	0.01415	0.1189	1.850	13.07
	0.3891	0.02356	0.1535	2.805	11.91
	0.6211	0.03761	0.1939	4.013	10.67
	0.8800	0.05329	0.2308	5.187	9.733
	1.2112	0.07335	0.2708	6.491	8.849
	1.4187	0.08592	0.2931	7.250	8.438

SeF₄TaF₅

$$K_o = 3 \times 10^{-7} \text{ ohm}^{-1} \text{cm}^{-1}$$

Expt. 137	w(g)	m	\sqrt{m}	$K \times 10^4 (\text{ohm}^{-1} \text{cm}^{-1})$	Λ_m
	0.0850	0.004429	0.06655	1.252	28.27
	0.1874	0.009764	0.09881	2.050	21.00
	0.4455	0.02321	0.1523	3.709	15.98
	0.5294	0.02758	0.1661	4.188	15.18
	0.7445	0.03879	0.1970	5.591	14.41
	1.0226	0.05328	0.2308	6.977	13.10

Conductivity Measurements in Fluorosulfuric Acid

The conductivity results for SeF_4SO_3 and SeF_4 in fluorosulfuric acid are given in Table 5.3, and a plot of the specific conductance, K , against molality is given in Fig. 5.4. The conductivity of the SeF_4SO_3 solution decreases slowly with time, and the low values of K for the final points in Ex. 37 are likely due to the change in the solution overnight.

Both compounds ionize as bases in fluorosulfuric acid as an addition of potassium fluorosulfate, KSO_3F , at the end of the experiment produced a further increase in conductivity for both compounds.

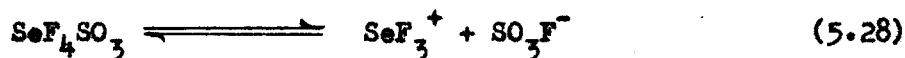
The degree of ionization of a weak base can be found from the ratio of the concentration of the base to that concentration of a fully ionized reference base (eg. KSO_3F) necessary to give the same conductivity as the weak base. This method assumes that the conductivity of the solution is almost entirely due to the self-dissociation ions and that the difference in the mobilities of the two protonated bases can be neglected. For a base, ionizing as in equation (5.26),



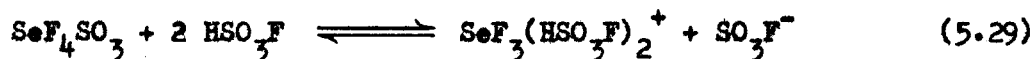
the dissociation constant, K_b , can be calculated from the relation

$$K_b = \frac{[\text{BH}^+][\text{SO}_3\text{F}^-]}{[\text{B}]} = \frac{\alpha^2 m}{1-\alpha} \quad (5.27)$$

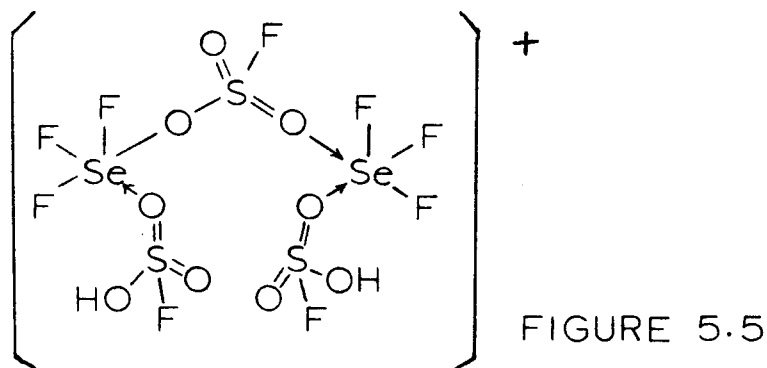
where all concentrations are in molal units. The curve A in Fig. 5.4 corresponds to the conductivity of KSO_3F from Barr, Gillespie and Thompson⁽⁷⁴⁾, and when this curve is used for the reference base, the value of K_b for SeF_4SO_3 increases with concentration. Thus SeF_4SO_3 cannot be ionizing as a simple base according to the equation



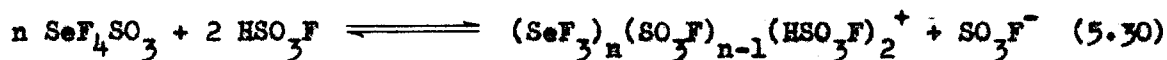
As shown in Chapter III, the SeF_3^+ ion must be solvated in fluorosulfuric acid, and if the solvated ion is written in equation (5.24) we have



The tendency for SeF_4SO_3 to polymerize is indicated by the cryoscopic data in nitrobenzene, and some polymerization might be expected in fluorosulfuric acid. Polymerization of the $\text{SeF}_3(\text{HSO}_3\text{F})_2^+$ ion would involve the formation of a bridging fluorosulfate group in place of two solvating molecules. The dimeric ion would have the structure



For varying degrees of polymerization, the overall reaction can be represented by the equation



For $n=1$, this equation is the same as equation (5.29). It can be seen from equation (5.30) that the extent to which polymers are formed in solution can be obtained from the ratio of the stoichiometric concentration of the compound to the concentration of fluorosulfate ion in solution, i.e.,

$$n = \frac{[\text{SeF}_4\text{SO}_3]_s}{[\text{SO}_3\text{F}^-]} \quad (5.31)$$

The concentration of the fluorosulfate ion at a given concentration of SeF_4SO_3 can be obtained from the concentration of KSO_3F required to give the same conductivity as the solution of SeF_4SO_3 . In this manner, values for n (Table 5.4) at interpolated values of the concentration of SeF_4SO_3 were obtained.

TABLE 5.4

m	n
0.0156	1.66
0.0214	1.69
0.0274	1.65
0.0368	1.58
0.0461	1.61
0.0604	1.65
0.0765	1.72
0.0938	1.80
0.1120	1.87
0.1312	1.94
0.1520	2.01
0.1750	2.09

These values are plotted in Fig. 5.4 using the scale on the right. It is apparent that SeF_4SO_3 is associated to a considerable extent even in dilute solution, and at approximately 0.15 m. it is ionizing in solution principally as the dimeric ion illustrated above.

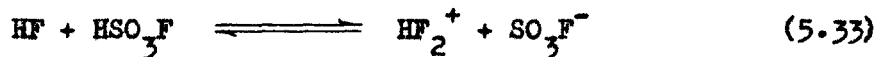
This interpretation of the conductivity of SeF_4SO_3 in fluorosulfuric acid is correct where the $(\text{SeF}_4\text{SO}_3)_n$ species are completely ionized. However, if any of these species is only partially ionized, this will result in higher values for n than expected for the true extent of polymerization in solution (i.e., the true extent of polymerization is less than the value of n would indicate). It is not possible to distinguish between these two effects, but in view of the other properties of SeF_4SO_3 , polymerization in solution is likely the dominant factor.

The conductivity of SeF_4 in fluorosulfuric acid can be interpreted by the reaction



The evolution of hydrogen fluoride gas can be observed from concentrated solutions of SeF_4 in fluorosulfuric acid. The conductivity of the solution increases slowly with time, and the reaction may not proceed immediately to completion; this may be partially responsible for the lower conductivity for SeF_4 than for SeF_4SO_3 observed at higher concentrations.

Hydrogen fluoride ionizes as a weak base in fluorosulfuric acid (74) according to the reaction



However, the ionization of HF in the solution of SeF_4 in HSO_3F should result in a slightly higher specific conductance in HSO_3F for SeF_4 than for SeF_4SO_3 .

The observed deviation of the SeF_4 conductivity curve is likely due to faulty experimental technique. Incomplete mixing of the stock solution of SeF_4 in HSO_3F which was used to add the SeF_4 to the conductivity cell results in a high observed conductance at low concentration and a low conductance at higher concentration, the amount of deviation depending on how poorly the solution was mixed. This explains why the initial specific conductance of the SeF_4 solution is higher than that for the SeF_4SO_3 solution, and this explains the low values at higher concentration.

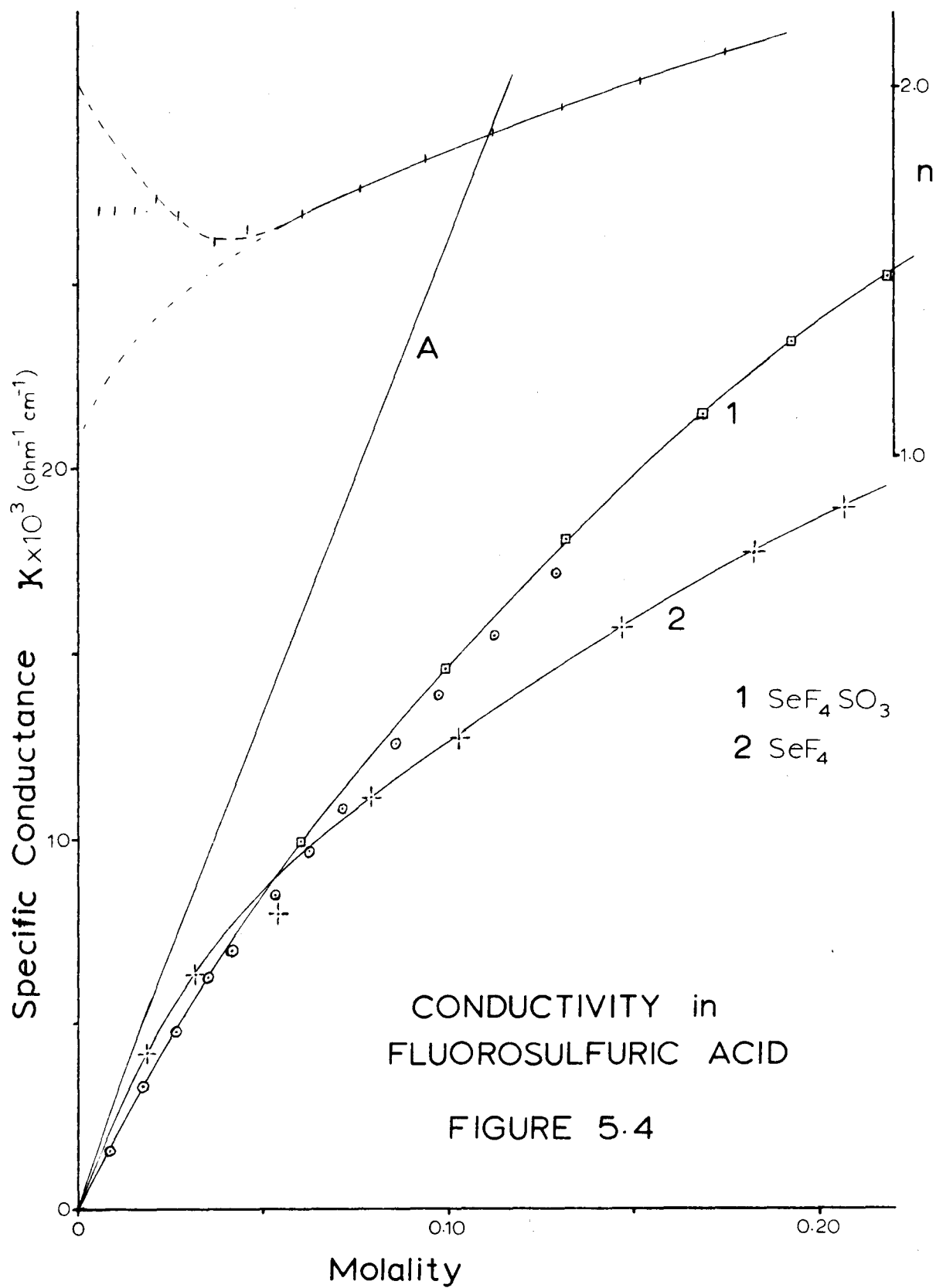


TABLE 5.3

CONDUCTIVITY MEASUREMENTS IN FLUOROSULFURIC ACID

<u>SeF₄SO₃</u>		F.W. = 235.026	
Expt. 36	w(g)	m	K x10 ³ (ohm ⁻¹ cm ⁻¹)
K _o = 2.59x10 ⁻⁴ ohm ⁻¹ cm ⁻¹	1.2974	0.05984	9.913
	2.1400	0.09869	14.58
	2.8603	0.1319	18.06
	3.6608	0.1688	21.42
	4.2734	0.1925	23.40
	4.7401	0.2186	25.18
Expt. 37			
K _o = 1.588x10 ⁻⁴ ohm ⁻¹ cm ⁻¹	0.2109	0.00847	1.565
	0.4333	0.01741	3.254
	0.6515	0.02617	4.773
	0.8732	0.03508	6.214
	1.0372	0.04167	6.961
	1.3174	0.05292	8.452
	1.5462	0.06212	9.653
	1.7706	0.07113	10.81
	2.1241	0.08533	12.53
	2.4111	0.09686	13.85
	2.7908	0.1121	15.45
	3.2153	0.1292	17.16
<u>SeF₄</u>		K x10 ³ (ohm ⁻¹ cm ⁻¹)	
Expt. 13	m		
K _o = 1.112x10 ⁻⁴ ohm ⁻¹ cm ⁻¹	0.01834	4.182	
	0.03148	6.314	
	0.05381	7.985	
	0.07862	11.09	
	0.1026	12.70	
	0.1465	15.69	
	0.1824	17.76	
	0.2068	18.94	

CHAPTER VI

X-ray Powder Diffraction

Theory

A crystalline solid consists of an arrangement of atoms or molecules which are ordered in three dimensions, such that a periodic repetition of a basic unit extended indefinitely in three dimensions produces the structure of the solid. About any one point in such an arrangement, the environment is reproduced exactly at regular intervals along straight lines passing through that point. A selection of any three non-coplanar lines with their identity period describes exactly the periodicity of the structure and defines a lattice for the crystal system. The structure is the arrangement of atoms in space; the lattice is related to the structure, but its origin is arbitrary and is chosen for convenience. It is generally most convenient to choose the three directions with the shortest identity period as the coordinate axes, and these define the unit cell for the crystal; such cells are primitive. In certain cases it is possible to obtain higher symmetry for the unit cell by selection of a non-primitive unit cell, which simplifies the interpretation of the structure.

In a three dimensional lattice, a plane passing through any three non-collinear lattice points passes through an infinite number of lattice points. Such a plane is called a rational plane. The action of lattice

translations on a rational plane generates a family of parallel planes. The perpendicular distance between planes is the only convenient single parameter, and it is just this quantity which is determined directly from X-ray powder diffraction.

The rational planes have intercepts with the coordinate axes which are some multiple or fraction of the translational period. In practice, such planes are referred to by the reciprocal of the intercept along each coordinate axis. If a plane divides the translation distance along the coordinate axes into h , k and l units respectively, then the plane has the designation hkl . The numbers h , k and l are the Miller indices for the particular set of coordinate axes and must be integers because every lattice point has one of the planes passing through it.

As a first approximation, the solid can be considered as an arrangement of similar electric charges at the points of a space lattice. When a beam of X-rays impinges on such an assembly, oscillations of the same frequency as the incident radiation are induced in each point charge such that each becomes a point source of coherent scattered radiation. With regularly spaced point sources interference effects are produced, and scattered radiation is only observed along those directions for which the linear difference in path length from adjacent point sources is an integral number of wavelengths. For an arrangement of points in a space lattice, diffraction of X-rays is only observed when

$$n\lambda = 2d \sin \theta$$

(6.1)

where d is the interplanar spacing, λ , the wavelength of the radiation, θ , the angle between the incident radiation and the rational plane, and n , the order of diffraction. By convention, n is incorporated in the indices of the plane, the n^{th} order diffraction from plane hkl being considered as the first order from the plane nh, nk, nl . Since $d_{nh,nk,nl} = d_{hkl}/n$, equation (6.1) becomes

$$\lambda = 2d \sin \theta \quad (6.2)$$

This equation is known as Bragg's Law.

For a specific wavelength, the direction in which diffraction is observed is determined by the interplanar spacings. This is a property of the lattice and not of the distribution of the atoms in the unit cell. The diffracted waves from different points in the unit cell differ in phase by an amount which is a function of their relative coordinates and of the direction of diffraction. In this manner, the intensities of the reflections depend on the arrangement of atoms within the unit cell.

The unit cell of a crystal often possesses certain symmetry elements such as axes of rotation, reflection planes, a centre of symmetry, and rotation-inversion axes. Crystals can be grouped into seven systems, each having certain minimum symmetry requirements as indicated in Table 6.1.

For the crystal systems with higher symmetry, considerable simplification is observed in the X-ray diffraction pattern, and generally it is possible to determine the crystal system of a substance from the powder diffraction pattern only for the crystal systems of higher symmetry.

TABLE 6.1

System	Lattice constants	Characteristic symmetry
Triclinic	$a \neq b \neq c$ $\alpha \neq \beta \neq \gamma \neq 90^\circ$	1-fold rotation or rotation-inversion axis. No axis of higher symmetry.
Monoclinic	$a \neq b \neq c$ $\alpha = \gamma = 90^\circ \neq \beta$	One 2-fold rotation or rotation-inversion axis. No axes higher than 2-fold.
Orthorhombic	$a \neq b \neq c$ $\alpha = \beta = \gamma = 90^\circ$	Three mutually perpendicular 2-fold axes, any of which can be either rotation or rotation-inversion axes. No axes higher than 2-fold.
Tetragonal	$a = b \neq c$ $\alpha = \beta = \gamma = 90^\circ$	Only one 4 or $\bar{4}$ axis.
Rhombohedral or Trigonal	$a = b = c$ $\alpha = \beta = \gamma \neq 90^\circ$	Only one 3 or $\bar{3}$ axis.
Hexagonal	$a = b \neq c$ $\alpha = \gamma = 90^\circ$ $\beta = 120^\circ$	Only one 6 or $\bar{6}$ axis.
Cubic	$a = b = c$ $\alpha = \beta = \gamma = 90^\circ$	Three 3-fold axes parallel to the body diagonals of the unit cell.

X-ray Powder Diffraction Data

The X-ray powder diffraction data for each complex are given in Table 6.1. The diffraction pattern for SeF_4BiF_5 was not obtained as the background on the film was too dense. The X-ray beam causes fluorescence in SeF_4BF_3 , and it was necessary to place a strip of black paper over the film in the powder camera.

The compounds SeF_4NbF_5 and SeF_4TaF_5 are isomorphous, SeF_4NbF_5 having a slightly smaller unit cell. This deduction is apparent from a visual comparison of the two films. The background on the film obtained from SeF_4NbF_5 is dense, which leads to some uncertainty in the intensity of the lines for this compound.

It was not possible to index any of the diffraction patterns by the usual procedures, and it is likely that all these compounds have unit cells of low symmetry.

TABLE 6.2*

X-Ray Powder Diffraction Data for Complexes*

$\frac{\text{SeF}_4\text{SO}_3}{d(\text{\AA})}$		$\frac{\text{SeF}_4\text{BF}_3}{d(\text{\AA})}$		$\frac{\text{SeF}_4\text{SbF}_5}{d(\text{\AA})}$		
5.007	1.195 (1)	5.413	1.220 (1)	4.500	1.244 (1)	0.8668
3.482	1.161	3.290	1.184	4.362 (1)	1.233	0.8653
2.606	1.140	3.005	1.175 (1)	3.512	1.221 (1)	0.8642
2.544 (2)	1.133	2.613 (9)	1.167	3.425 (3)	1.211	0.8621
2.456 (1)	1.126	2.599 (2)	1.145	3.421 (4)	1.198	0.8589
2.426 (2)	1.111	2.540 (1)	1.127 (1)	2.410 (1)	1.182	0.8498
2.351	1.089	2.442	1.099 (1)	2.491 (1)	1.179	0.8439
2.310 (6)	1.078 (1)	2.236 (9)	1.090 (1)	2.371 (1)	1.149 (1)	0.8227
2.284 (8)	1.064 (1)	2.197 (7)	1.073	2.346 (2)	1.143 (1)	0.8205
2.262 (10)	1.031 (2)	2.095 (2)	1.036	2.251 (2)	1.134 (1)	0.8092
2.196	1.016 (2)	2.063 (4)	1.016	2.218 (10)	1.083	0.8068
1.981 (1)	0.9961	1.953 (10)	0.9877	2.188 (5)	1.080 (1)	0.8028
1.957 (2)	0.9944	1.917 (1)	0.9529	2.164 (1)	1.076	0.7920
1.944 (4)	0.9885	1.899 (1)	0.9444	2.108	1.073	0.7913
1.920 (2)	0.9743 (1)	1.869 (1)	0.9353 (1)	2.054 (2)	1.068 (2)	
1.907 (3)	0.9628	1.807	0.9316 (2)	2.033 (5)	1.056	
1.890 (6)	0.9507	1.744	0.9257	2.018 (4)	1.049	
1.842 (2)	0.9342 (1)	1.673 (3)	0.9154	1.989 (8)	1.036 (1)	
1.814 (7)	0.9314	1.659 (6)	0.9119	1.967 (4)	1.027 (1)	
1.782 (5)	0.9300 (2)	1.625 (2)	0.8972	1.945 (3)	1.020	
1.745	0.9135	1.601 (1)		1.854	1.017	
1.725 (2)	0.9118	1.559		1.822	1.010	
1.641	0.9069 (1)	1.527		1.723	1.007	
1.582	0.8873	1.481		1.707 (3)	1.004	
1.574 (2)	0.8858	1.449		1.656	1.002	
1.561	0.8747	1.423		1.640	0.9992	
1.547	0.8617	1.414 (1)		1.616	0.9974	
1.528 (1)	0.8400	1.399		1.582 (1)	0.9903	
1.512 (4)	0.8368	1.388		1.562 (1)	0.9867	
1.437 (1)	0.8257	1.381 (1)		1.533 (2)	0.9816	
1.409 (4)		1.352		1.517 (1)	0.9779	
1.325		1.341		1.497 (1)	0.9701	
1.312 (5)		1.307		1.465	0.9668 (1)	
1.302 (1)		1.292 (1)		1.449	0.9651 (1)	
1.289 (5)		1.264 (1)		1.357	0.9619	
1.269		1.246		1.343	0.9493	
				1.334 (3)	0.9481	
				1.308	0.9456	
				1.300 (2)	0.9168	
				1.292 (2)	0.8940	
				1.277	0.8921 (1)	
				1.261	0.8897	
				1.255 (1)	0.8868	

*The figures in brackets following the values of d correspond to the relative intensity of the line giving the strongest line a value of 10. Lines with no intensity given have an intensity less than 1 on this scale

TABLE 6.2, cont'd.

SeF_4AsF_5 d(Å)		SeF_4TaF_5 d(Å)		SeF_4NbF_5 d(Å)		SeF_4VF_5 d(Å)	
3.175(2)	1.044(3)	4.536(1)	1.172	0.8759	4.145(1)	4.232(1)	1.137(3)
3.110(3)	0.9923	4.453(1)	1.170	0.8706(4)	3.736(1)	3.311	1.127
2.583(3)	0.9900	3.813	1.150(2)	0.8682(2)	2.931(2)	3.229	1.100(1)
2.552(4)	0.9634(1)	3.259	1.145(2)	0.8650	2.838(1)	2.977(2)	1.091
2.533(4)	0.9611(2)	3.219(1)	1.132(9)	0.8626(1)	2.230(5)	2.871(4)	1.054(1)
2.238(2)	0.9525	3.057(1)	1.111	0.8571(1)	2.180(10)	2.746(1)	1.050(1)
2.217(3)	0.9483(2)	2.683	1.108(1)	0.8560(1)	2.055(3)	2.710(1)	1.032(1)
2.015(7)	0.9238(1)	2.631(1)	1.102(2)	0.8506	2.030(4)	2.479	1.027(1)
1.987(10)	0.9129	2.289(2)	1.096(2)	0.8462	2.012(8)	2.340(1)	1.019(1)
1.848(3)	0.8930(1)	2.266(4)	1.082	0.8416	1.957(5)	2.290(2)	0.9996
1.824(5)	0.8838	2.244(9)	1.078	0.8394	1.927(9)	2.074(3)	0.9933
1.613(1)	0.8776	2.094(1)	1.073	0.8348	1.861(4)	2.035(5)	0.9893(1)
1.593(2)	0.8754	2.061(6)	1.070	0.8328	1.824(3)	2.004(5)	0.9657(2)
1.525(1)	0.8738	2.009(3)	1.061(1)	0.8249	1.807(1)	1.968(10)	0.9618(1)
1.511(2)	0.8695	1.980(10)	1.053	0.8227	1.578(1)	1.871(3)	0.9583(2)
1.450	0.8688	1.934(2)	1.046(1)	0.8218	1.543(3)	1.838(8)	0.9489(1)
1.441(1)	0.8602	1.903(7)	1.041	0.8050	1.411(2)	1.805(2)	0.9425(2)
1.408	0.8465	1.868(5)	1.033	0.8004	1.136(1)	1.753(5)	0.9308
1.390(2)	0.8448	1.841	1.028(1)	0.7995(1)	1.117(9)	1.712(1)	0.9278
1.379(4)	0.8351	1.576(4)	1.011(1)	0.7985	1.087(1)	1.614(2)	0.9249
1.334	0.8321	1.537	1.007(1)	0.7961	1.080(1)	1.533(1)	0.9167
1.326(1)	0.8287	1.528	0.9976	0.7939	0.8577(4)	1.509(2)	0.9141
1.283	0.8234	1.486	0.9954	0.7891		1.502(2)	0.9116
1.242	0.8185	1.455(1)	0.9927(1)	0.7884		1.489(2)	0.9044
1.238	0.8139	1.438(3)	0.9879	0.7865		1.404	0.9001
1.175	0.8093(1)	1.420	0.9808	0.7857		1.396(1)	0.8956
1.168	0.8054	1.405(2)	0.9741	0.7846		1.388(1)	0.8917
1.139	0.7917	1.370	0.9717	0.7822		1.366	0.8705
1.118(1)	0.7841	1.359	0.9674(1)	0.7809		1.283	0.8652
1.116(2)	0.7834	1.351	0.9573	0.7804		1.244	0.8641
1.112(3)	0.7824	1.322	0.9512	0.7799		1.234(1)	0.8357
1.094	0.7717	1.312	0.9477(1)	0.7769		1.219(3)	
1.092		1.303	0.9433(1)			1.207(2)	
1.086(1)		1.291(1)	0.9382			1.202	
1.071		1.278(1)	0.9323			1.186(2)	
1.068		1.268	0.9241			1.179(1)	
1.065(1)		1.253	0.9221			1.161(1)	
1.050		1.238	0.8969			1.156(1)	
1.047(2)		1.219				1.150(2)	

CHAPTER VII

Conclusions

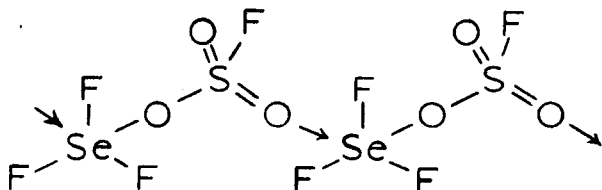
In the preceding chapters, the data from individual physical techniques has been presented with little attempt to show the relationship among the possible interpretations. In this chapter an attempt is made to give a consistent interpretation of all the results for each compound and to summarize the characteristic properties of these selenium tetrafluoride adducts.

SeF₄SO₃

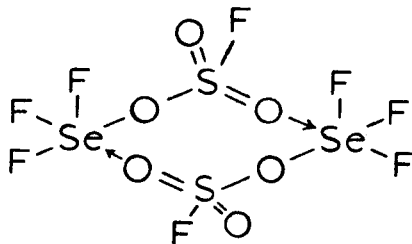
The compound SeF₄SO₃ has vibrational spectra which are consistent with either a covalent, fluorosulfate-bridged polymeric structure or an ionic structure with strong interaction between ions. The properties of the melt are more consistent with a covalent structure; the conductivity of the melt indicates only slight dissociation into ions, and the n.m.r. spectrum is consistent with a covalent polymer. In solution in fluorosulfuric acid, the presence of polymeric ^{solvated} SeF₃⁺ ions (Fig. 5.5) is indicated by the conductivity, and an environment of six electron pairs about the selenium atom in SeF₃⁺ is consistent with the n.m.r. spectrum. (Although a disolvated cation (Fig. 3.1) is the simplest species to provide this environment, polymeric cations, (SeF₃)_nSO₃F_{n-1}(HSO₃F)₂⁺, also have the same environment about the SeF₃⁺ group.) The conductimetric and cryoscopic measurements in nitrobenzene both show considerable polymerization of SeF₄SO₃,

and the cryoscopic results indicate the predominant formation of dimeric species in solution. Thus each of the measurements can be explained by a fluorosulfate-bridged polymeric structure.

The solid probably contains the linear polymers shown below



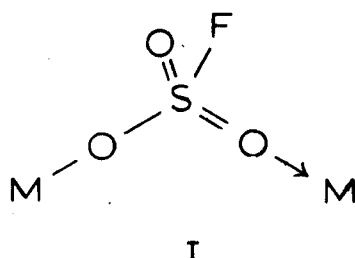
or possibly dimeric molecules, i.e.,



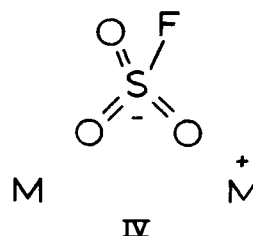
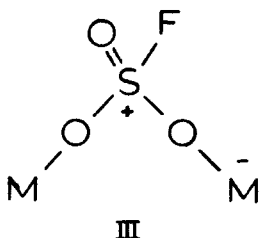
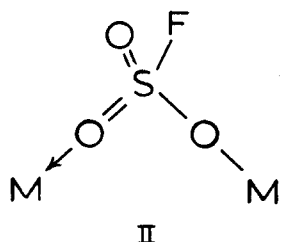
The low melting point suggests that the polymer units are small, which favours the second suggestion above. The vapour pressure of the compound is likely due to the presence of molecular units in the vapour, and sublimation probably proceeds via such species. This postulate is supported by the fact that sublimation occurs without fractionation, and by the infra-red spectrum of the condensed solid. If the vapour were completely dissociated, under the conditions used to obtain the infra-red spectrum, one would expect to see only the spectrum of the dissociation products since recombination should be slow at the temperature of the infra-red window. Thus the presence of molecular units in the vapour, probably dimers, is consistent with the available data.

The Fluorosulfate Bridge

The only other compound known to show fluorosulfate bridging is $\text{SbF}_4\text{SO}_3\text{F}$.⁽⁴⁷⁾ In this compound the bridging fluorosulfate groups complete the six coordination about antimony, and in $\text{SeF}_3\text{SO}_3\text{F}$ six electron pairs surround the selenium atom as a result of the bridging fluorosulfate groups. The valence-bond description of the fluorosulfate bridge involves one coordinate covalent bond and one normal covalent bond, viz.



There will also be some contribution from the following structures:



Structure II is the resonance form of structure I, and resonance between these two forms will result in a plane of symmetry for the bridging group. Structures III and IV also have a plane of symmetry, and thus this description of the bonding requires a symmetrical fluorosulfate bridge when bridging occurs between identical groups. This conclusion is valid only if structure I and II are true resonance forms, and it seems likely

that strong fluorosulfate bridging will satisfy this condition. However, it is possible that the fluorosulfate group is bonded more strongly by the covalent bond, and structures I and II are not true resonance forms. Thus bridging would involve one strong interaction and one weak interaction, and we do not know how strong the coordinate bond must be in order to produce the symmetrical bridge.

The reaction of SO_3 with SeF_4 or SbF_5 replaces the fluorine-bridged interactions in the fluoride with fluorosulfate bridges. This preferential formation of the fluorosulfate bridge shows the greater strength of fluorosulfate bridging over fluorine bridging.

SeF_4SbF_5

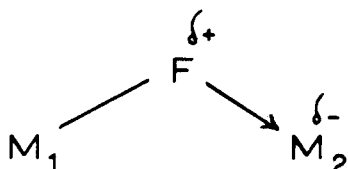
The vibrational spectra and many of the other properties of SeF_4SbF_5 can be interpreted in terms of an ionic structure with strong interaction between the ions. From a detailed examination of these properties, one can evaluate to what extent fluorine bridging is important as a means of interaction between ions. The n.m.r. spectrum gives no definite information, but it is consistent with some fluorine bridging. The conductivity of the melt shows incomplete dissociation into ions, and it seems likely that the incomplete dissociation is due to fluorine-bridged interactions. The conductivities and freezing points of solutions in nitrobenzene are typical of a strong electrolyte at low concentration but indicate significant association at concentrations above ~ 0.03 m. Thus it is reasonable to expect fluorine-bridged interaction between the

ions in this compound, which therefore has a linear, or cyclic, fluorine-bridged polymeric structure (Fig. 2.9). The infra-red frequencies at 908 and 942 cm^{-1} in SeF_4SbF_5 may be a criterion of fluorine-bridged interaction: the greater the intensity of these bands, the stronger the fluorine-bridged interaction between the ions. It seems unlikely that these frequencies are characteristic of the bridging fluorine atoms alone; their origin is more likely $\nu_2(\text{O}_h)$ of the octahedral ion, the degeneracy being removed and the frequency probably shifted by the fluorine bridging. In SeF_4SbF_5 , these frequencies are weak compared with the intensity of the stretching frequencies, and thus the fluorine bridging in SeF_4SbF_5 is probably weak (i.e., the fluorine atoms in such bridges are displaced towards the antimony atom, thereby giving greater ionic character).

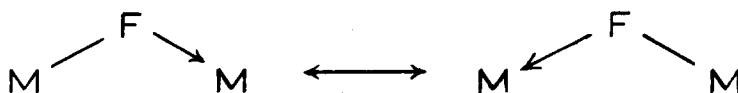
Thus the compound SeF_4SbF_5 has a structure involving fluorine-bridged interactions between SeF_3^+ and SbF_6^- ions, the bridging fluorine atoms being displaced towards the antimony atom.

The Fluorine Bridge

The fluorine bridge involves the donation of a pair of electrons from a bonded fluorine atom to another metal atom, i.e.,



In the extreme case this can be regarded as the formation of two bonds by an F^+ ion. The charge distribution indicates that the electron density about the bridging fluorine atom is lower than that for the same fluorine atom without bridging. In terms of localized molecular orbitals, a molecular orbital can be formed between one p or sp^3 orbital on fluorine and a suitable orbital on M_1 (d^2sp^3), and a second molecular orbital can be formed between a second p or sp^3 orbital on fluorine and a suitable orbital on M_2 . Four molecular orbitals can be formed, two bonding and two anti-bonding. There are four electrons available for these orbitals, one from M_1 or M_2 and three from fluorine, and thus the two bonding orbitals are completely filled. If the metal atoms are identical, and if the overlap of the atomic orbitals is the same in both molecular orbitals, then the bonding must be symmetrical about the bridging fluorine atom. However, it is possible that the interaction is not sufficiently strong, and a more stable bonding results if one of the molecular orbitals is of lower energy than the other (i.e., there is more overlap of the atomic orbitals). Thus an asymmetric fluorine bridge may be observed where the interaction is relatively weak. From a valence-bond approach, one bond is formed by the overlap of a partially filled orbital (d^2sp^3) on M_1 with a partially filled p or sp^3 orbital on the fluorine atom. The second bond is formed between a filled p or sp^3 orbital on fluorine and a vacant d orbital (or suitable hybrid) on M_2 . When the bonding interaction is sufficiently strong, the two resonance forms



are of equal energy, and the bridging fluorine atom must lie in a plane of symmetry between the atoms. However, when the interaction is weak one structure may be more stable than the other, and an asymmetric fluorine bridge which favours the more stable form will give a system of lower energy. Thus it is likely that the fluorine bridge is symmetrical for strong interaction, but as the strength of the fluorine bridge decreases, the asymmetric bridge is more likely to occur.

It may be noted here that fluorine bridging and hydrogen bonding are not analogous. Hydrogen bonding can be described most readily in terms of three-centred molecular orbitals. The hydrogen bonded system in liquid hydrogen fluoride may be used as a typical example. The hydrogen 1s orbital, the fluorine p or sp^3 orbital, and a p or sp^3 orbital from an adjacent fluorine are used to construct three-centred molecular orbitals. Three molecular orbitals can be formed, one bonding, one non-bonding, and one anti-bonding. There are four electrons available to fill these orbitals, and they occupy the bonding and the non-bonding orbitals. The non-bonding orbital makes essentially no contribution to bonding for a symmetrical arrangement of the hydrogen atom, but if the hydrogen atom is displaced towards one of the fluorine atoms, this orbital is lowered in energy resulting in partial bonding. Thus the hydrogen bond tends to be asymmetric, the hydrogen atom displaced towards one fluorine atom in order to lower the total energy of the system. Although the fluorine bridge can be described in terms of three-centred orbitals using one of the 2p orbitals on fluorine, such molecular orbitals are of higher energy than simple localized molecular orbitals. Thus, contrary to the situation with

hydrogen bonding, three-centred molecular orbitals give an unsatisfactory explanation of the bonding in the fluorine bridge, and a simple localized molecular orbital approach can account for both the symmetric and the asymmetric bridge.

The fluorine bridge will in general be asymmetric when bridging occurs between two different metal atoms. In this situation, the fluorine atom may bond more strongly to one atom than to the other (i.e., the fluorine atom has a greater share of one pair of electrons than the other). This is directly analogous to the bonding with relatively weak interaction described above and can be related to the electronegativity of the two metal atoms. The fluorine atom is displaced towards the atom with the greater electronegativity.

Fluorine bridging has only been observed directly for compounds in which both metal atoms are identical. The n.m.r. spectrum of SbF_5 ⁽⁵⁷⁾ shows fluorine bridging in the liquid, and the X-ray crystal structures of MoF_5 ⁽⁷⁸⁾ and RuF_5 ⁽⁷⁹⁾ show that both compounds exist as fluorine-bridged tetramers. In both MoF_5 and RuF_5 , the bridging fluorine atoms were found to be situated symmetrically between the metal atoms. This is the result expected for strong fluorine bridging and supports the description of the bonding given above. There are no well established examples of fluorine bridging between two different metal atoms, although fluorine bridging has been suggested to explain the observed n.m.r. spectrum of AsF_3SbF_5 ⁽⁷¹⁾.

SeF₄AsF₅

The data obtained for SeF₄AsF₅ are consistent with an interpretation similar to that for SeF₄SbF₅. The vibrational spectra for SeF₄AsF₅ can be explained by an ionic model with strong interaction between ions; the infra-red bands at 922 and 953 cm.⁻¹ are somewhat stronger for this compound than the corresponding frequencies for SeF₄SbF₅. The higher conductivity of the melt of SeF₄AsF₅ than that of the melt of SeF₄SbF₅ may be due to the higher melting point of SeF₄AsF₅. Conductimetric and cryoscopic measurements in nitrobenzene show somewhat greater ionic association for SeF₄AsF₅ than for SeF₄SbF₅. The n.m.r. spectrum for SeF₄AsF₅ has one resonance, presumably because there is complete exchange between the fluorine atoms on arsenic and selenium via fluorine-bridged structures. Although this is good indication of fluorine bridging in SeF₄AsF₅, it does not necessarily indicate a faster exchange rate and thus a greater interaction than in SeF₄SbF₅ since the smaller chemical shift between SeF₃⁺ and AsF₆⁻ facilitates collapse of the two expected signals into the single resonance which is observed. This observation which can be attributed to fluorine bridging, combined with the close similarity between SeF₄AsF₅ and SeF₄SbF₅ as indicated by other physical data, supports the conclusion that fluorine bridging is significant in both compounds. Thus the structure of SeF₄AsF₅ is related to that of SeF₄SbF₅, the fluorine bridge being somewhat less asymmetric in SeF₄AsF₅ than in SeF₄SbF₅.

The fact that sublimation occurs without fractionation suggests that the sublimation is proceeding via molecular species rather than by dissociation followed by recombination. If dissociation were the predominant mechanism, one might expect a concentration of the higher boiling component in the sublimate. Also the spectra of the starting compounds are not observed under the conditions used to obtain the infra-red spectrum.

SeF_4BiF_5

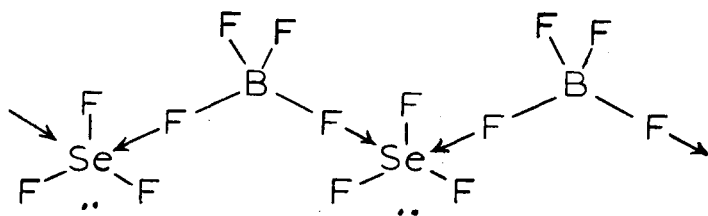
The data obtained for SeF_4BiF_5 indicate a close similarity between SeF_4SbF_5 and SeF_4BiF_5 . The higher temperature necessary to sublime SeF_4BiF_5 indicates greater ionic character, and such an interpretation would result in a gradual increase in ionic character for the sequence $\text{SeF}_4\text{AsF}_5 < \text{SeF}_4\text{SbF}_5 < \text{SeF}_4\text{BiF}_5$. This would be consistent with increasing Lewis acid strength in the order $\text{AsF}_5 < \text{SbF}_5 < \text{BiF}_5$.

SeF_4HF_3

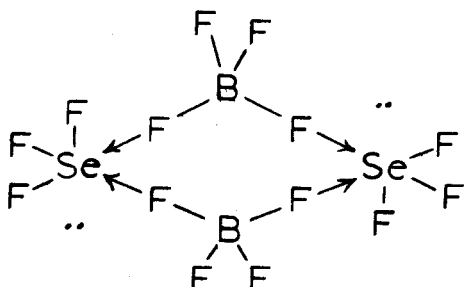
The compound SeF_4HF_3 presents much the same problem for interpretation as SeF_4SbF_5 , the best description of the structure depending on the importance of fluorine-bridged interactions. The vibrational spectra are consistent with an ionic structure with strong interaction between ions, and it is difficult to assess the importance of fluorine bridging from the spectra alone. The n.m.r. spectrum gives strong evidence for fluorine bridging in that only one signal is observed. The chemical shift between SeF_3^+ and HF_4^- is even greater than the shift between

SeF_3^+ and SbF_6^- in SeF_4SbF_5 , and in SeF_4BF_3 the exchange rate is sufficiently rapid to collapse the signals of the two expected resonances. This exchange is likely to occur through fluorine bridged interaction between the ions, and the rapid exchange rate probably indicates a more symmetrical bridge in SeF_4BF_3 than in SeF_4SbF_5 . The conductivity of the melt is higher than would be expected from this interpretation, the calculated dissociation being 22%. The assumption that $\mu_{\text{SeF}_4\text{SbF}_5} = \mu_{\text{SeF}_4\text{BF}_3}$ may not be valid for SeF_4BF_3 , and it may have a lower viscosity than expected from this assumption. Although the origin of this high conductance is not understood, the observed value is not inconsistent with extensive fluorine bridging in the compound. The conductimetric and cryoscopic measurements in nitrobenzene indicate considerable association in solution, and such association is likely to occur by fluorine bridging.

Thus the behaviour of SeF_4BF_3 is consistent with a fluorine-bridged structure which has considerable covalent character, i.e.,



or



Such structures could easily give rise to fluorine-bridged molecular species which would explain the high vapour pressure of the compound. The presence of such species in the vapour is consistent with the fact that no change in composition occurs on sublimation and with the infra-red spectrum of the condensed solid directly after sublimation.

The Group Va Pentafluoride Adducts

As for the group Vb pentafluoride adducts, the addition compounds with the group Va pentafluorides show increasing ionic character with increasing atomic weight of the metal atom. The compound SeF_4VF_5 has a vibrational spectrum which is similar to that for SeF_4SbF_5 . The relative intensity of the lines at 1022 and 962 cm^{-1} is greater in SeF_4VF_5 than that of the lines at 942 and 908 cm^{-1} in SeF_4SbF_5 . As mentioned above, the increased intensity of these lines may indicate strong fluorine-bridged interaction between the ions.

Conductivity measurements in nitrobenzene support this interpretation of the structure, as association of the same order as that for SeF_4BF_3 is observed. Also the high vapour pressure of the compound is another similarity between SeF_4VF_5 and SeF_4BF_3 . Thus it is likely that SeF_4VF_5 has a structure having strong fluorine bridging between ions.

The compounds SeF_4NbF_5 and SeF_4TaF_5 are isostructural as indicated by their X-ray powder patterns, and both compounds show considerably more ionic character than SeF_4VF_5 . As for SeF_4SbF_5 the vibrational spectra can be interpreted on the basis of an ionic model with strong interaction between ions. A moderately strong band is observed at 955 cm^{-1} in

SeF_4TaF_5 , and a somewhat weaker band is observed at 943 cm^{-1} in SeF_4NbF_5 . This would indicate somewhat greater fluorine-bridged interaction for SeF_4TaF_5 . The n.m.r. spectrum of each compound shows only one resonance, which is consistent with some fluorine bridging in these compounds. Also the results of conductimetric and cryoscopic measurements in nitrobenzene indicate some ionic association for these compounds at concentrations higher than $\sim 0.02\text{ m}$. The cryoscopic results show SeF_4TaF_5 to be somewhat less associated than SeF_4NbF_5 , and a similar deduction can be made from the conductivity results. Thus both compounds exhibit considerable ionic character, but fluorine bridging between the ions is fairly strong, the relative importance of fluorine bridging probably being slightly greater in SeF_4NbF_5 than in SeF_4TaF_5 . The infra-red results lead to the opposite conclusion, but this may be a result of the low temperature at which the infra-red data were obtained.

The structures of SeF_4NbF_5 and SeF_4TaF_5 are related to that of SeF_4SbF_5 and involve fluorine-bridged interactions between the ions, the fluorine bridges being somewhat less ionic than in SeF_4SbF_5 .

General Observations

The structures proposed for these compounds are consistent with their chemical properties. The observation that the anion is obtained in solution after hydrolysis has been cited as evidence in support of ionic structures for these compounds.⁽¹⁰⁾ However, initial attack by

water at the SeF_3 group could lead to complete hydrolysis of the SeF_3 group with liberation of the free anion. Thus the proposed structures can explain the observed hydrolysis of the compounds. The vapour pressure of the compounds follows the strength of fluorine bridging in the compounds. The compounds SeF_4BF_3 and SeF_4VF_5 show the highest vapour pressure as well as the strongest fluorine bridging, and the vapour pressure of the other compounds is in the order $\text{SeF}_4\text{NbF}_5 > \text{SeF}_4\text{TaF}_5 \sim \text{SeF}_4\text{AsF}_5 > \text{SeF}_4\text{SbF}_5 \sim \text{SeF}_4\text{BiF}_5$, which parallels the increasing ionic character of the fluorine bridging in these compounds.

Certain structural characteristics can be observed which are common to each of the addition compounds. The anionic species for each compound is either four or six coordinate. The addition compounds are found with strong fluorine ion acceptors, and the favourable four or six coordination is achieved by donation of a fluoride ion from SeF_4 . The extent to which the donation of F^- from SeF_4 is complete varies from one compound to another.

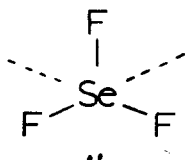
A second observation, and possibly the most significant as far as the stability of the compounds is concerned, is the environment about the SeF_3^+ group. For each compound, the selenium atom is surrounded by six electron pairs, and the ability of the anionic species to provide this stable environment for the SeF_3^+ ion probably is the most significant feature of these structures. The fluorine bridging which is found for each of these compounds is essential to provide the stable environment for the SeF_3^+ ion. This fact may explain the difficulty in isolating the adduct with phosphorus pentafluoride (PF_5). Although PF_5 is a strong

fluoride ion acceptor, the higher electronegativity of the phosphorus may reduce the donor ability of the fluorine atoms in PF_6^- to the extent that they can no longer engage in fluorine-bridged interactions with the SeF_3^+ group which are sufficiently strong to provide stability for the cation.

This necessity to provide the stable pseudo-six-coordinate environment for the SeF_3^+ ion is confirmed by the behaviour of the adducts in solution. As shown by n.m.r. and conductivity measurements in fluorosulfuric acid, SeF_4SO_3 forms polymeric cationic species. The conductimetric and cryoscopic measurements in nitrobenzene can be interpreted to show the extent to which the solvent participates in stabilizing the SeF_3^+ group. The least stable compounds in solution are those where the solvent has the most interaction with the SeF_3^+ ion, and it is likely that it is these solvated SeF_3^+ ions which undergo decomposition.

This instability of the free SeF_3^+ ion is again demonstrated by the Raman spectra of SeF_4SO_3 and SeF_4BF_3 in more strongly coordinating solvents than nitrobenzene, such as dimethylformamide, formamide and nitromethane. These Raman spectra of solutions of SeF_4SO_3 and SeF_4BF_3 indicate clearly the strong interaction between the solvent and the SeF_3^+ ion. In dimethylformamide and formamide, the interaction is such that the characteristic frequencies of the SeF_3^+ group cannot be recognized, and in nitromethane the frequencies observed are consistent with strong interaction with the solvent. Thus it appears that the SeF_3^+ ion cannot exist as a free ion, but it must be stabilized by coordination with neighbouring groups. The

most stable configuration for the SeF_3^+ ion is that given below where the dotted lines indicate some coordination, whether through fluorine bridging or solvation.



Properties of Fluorine Bridging

Since these compounds all show behaviour which has been interpreted in terms of fluorine-bridged interaction between the ions, it should be possible to evaluate the various physical methods and properties for their ability to indicate when such interaction is significant. The infra-red and Raman spectra are of limited value, since the changes in the spectra are the same as for any anion-cation interaction. However, the relative intensity of bands which appear in the range $900\text{--}1050\text{ cm}^{-1}$ in the infra-red indicates the degree of interaction, and such bands are usually strong where fluorine bridging is significant. In the selenium tetrafluoride adducts, the vapour pressure of the compound is a good indication of the importance of fluorine bridging: the stronger the fluorine bridging, the more volatile the compound.

From cryoscopic or conductimetric measurements, the degree of ionic association in solvents with relatively high dielectric constants but with moderate solvating ability, as with nitrobenzene, appears to be

a reliable measure of the importance of fluorine bridging. In such solvents fluorine-bridged interaction can compete with solvation, and the amount of ionic association observed is a measure of the ability of the fluorine bridging to replace solvation. For a series of compounds in the same solvent, this is a good method for evaluating the relative importance of such interaction throughout the series.

In certain cases the n.m.r. spectrum gives strong indication of fluorine bridging. However, it is difficult to obtain any estimate of the asymmetry of the fluorine bridges for a series of compounds because of the changes in chemical shift between the exchanging species. In some cases a single resonance is observed when more than one n.m.r. signal is expected, and this observation can be explained by rapid fluorine exchange because of strong fluorine bridging. For slow exchange rates, the resonance of the bridging fluorine atoms can be observed directly (e.g., in SbF_5). However, for intermediate rates of exchange, no definite information can be obtained from the n.m.r. spectrum.

Measurement of the conductivity of the melt gives no direct evidence for fluorine bridging, but for compounds where fluorine bridging is possible the estimate of the degree of ionization which can be obtained from these results gives some indication of when such interaction may be significant. However, the approximations necessary to interpret these results make a comparison of the strength of fluorine bridging from one compound to another somewhat unreliable.

It is apparent from this discussion of the physical methods that no one method is suitable for detecting fluorine bridging in all compounds.

However, the combination of the indications of fluorine bridging from several physical measurements can lead to a definite conclusion regarding the importance of fluorine bridging in a given compound.

Summary

The compound SeF_4SO_3 has a fluorosulfate-bridged polymeric structure. The remaining compounds exhibit fluorine-bridged interaction between SeF_3^+ and the accompanying anion, such that the SeF_3^+ ion has six electron pairs about selenium. The fluorine bridges become less symmetrical (i.e., more "ionic") in the order $\text{SeF}_4\text{BF}_3 \sim \text{SeF}_4\text{VF}_5 > \text{SeF}_4\text{NbF}_5 > \text{SeF}_4\text{TaF}_5 > \text{SeF}_4\text{AsF}_5 > \text{SeF}_4\text{SbF}_5 \sim \text{SeF}_4\text{BiF}_5$.

The SeF_3^+ ion is only stable when there are six electron pairs surrounding the selenium atom; thus the free SeF_3^+ ion is not found.

Fluorine-bridged interactions can be detected by combinations of the following properties:

- 1) collapse of the expected n.m.r. resonances into a single line, or direct observation of the resonance of the bridging fluorine atoms.
- 2) appreciable ionic association in solvents such as nitromethane or nitrobenzene.
- 3) strong intensity of certain forbidden transitions in the infra-red.
- 4) appreciable ionic association in the molten state where fluorine bridging is a possible source of interaction.

Suggestions for Extension of This Work

Although it has been possible to obtain a description of the structure of these adducts of selenium tetrafluoride, the most complete answer to this problem would be given by a single crystal X-ray analysis. Such an approach would be interesting in view of the probability of fluorine bridging in these compounds. The most promising method to obtain single crystals would be vacuum sublimation, and a second possibility might be to grow the crystals from nitromethane if the solution could be kept cold enough to prevent decomposition.

It has been suggested that these addition compounds exist as molecular units in the vapour phase, rather than being completely dissociated. It should be possible to test this postulate by studying the infra-red spectrum of the vapour using a multiple reflection cell to increase the path length, and working at a sufficiently high temperature to ensure an adequate vapour pressure.

An investigation of the conductivity and freezing point depression of these compounds in nitromethane would complement the Raman spectral measurements in nitromethane, and the measurements we have obtained in nitrobenzene. Also, nuclear magnetic resonance spectra of the nitrobenzene and nitromethane solutions might give some further information about these compounds.

Finally, the techniques we have described could be applied to study the structures of other known adducts of selenium tetrafluoride. The preparation of further selenium tetrafluoride adducts could be attempted

by reacting SeF_4 with other strong fluoride ion acceptors which might be capable of stabilizing the SeF_3^+ ion. Such compounds as beryllium difluoride and aluminum trifluoride may form compounds, and the other transition metal pentafluorides, such as CrF_5 , MoF_5 , MnF_5 , and ReF_5 , are further possibilities.

CHAPTER VIII

Preparation and Purification of Materialsa) General Procedures

Kel-F 90 grease (Minnesota Mining and Manufacturing Co.) was used to grease all ground glass joints. Fluorolube grease (Hooker Chemical Corp.) was also used during the earlier part of the work.

Before use, all glass apparatus was cleaned in sulfuric acid - potassium dichromate cleaning solution, rinsed thoroughly with tap water and with distilled water, and dried overnight in an oven at 110°C.

Larger vacuum line assemblies were cleaned by boiling concentrated nitric acid in them until all surfaces of the assembly had been in contact with the hot acid. The apparatus was rinsed as well as possible with distilled water only, and dried overnight in the oven. Generally drying was completed by heating the line with a bunsen burner under vacuum.

Volatile materials were handled on a vacuum line equipped with an oil diffusion pump. The vacuum line had two liquid air traps before the diffusion pump to prevent volatile products from the preparative section of the line from entering the pump.

Manipulation of the compounds in the line was accomplished using liquid air unless otherwise indicated.

b) Purification of Materials

Nitrobenzene

Reagent grade nitrobenzene (Eastern Chemical Corp.) was distilled through a two-foot heated column of glass helices, and the product collected after a steady temperature was reached at the head of the column. The product was stored over a molecular sieve (Type 4A, Linde Company) to remove any traces of water.

1,3,5-Trinitrobenzene

Commercial trinitrobenzene (Eastman Kodak) was recrystallized from glacial acetic acid. The crystals were filtered and washed with small portions of cold glacial acetic acid, then stored over phosphorus pentoxide in a vacuum desiccator until used. The product had a melting point of 123.8 - 125.0°C (uncorr.).

Fluorosulfuric Acid

Technical fluorosulfuric acid (Allied Chemical) was distilled twice in all glass apparatus out of contact with the air. The low boiling fraction from the first distillation was collected in a tube, and, when the distillation temperature reached 152°C, the distillate was directed into the pot of the second distillation apparatus. A similar procedure was followed with the second distillation, the fraction boiling between 152-153°C being used. All ground glass joints which could come in contact with the hot acid were kept free of grease.

Nitromethane

Commercial nitromethane (Fisher Reagent) was redistilled through a fractionating column of glass helices. The product was stored in a flask with an ungreased ground glass stopper.

N, N-dimethylformamide

Commercial dimethylformamide (Fisher Reagent) was distilled through a heated fractionating column of glass helices, and the fraction boiling between 150.6 - 151.2°C was collected. The compound was stored in a flask with an ungreased ground glass stopper.

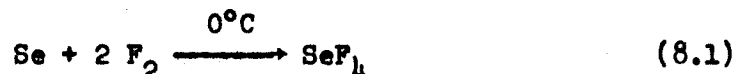
Formamide

Commercial formamide (Fisher Reagent) was used directly without further purification.

c) Preparation of Compounds

Selenium Tetrafluoride

Selenium tetrafluoride was prepared by the reaction



according to the procedure given by Dodd and Robinson⁽⁴⁾.

Selenium metal (30 g.)(Analar - pellets) was placed in the flask of the apparatus shown in Fig. 8.1; the system was attached to the fluorine line (Fig. 8.2) and evacuated. The system was dried for at least two days and heated periodically with a bunsen flame during this time.

After drying the apparatus, the selenium was sublimed onto the walls of the flask. A hole three inches in diameter was cut in an asbestos mat, and this was held beneath the flask so that the upper portion of the flask was protected from the flame. The upper part of the flask was wrapped with wet kleenex, and the selenium sublimed by heating the bottom of the flask with a steady flame. The kleenex was kept damp throughout the sublimation to prevent the selenium from converting to the gray form. The line was then brought to atmospheric pressure by cautiously filling with nitrogen. The receiver for the product was kept evacuated. Once the line was at atmospheric pressure, the nitrogen flow was adjusted at the inlet valve to give a flow of approximately 100 ml./min. During this time, the main flask was surrounded with an ice bath, and a dry ice - acetone bath was placed on the trap. When the nitrogen flow was steady, the fluorine cylinder was opened and the flow adjusted at the needle valve (Fig. 8.2,A)

until the flow rate was approximately twice that of the nitrogen alone (i.e., a dilution of $F_2:N_2 :: 1:1$). The reaction was continued, the ice bath being replenished as necessary, until most of the selenium had reacted (4 - 8 hr.). The fluorine flow was then stopped, and the line flushed with nitrogen for one hour.

The system was evacuated, and the selenium tetrafluoride remaining in the flask was distilled into the trap. The selenium tetrafluoride was distilled from the trap into the receiver (Fig. 8.1,B); then the receiver was sealed off at A.

The selenium tetrafluoride was stored at dry ice temperature until used, and was redistilled immediately before use.

Trifluoroselenium (IV) fluorosulfate

The vacuum manifold shown in Fig. 8.3,A was used. The reaction flask (Fig. 8.3,B), the B19 opening closed with a B19 cap, was placed on the centre position of the manifold. The flask for the sulfur trioxide (Fig. 8.3,D) was placed on one end, and the receiver of selenium tetrafluoride on the other. The receiver of SeF_4 was joined by glass blowing to the adaptor (Fig. 8.4,A) which held two nickel balls in the side arm to break the break-seal above the SeF_4 . The system was evacuated and, with the exception of the flask containing SO_3 , was dried by flaming with a bunsen burner.

The sulfur trioxide was obtained from 65% oleum (Allied Chemical) or from Sulfan B (Allied Chemical) by distillation into the reaction flask under reduced pressure. The flask in Fig. 8.3,D was used to prevent liquid

splashing into the manifold. Excess selenium tetrafluoride was then distilled onto the sulfur trioxide.

The reaction flask was removed from the manifold and immersed in an ice bath. As the selenium tetrafluoride became liquid, reaction started and heat was produced. At 0°C the reaction remained under control, but pressure could develop in the flask at higher temperatures. Once the violent reaction had subsided, the flask was warmed with hot water from the tap (50°C) until the solution was completely clear.

The flask was again placed on the manifold, and the excess selenium tetrafluoride distilled into a dried receiver (Fig. 8.4,B). The bulk of the excess selenium tetrafluoride was removed in this way, the receiver sealed off at A (Fig. 8.4,B), and the selenium tetrafluoride stored for future use.

The remaining selenium tetrafluoride was distilled directly into the traps of the vacuum line. Periodically, the reaction flask was removed from the manifold and shaken to break up lumps in the product. The flask was kept evacuated until the product was a free flowing powder. The reaction flask was then placed in the dry box, and the product transferred to dried tubes which were sealed off under vacuum.

The product was a fine white crystalline powder (m.p. 69.0 - 70.0°C) and could be used without further purification. After handling several times or on standing in the tubes for long periods, the product turned pale yellow and had a "wet" appearance. The compound could be purified by sublimation under vacuum in the apparatus shown in Fig. 8.5, using a heating

bath at 70 - 80°C and circulating cold water through the cold finger. The sublimed material was a white crystalline solid. The yellow product was left at the bottom of the sublimmer.

Trifluoroselenium (IV) tetrafluoroborate

The vacuum manifold (Fig. 8.3,A) was used. The reaction flask (Fig. 8.3,B) was attached at the end position. A bubble tube (Fig. 8.3,C) was inserted through the B19 joint, and this was connected to the boron trifluoride, BF_3 , cylinder with Teflon tubing. The Teflon tubing was heated carefully in a flame until clear, then pushed over the glass tubing which had a ring of Kel-F grease on it. In this manner, vacuum tight seals were readily obtained. A similar procedure was used to attach the tubing to the cylinder.

The container of SeF_4 was joined by glass blowing to the adaptor (Fig. 8.4,A) which held nickel balls in the side arm to break the break-seal above the SeF_4 . This assembly and a receiver (Fig. 8.4,B) were placed on the other two positions of the manifold. The system was evacuated and dried by periodic heating with a bunsen burner.

Selenium tetrafluoride was distilled into the reaction flask. The SeF_4 was allowed to warm to room temperature; then boron trifluoride (Matheson Co. Inc.) was bubbled slowly through the liquid in the flask. It was found that the best conversion was obtained when the reaction was allowed to proceed at its own temperature. The flask was only cooled with cold water when the temperature rose so much that SeF_4 was swept out in the gas stream.

Initially, the BF_3 was bubbled in with the system closed, but as soon as a slight pressure developed, the BF_3 was vented into the fume hood through a drying tube. Boron trifluoride was bubbled for approximately thirty minutes after atmospheric pressure had been attained, or approximately ten minutes after the first solid started to separate out of the solution. Then the bubble tube was sealed off at B (Fig. 8.3,C).

After reevacuating the reaction flask, any excess SeF_4 was distilled into the receiver. The complex is sufficiently volatile that under these same conditions it also sublimes to some extent. Periodically, the reaction flask was removed and shaken to break up any lumps in the product. Finally, the solid was opened directly to the vacuum system for a few minutes. The reaction flask was placed in the dry box, and the product transferred to dried tubes which were sealed off under vacuum. The product was a fine white crystalline solid (m.p. $54.0 - 55.3^\circ\text{C}$), and was used directly.

On handling, the compound gradually turned pale yellow. It could be purified again by sublimation under vacuum using the apparatus shown in Fig. 8.5. The sublimation proceeded rapidly at room temperature with ice placed in the cold finger.

Trifluoroselenium (IV) hexafluoroarsenate

The same apparatus was used as in the preparation of trifluoroselenium (IV) tetrafluoroborate. The cylinder of arsenic pentafluoride (Ozark-Mahoning) was connected via a piece of Teflon tubing as described above. The AsF_5 was used without further purification.

The system was dried under vacuum by flaming with a bunsen burner. Selenium tetrafluoride was distilled into the reaction flask. The flask was cooled with ice, and AsF_5 was bubbled through the SeF_4 . The excess AsF_5 was allowed to escape into the fume hood through a tube of P_2O_5 on glass wool. After the reaction mixture turned solid, the flow of AsF_5 was reduced and continued at the slower rate for another ten minutes. The bubble tube was then sealed off at B (Fig. 8.3,C).

After reevacuating the reaction flask, any excess SeF_4 was distilled into the receiver. The reaction flask was removed periodically and shaken to break up the lumps in the product. Finally, the product was opened to a vacuum directly to remove the last traces of SeF_4 . The reaction flask was placed in the dry box, and the product transferred to dried tubes which were sealed off under vacuum. The product was a fine white powder and was used directly.

After handling a number of times, the compound gradually assumed a pale yellow colour. The compound could be purified again by sublimation under vacuum using the apparatus shown in Fig. 8.5. The sublimation proceeded readily with a heating bath at $50 - 60^\circ\text{C}$ and cold water circulating through the cold finger.

The compound melted at 135°C with dissociation.

Trifluoroselenium (IV) hexafluoroantimonate

The same apparatus was used as in the preparation of trifluoroselenium (IV) fluorosulfate. Commercial antimony pentafluoride (Allied Chemical) was distilled twice in all glass apparatus; the fraction boiling

between 140-142°C was collected and distilled into the reaction flask under vacuum.

Excess SeF_4 was distilled onto the SbF_5 . The reaction flask was removed from the line and immersed in a bath of crushed ice. When the selenium tetrafluoride was liquid, the exothermic reaction began. The flask was swirled to bring all the SbF_5 into contact with the SeF_4 . After the bulk of the reaction was complete, the flask was warmed to approximately 50°C until all the solid went into solution, leaving a clear colourless liquid.

The flask was reevacuated, and the excess SeF_4 distilled into a dried receiver (Fig. 8.4,B) placed where the SeF_4 sample had been previously. The solid product was then opened to the vacuum system directly to remove the last traces of SeF_4 .

The product was a fine white powder (m.p. 120.5-121.5°C) and was used without further purification.

Trifluoroselenium (IV) hexafluoroniobate and Trifluoroselenium (IV) hexafluorotantalate

The vacuum line used for the preparation of these compounds is shown in Fig. 8.6. Commercial niobium and tantalum pentafluorides (Ozark-Mahoning) were transferred in a dry box to the tube shown in Fig. 8.6,B. The pentafluoride was introduced into the vacuum system at A, the transfer being performed under a large inverted funnel through which a stream of nitrogen was flowing. The system was sealed off immediately at 'a' and evacuated. The vacuum line was then dried by heating with a flame.

The end trap was wound with heating tape, and the pentafluoride was sublimed into the reaction flask, C, by gradually increasing the temperature from 90°C to 140°C. The line was sealed off at 'b'.

Selenium tetrafluoride was distilled into the reaction vessel, and was allowed to warm to room temperature. No violent reaction was observed, and it was necessary to warm the vessel to 40°C to dissolve the pentafluoride in the excess SeF_4 . Then the excess SeF_4 was distilled off into the trap leaving a grayish-white solid. The system was sealed off at 'c' and 'd'.

In the dry box, the solid was transferred to the sublimation apparatus (Fig. 8.5). The niobium compound sublimed readily at 55°C, and the tantalum compound at 70°C. Both compounds were white solids. The melting point of trifluoroselenium (IV) hexafluoroniobate was 102.8-104.3°C, and that of trifluoroselenium (IV) hexafluorotantalate was 122.6-123.6°C.

Trifluoroselenium (IV) hexafluorobismuthate(V)

1) Preparation of bismuth (III) fluoride

Bismuth trifluoride was prepared according to the method of Brauer⁽⁸¹⁾.

In a 150 ml. beaker, 8.5 g. bismuth (III) oxide were dissolved in a minimum amount of concentrated hydrochloric acid and filtered to remove foreign particles. Then concentrated ammonia was added to bring down bismuth (III) hydroxide, which was filtered and washed with water. The

bismuth (III) hydroxide was transferred to a platinum evaporating dish, and evaporated to dryness with 45% hydrofluoric acid. This process was repeated three times to ensure complete conversion to the fluoride. The product was then heated to drive off the excess hydrogen fluoride.

2) Preparation of bismuth (V) fluoride

Bismuth (V) fluoride was prepared from bismuth (III) fluoride by reaction with fluorine at 500°C. (82)

A nickel boat containing BiF_3 was placed inside the monel tube shown in Fig. 8.7. The system was evacuated and dried by periodic flaming with a bunsen burner. The monel tube was heated under vacuum at 200°C overnight.

The line was brought up to atmospheric pressure by letting nitrogen into the line. The nitrogen flow was regulated to approximately 100 ml./hr., and the fluorine flow adjusted to give approximately 1:1 dilution with nitrogen. The temperature of the tube furnace was then raised to 500°C. The first product appeared around 450°C. The product was a white crystalline solid which condensed in the cool portion of the monel tube. It was found preferable to tip the product from the tube into the glass system rather than to transfer it by distillation, since the high temperature necessary lead to some decomposition.

3) Preparation of the adduct

Once the bismuth (V) fluoride was in the end trap, the system was sealed off at 'a' (Fig. 8.7). Selenium tetrafluoride was distilled onto

the product. The mixture was allowed to come to room temperature, and, to ensure complete reaction, was warmed with hot water (50°C). The excess selenium tetrafluoride was distilled off into trap B, and the system sealed off at 'b', 'c' and 'd'.

The trap containing the white product was opened in the dry box, and the contents transferred to the sublimation apparatus (Fig. 8.5). With cold water circulating through the cold finger, the first sublimation started around 100°C , and the sublimation proceeded rapidly with a bath at 110°C .

The product was a white solid. In a sealed melting point capillary, the compound attacked the glass and decomposed. The first melting was around 90°C and melting continued to 105°C leaving a cloudy liquid. The bulk melted between $91-94^{\circ}\text{C}$.

Trifluoroselenium (IV) hexafluorovanadate

The vacuum line used for this preparation is shown in Fig. 8.9. The system was attached to the cylinder of vanadium pentafluoride (Ozark-Mahoning) by a Teflon seal as described in the preparation of trifluoroselenium (IV) tetrafluoroborate. Dried sodium fluoride or potassium fluoride was placed in the end trap, A.

The vanadium pentafluoride was distilled onto the alkali fluoride in the end trap cooled in a dry ice-acetone bath. The line was sealed off at 'a'.

The vanadium pentafluoride was distilled off the alkali fluoride into the reaction flask, B. The intervening trap was to catch any alkali fluoride which was carried along in the distilling vapours. The line was sealed off at 'b'.

Selenium tetrafluoride was distilled onto the vanadium pentafluoride, leaving the vanadium pentafluoride in excess. The reaction flask was warmed to room temperature and then to 40°C to liquify the mixture. The excess VF_5 was distilled off into the trap, leaving a white powder behind. The system was sealed off at 'd', 'e' and 'f'.

The compound was an extremely hygroscopic white powder. In a sealed capillary, melting occurred at $112\text{--}114^{\circ}\text{C}$, and the compound boiled at 120°C .

Trifluoroseelenium (IV) hexafluorophosphate

We were unable to obtain any appreciable amount of this compound although several methods of preparation were attempted. Phosphorus pentafluoride (Ozark-Mahoning) was used directly after passage through a dry ice trap to remove higher boiling impurities.

Bubbling phosphorus pentafluoride through liquid selenium tetrafluoride, even at 55°C , gave no apparent reaction. Removal of the selenium tetrafluoride left only a trace of white solid.

Condensation of 8.2 g. phosphorus pentafluoride with 9.3 g. selenium tetrafluoride in a stainless steel bomb of 30 ml. volume and heating the bomb at 95°C overnight gave little evidence of reaction. No volatile products

other than PF_5 and SeF_4 were detected. After removal of all volatile substances, the bomb increased in weight by 0.5 g. On opening the cylinder, a white solid was removed which fumed in moist air, and which on hydrolysis gave a positive test for selenium and a precipitate with nitron (PF_6^-).

It is likely that under the correct reaction conditions selenium tetrafluoride will combine with phosphorus pentafluoride. However, considering the instability of the arsenic pentafluoride compound, it is possible that the phosphorus pentafluoride compound is not stable at room temperature.

Analyses of Compounds

Selenium: Selenium was determined as the metal by reduction with hydroxylamine hydrochloride in slightly basic solution. The precipitate was digested at 80°C for one hour. It was then filtered, washed with water dried at 110°C for one hour, and weighed as selenium metal.

In SeF_4VF_5 , the reduction was accomplished with Na_2SO_3 in strong HCl .

Fluoride: In all cases, a fluoride separation was made by distillation as hydrofluorosilicic acid using perchloric acid (Scott, p.408⁽⁸³⁾). The fluoride was determined gravimetrically as PbClF according to Scott p.406.⁽⁸³⁾

Sulfate: Sulfur trioxide in SeF_4SO_3 was determined on the filtrate after the selenium determination. The filtrate was evaporated to dryness several times with concentrated HCl to remove the fluoride. The residue was dissolved in a little dilute HCl and filtered to remove any silica. Sulfate was precipitated as BaSO_4 from a hot solution and digested for one hour at $90\text{--}100^{\circ}\text{C}$. The precipitate was filtered on a glass filter crucible, washed with hot water, ethanol and a small quantity of ether, dried at 110°C and weighed as BaSO_4 .

Boron: Boron was determined as nitron tetrafluoroborate according to Vogel, p.578.⁽⁸⁴⁾ This method gives some difficulty with a gelatinous precipitate, and large quantities of wash water are necessary to remove the gelatinous material.

Antimony: This was determined using the method of Scott, p.76.⁽⁸³⁾

After the reduction, antimony was determined by titration with standard potassium permanganate. The end point was obscured somewhat by the yellow-brown colour of the solution, and this leads to some uncertainty in the final value.

Arsenic: Arsenic was determined according to Vogel, p.367.⁽⁸⁴⁾

The analysis was performed on the filtrate from the selenium analysis. The method involves the titration of iodine, liberated by the addition of an excess of potassium iodide, with standard thiosulfate.

Vanadium: Vanadium was determined by titration with standard permanganate. (Scott p.1038⁽⁸³⁾). A small quantity of sodium sulfite was added to the filtrate from the selenium analysis to ensure complete reduction to V (IV). The solution was heated to boiling to expel the excess reducing agent and then titrated with standard permanganate.

Niobium, Tantalum: These elements were precipitated as the hydrous oxide with concentrated ammonia. The precipitate was digested at 80-100°C, filtered and washed with dilute ammonia. A second precipitation after reducing the volume of the filtrate gave additional precipitate which was added to the first. The precipitate was ignited at 700°C and weighed as M_2O_5 .

Results of Determinations

SeF_4 : Se, 50.2%; calc. Se, 51.0%

SeF_4SO_3 : found Se, 34.1%; F, 32.5%; SO_3 , 33.4%
calc. Se, 33.60%; F, 32.34%; SO_3 , 34.07%

SeF_4BF_3 : found Se, 35.3%; F, 54.5%
calc. Se, 35.44%; F, 59.70%; B, 4.857%

SeF_4SbF_5 : found Se, 21.2%; F, 46.3%; Sb, 31.6%
calc. Se, 21.24%; F, 46.00%; Sb, 32.76%

SeF_4AsF_5 : found Se, 24.4%; F, 52.3%
calc. Se, 24.30%; F, 52.64%; As, 23.06%

SeF_4NbF_5 : found Se, 21.0%; F, 50.8%; Nb, 30.5%
calc. Se, 23.03%; F, 49.87%; Nb, 27.10%

SeF_4TaF_5 : found Se, 17.9%; F, 38.1%; Ta, 45.2%
calc. Se, 18.32%; F, 39.68%; Ta, 42.00%

SeF_4VF_5 : found Se, 26.7%; F, 46.0%; V, 22.0%
calc. SE, 26.24%; F, 56.84%; V, 16.93%

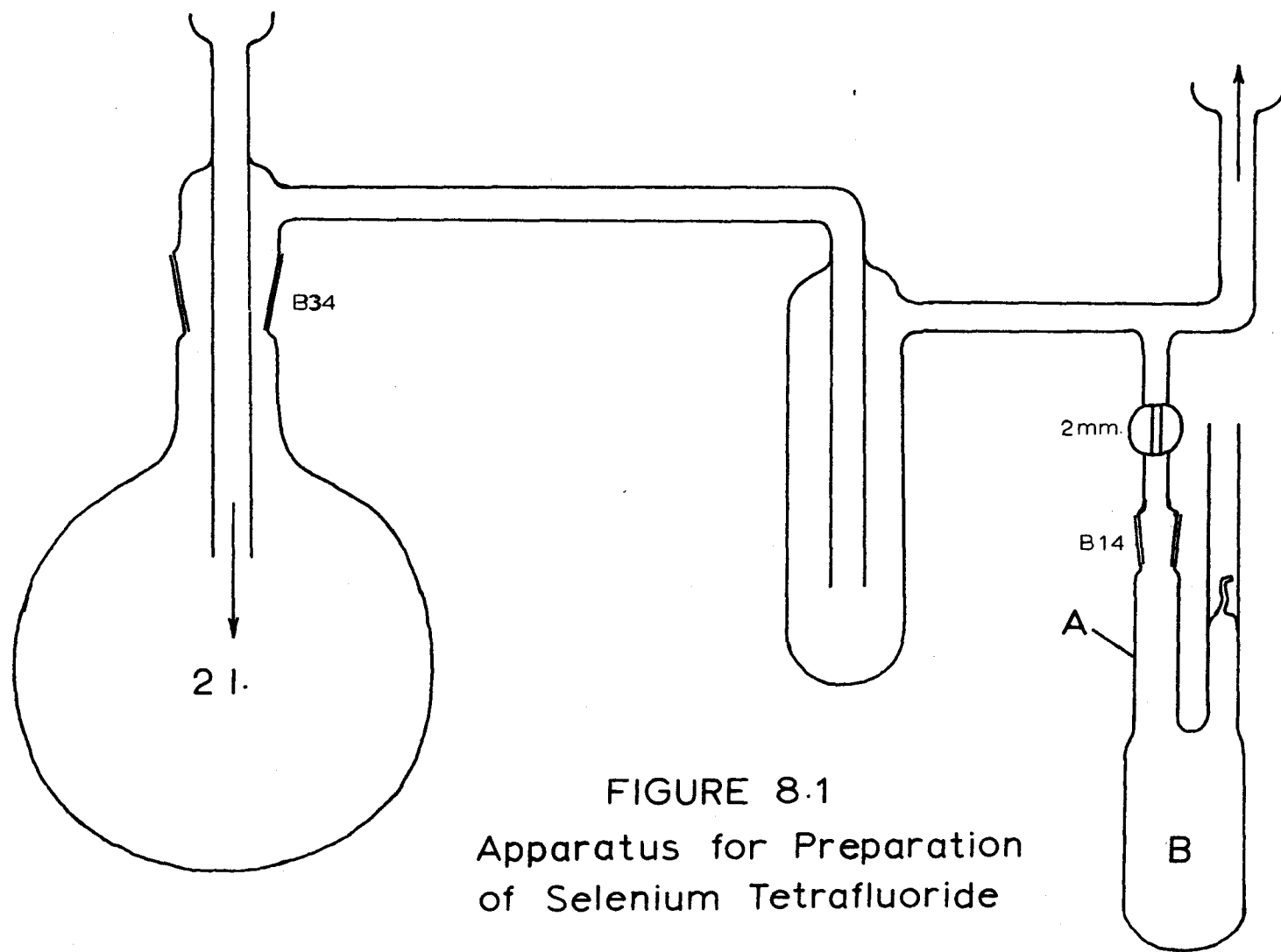


FIGURE 8.1
Apparatus for Preparation
of Selenium Tetrafluoride

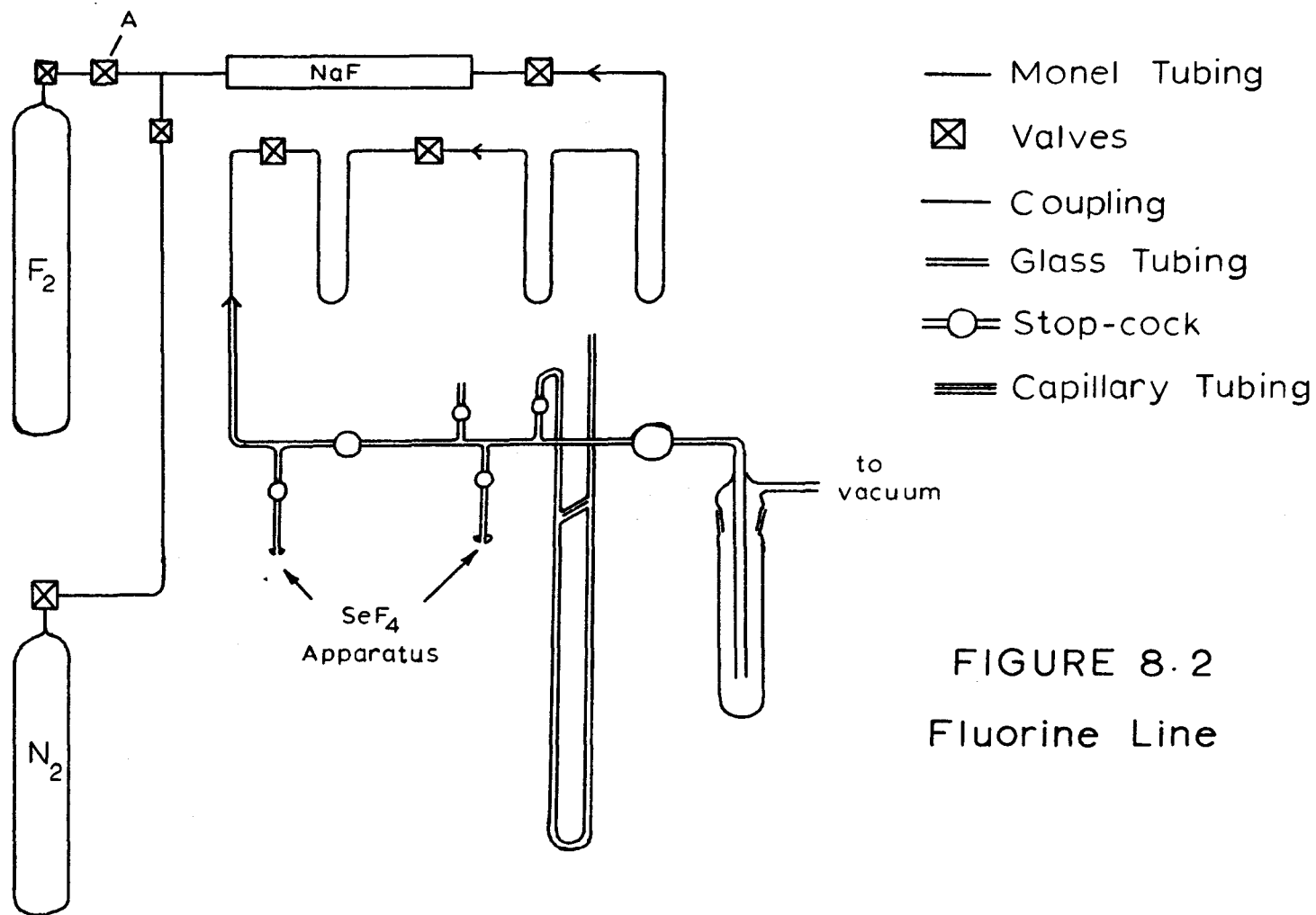
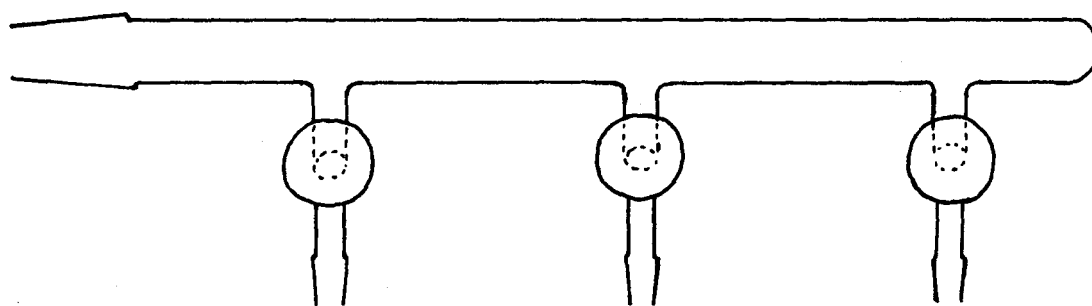
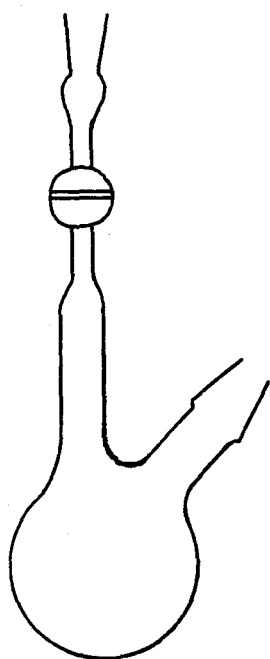


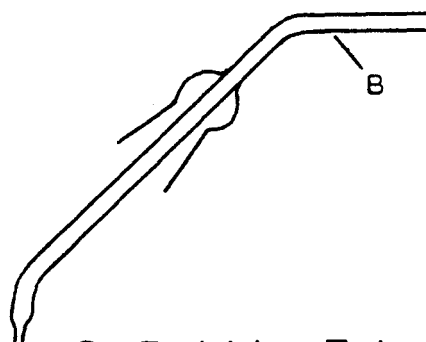
FIGURE 8.2
Fluorine Line



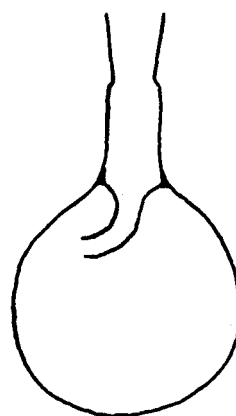
A Vacuum Manifold



B Reaction Flask



C Bubble Tube



D Anti-Bumping Flask

FIGURE 8.3

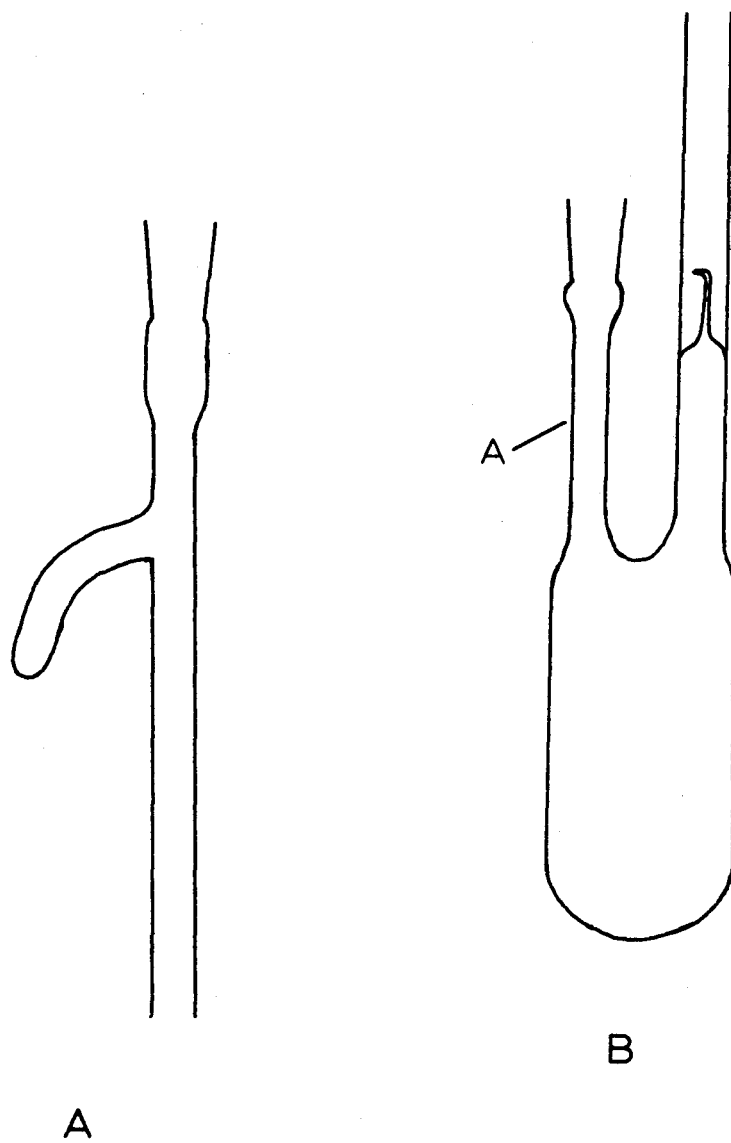


FIGURE 8.4

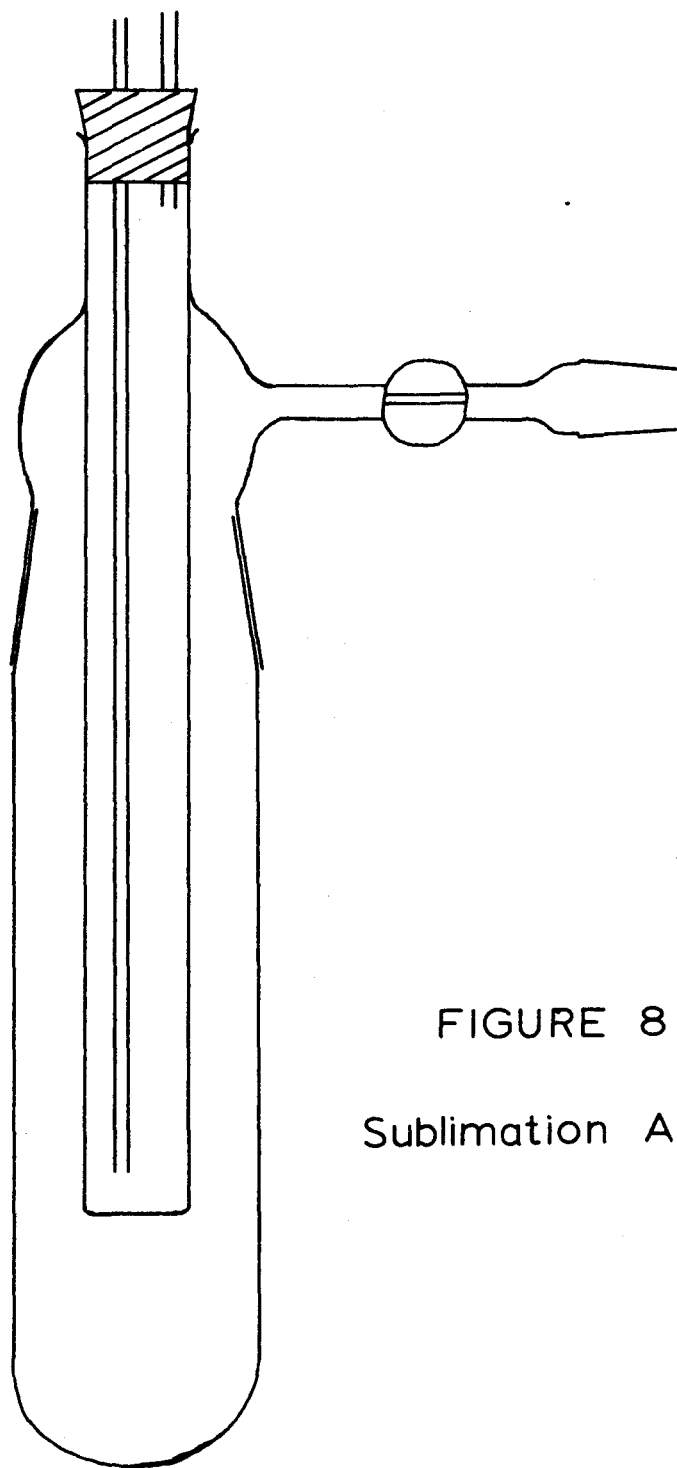


FIGURE 8.5
Sublimation Apparatus

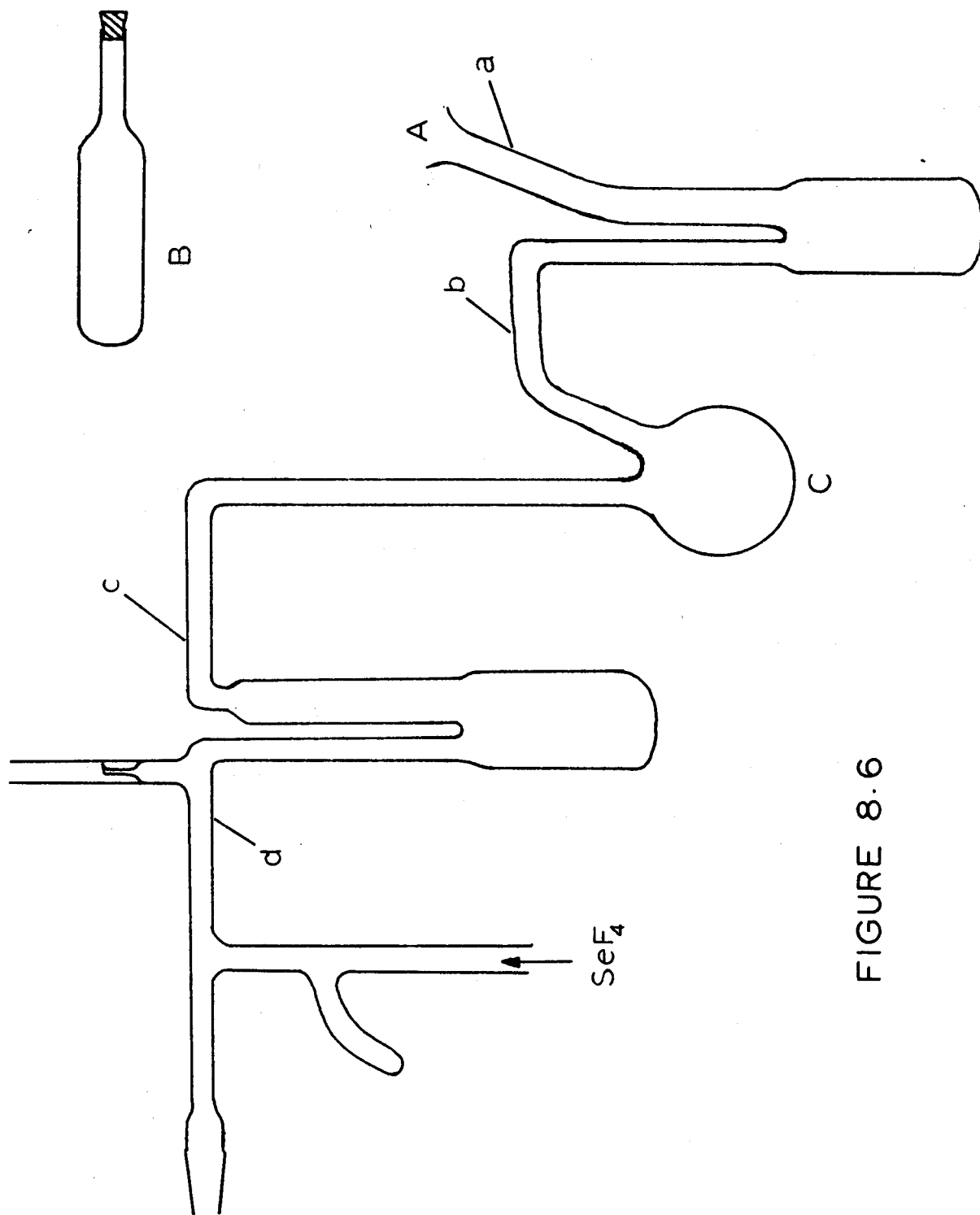


FIGURE 8.6

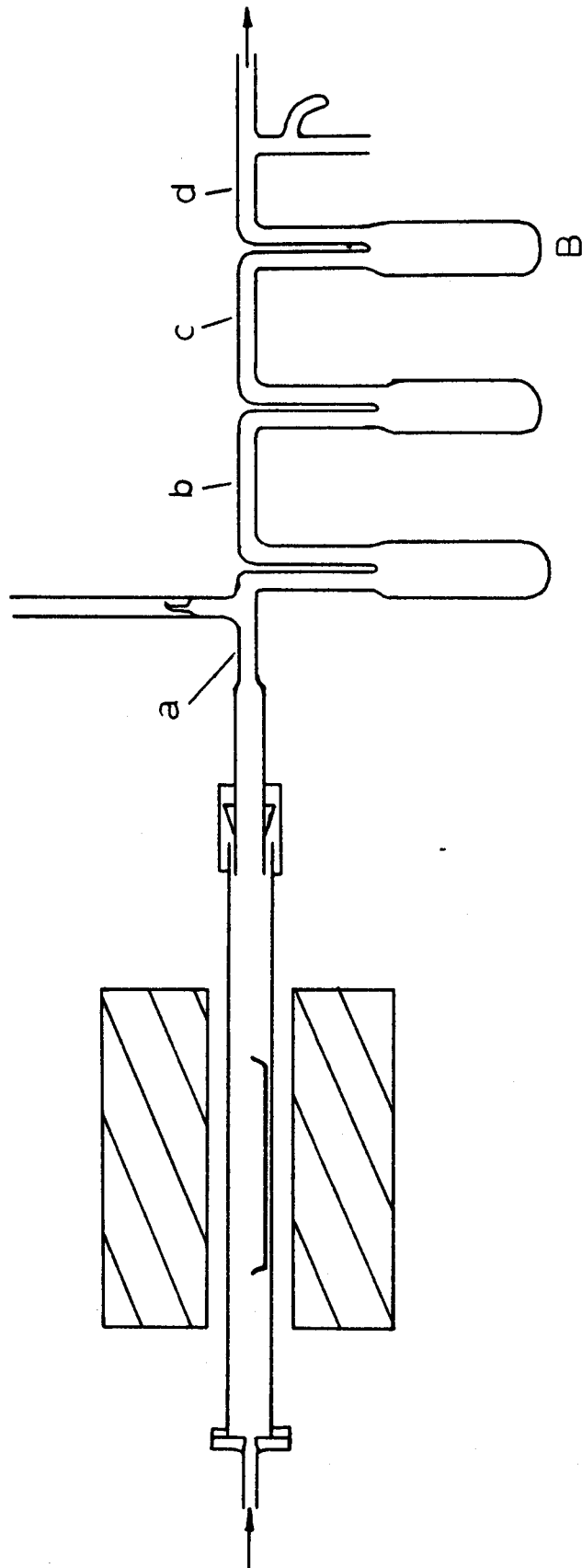
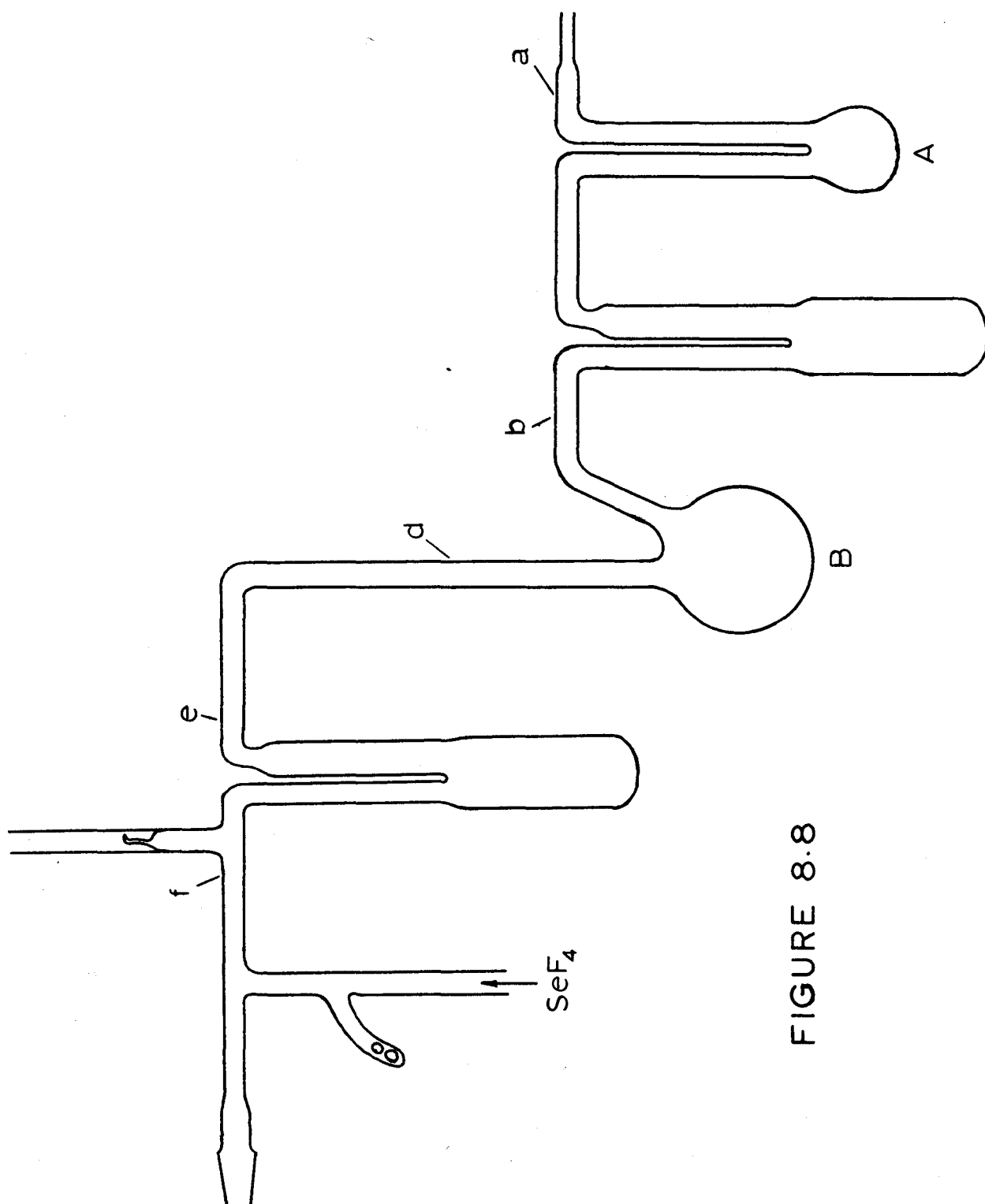


FIGURE 8.7



CHAPTER IX

Experimental Techniques

1. Raman Spectroscopy

The Raman spectrometer consisted of a Hilger E612 Raman spectrograph with glass prisms used in conjunction with a water cooled, Toronto-type mercury-arc lamp. After the spiral of the lamp had been heated with infra-red lamps, and the mercury pool electrodes heated with nichrome heaters, the arc was easily struck by using the discharge from a "tesla coil". A 250 DC. power supply was used at an operating current of 12 amps. A prism was used to reflect the Raman radiation through 90° and a two lens system ensured that most of the light from the sample was collected. Kodak IIa-0 spectroscopic plates were used generally, although occasionally 103a-0 plates were also used. The spectra were measured from microdensitometer tracings of the photographic plates (Leeds and Northrup Recording Photometer, Type 6700 P-1, No. 1518677) using the 4339 Å line in the mercury spectrum as reference. The calibration chart was obtained from iron arcs superimposed onto the mercury spectrum using the same mercury line as reference. The uncertainty of the Raman frequencies reported is $\pm 3 \text{ cm}^{-1}$. Polarization measurements were carried out using cylinders of polaroid cut parallel to and perpendicular to the plane of the incident light and placed inside the filter jacket (Fig. 9.1,A).

Raman tubes similar to that in Fig. 9.1,B were used for each compound. The Raman tubes were filled in the dry box and sealed off under vacuum immediately on removal from the dry box.

The samples were mounted inside the filter jacket (Fig. 9.1,A) containing a saturated solution of sodium nitrite which was circulated and cooled so that it served both as a filter to reduce the intensity of the 4061 Å mercury line and as the cooling medium for the sample.

The samples were mounted in a glass tube with a B24 joint which fitted into the filter jacket. The Raman tube (Fig. 9.1,B) was held in a rubber stopper cut to fit the mounting tube tightly and to hold the bottom of the Raman tube in the centre of the holder. The top of the Raman tube was held in the centre of the holder by pieces of cork which were wedged between the Raman tube and the tubing of the holder. To prevent stray light entering the optics other than through the Raman tube, the holder was painted black from the position of the lower support to the bottom of the joint.

The Raman spectra of the solid compounds were obtained with this method of mounting the sample. Several variations were found useful to reduce the background scattering in the solid spectra. A finely powdered sample gave less background than a polycrystalline sample in most cases. The crystalline nature of the sample was the main difficulty with the spectra of the arsenic pentafluoride adduct. The background could also be reduced by masking out the lower 1/8" to 3/16" of the sample with black tape. This increased the exposure time, but often the relative

intensity of the spectrum to the background was improved. For the Raman spectrum of a solid, 1 - 2 cm. of solid packed in the bottom of the Raman tube was sufficient to give a good spectrum.

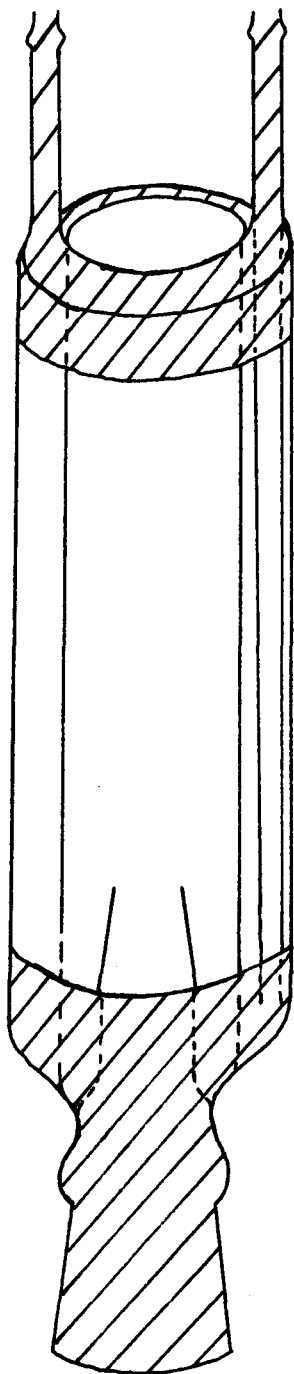
The Raman spectra of the molten complexes were obtained, in most cases, using the same samples used for the solid spectra. The same method of mounting the Raman tubes was used.

The high temperature necessary to melt the compounds was obtained by heating a stream of air with the heater shown in Fig. 9.2. The stream of air was regulated with a needle valve attached to the compressed air line, and the temperature of the air emerging from the heater was regulated by the voltage applied to the heater from a variable transformer. The stream of heated air was directed through a glass tube into the space between the Raman tube and the holder. The temperature of the air surrounding the Raman tube was measured with a copper-constantan thermocouple and a Leeds and Northrup temperature potentiometer. Once equilibrium was established with the surroundings, the sample temperature could be maintained constant for several hours at temperatures up to 150°C. The variation in temperature from the top to the bottom of the Raman tube was 2 - 3 C°.

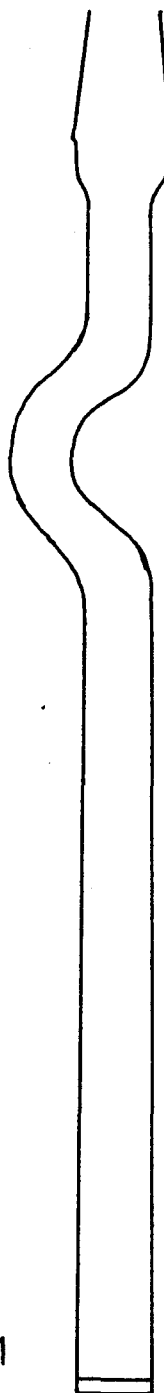
The conditions necessary to obtain the Raman spectra of the melts did not appear to decompose the compounds. Even trifluoroselenium (IV) hexafluoroarsenate, the adduct which is the least thermally stable of those studied, appeared to be stable in the sealed Raman tube up to 150°C.

The spectra of the complexes in solution were obtained using the Raman tube shown in Fig. 9.3,A. The solutions were made up in the dry box and were filtered into the Raman tube.

The Raman tube shown in Fig. 9.3,B was used for solutions which had to be kept cold to prevent decomposition. Air from a liquid air boiler was passed through the jacket around the tube. This Raman tube had two windows, and the space between them was evacuated. In this way, condensation on the outer window was prevented. The condensation on the outer jacket was controlled by flushing the space between the Raman tube and the filter jacket with a stream of nitrogen, then closing off this space with glass wool.



A Raman Filter Jacket



B Raman Tube

FIGURE 9.1

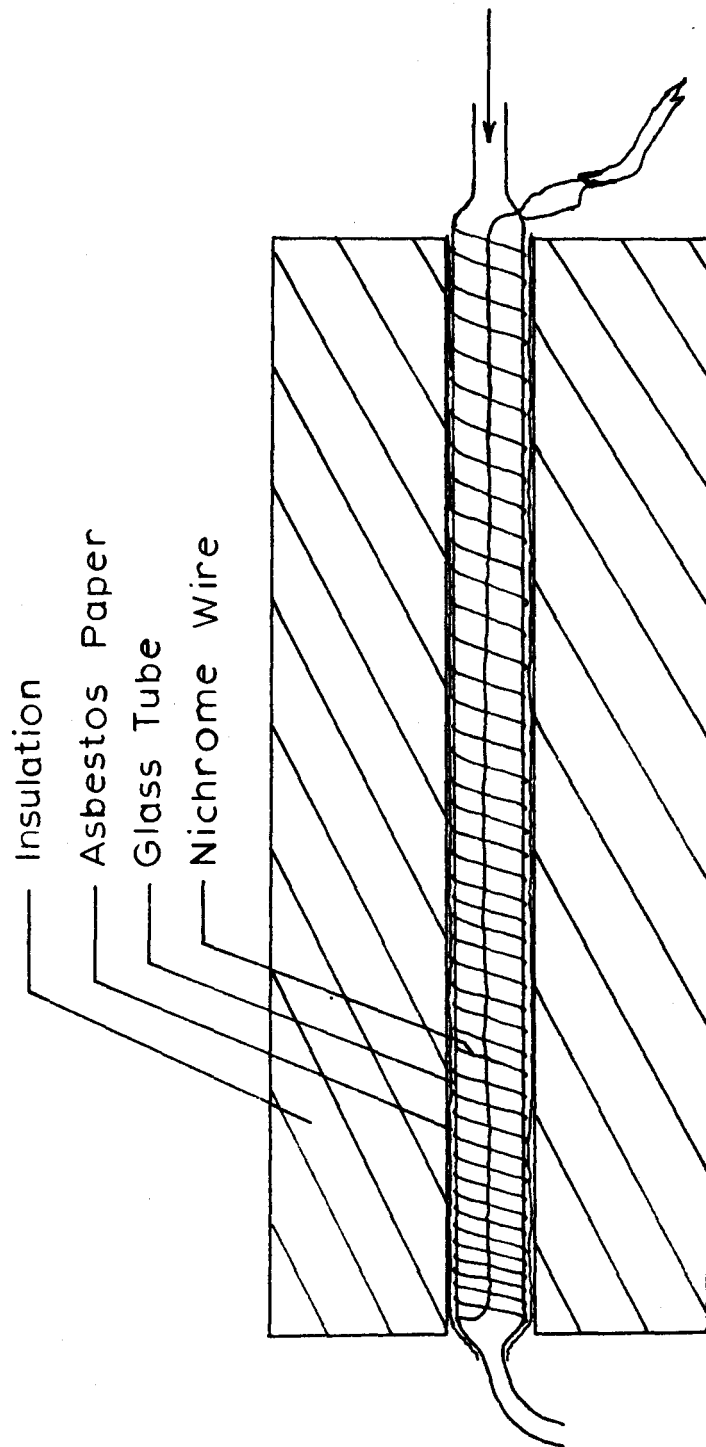
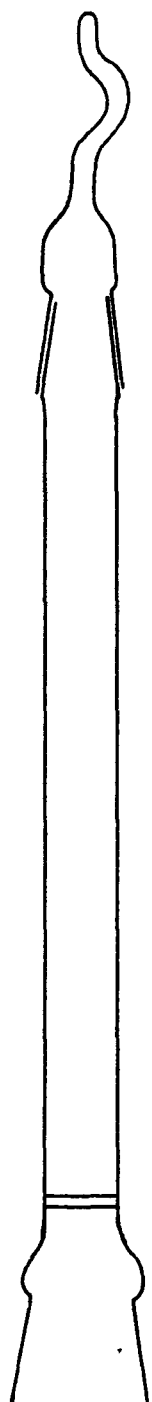


FIGURE 9.2

Air Heater



A Raman Tube

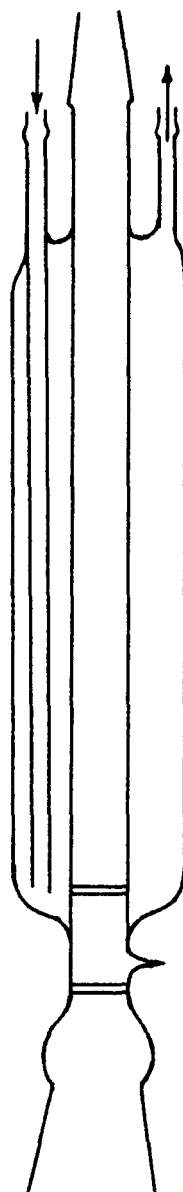
B Low-Temperature
Raman Tube

FIGURE 9.3

2. Infra-red Spectroscopy

The infra-red spectra were obtained using a Perkin-Elmer model 521 grating infra-red spectrometer with extended range interchange. Silver chloride and polythene windows were used in order that the entire spectral range available, from 4000 cm^{-1} to 250 cm^{-1} , could be recorded.

The usual sample techniques for infra-red spectroscopy were not available for the compounds studied. Nujol, even when dried with molecular sieves, immediately decomposed the compounds. The same was true of potassium bromide pellets. Thus it was necessary to develop special cells which allowed the samples to be mounted in anhydrous conditions.

Two cells, based on the same principle, were used. The first cell (Fig. 9.4,A) was used for compounds which did not have sufficient vapour pressure at room temperature to sublime readily in the cell at this temperature. After drying in the oven overnight, the cell was evacuated for several hours to remove as much water as possible. The cell was transferred to the dry box where one of the windows was removed, and the sample introduced into the side-arm of the cell (S, Fig. 9.4,A). The window was replaced, and the cell reevacuated immediately on removal from the dry box.

To prepare the compound to obtain its infra-red spectrum, the cold finger (Fig. 9.4,B), holding a $1\frac{1}{2}$ " by $\frac{3}{4}$ " window of the appropriate window material, was turned so that the window was directed toward the side arm of the cell. Liquid air was poured down the glass tube into the cold finger to cool the brass mounting and thence the cell window. Five

to ten minutes were sufficient to cool the window to operating temperatures. Once the window was cold, a low voltage, controlled with a variable transformer, was applied to the heating coil wound around the side arm of the cell. The amount of the compound sublimed in this manner onto the window was controlled by the heating time. The presence of the compound on the window could be detected by observing reflected light from the surface of the window. As the compound deposited on the window, diffraction rings appeared, and with experience the number and colour of the rings could be used to determine when sufficient compound had accumulated on the window. In practice, it was found best to stop the sublimation before sufficient compound was on the window and to record the spectrum. The sublimation process was then repeated several times, and the spectrum recorded each time so that the amount of compound on the window was gradually increased up to and past the amount which gave the best spectrum of the compound.

When sufficient compound was judged to be on the window, the liquid air was allowed to boil out completely from the cold finger, and the joint between the cell and the cold finger was warmed up with the hands until the grease was warm enough to allow rotation of the cold finger so that the window could be turned into the path of the infra-red beam passing through the main windows of the cell. The cold finger appeared to warm up very little during this time. Once this rotation of the cold finger was accomplished, liquid air was immediately poured into the cold finger. While the infra-red spectrum was recorded, the cold finger was kept filled with liquid air.

The second infra-red cell, shown in Fig. 9.5,A, was designed to handle the compounds whose vapour pressures at room temperature were too high to allow the amount of compound sublimed onto the window to be controlled in the manner described above.

The cell was evacuated and dried as above. In the dry box, the sample was introduced into the sample reservoir by removal of the B14 cap. The cell was reevacuated immediately on removal from the dry box, and the sample reservoir was cooled with powdered dry ice. The cold finger was cooled with liquid air, and, when the window had reached operating temperatures, the dry ice was removed from the sample reservoir, and the sample allowed to warm slowly to room temperature. When sufficient sample was observed to be present on the window, the dry ice was replaced around the sample reservoir. The cold finger was rotated into the path of the infra-red beam, and the infra-red spectrum of the material on the window obtained. It was again found most convenient to increase the amount of material on the window in several stages in order to obtain spectra with the optimum amount of sample.

One difficulty was encountered with the use of these cells. The fluoride resistant greases which were in general use during this work, i.e., Fluorolube and Kel-F grease, both have sufficient vapour pressure that they will sublime onto the surface of the window held in the cold finger. Thus it was necessary to use Apiezon T grease to seal the main windows to the cells, and for the stop-cocks on the cells. Fortunately, under the conditions used to prepare the sample, little attack of the

Apiezon grease was observed until the cell was allowed to warm to room temperature after the spectrum had been measured. Kel-F grease was used for the joint between the cell and the cold finger. Since the grease on this joint is at approximately the same temperature as the cold finger itself, there is no possibility of it subliming onto the cold finger.

Silver chloride windows were used to obtain the spectra of the compounds between 4000 cm^{-1} and 500 cm^{-1} . No compensating windows were placed in the reference beam, and the cell was balanced by partially closing the reference beam of the spectrometer.

Polythene windows were used to obtain the spectra between 600 cm^{-1} and 250 cm^{-1} . The windows were cut to $3/16$ " thickness from a polythene block, and the surfaces polished smooth. The cell was balanced by a $3/8$ " window of the same polythene, finished in the same manner. To bring the recorder pen further down scale, the reference beam was partially closed as well.

To obtain a vacuum tight seal of the polythene windows, it was necessary to apply pressure around the edges of the window in contact with the cell. This was accomplished with the clamp shown in Fig. 9.5,B. These measures were necessary since the polythene windows buckled slightly under vacuum.

The frequency calibration of the spectra was accomplished by superimposing onto the spectrum of each compound several of the peaks of known frequency from the spectrum of polystyrene. Thus the observed infrared frequencies have an uncertainty of less than $\pm 2\text{ cm}^{-1}$.

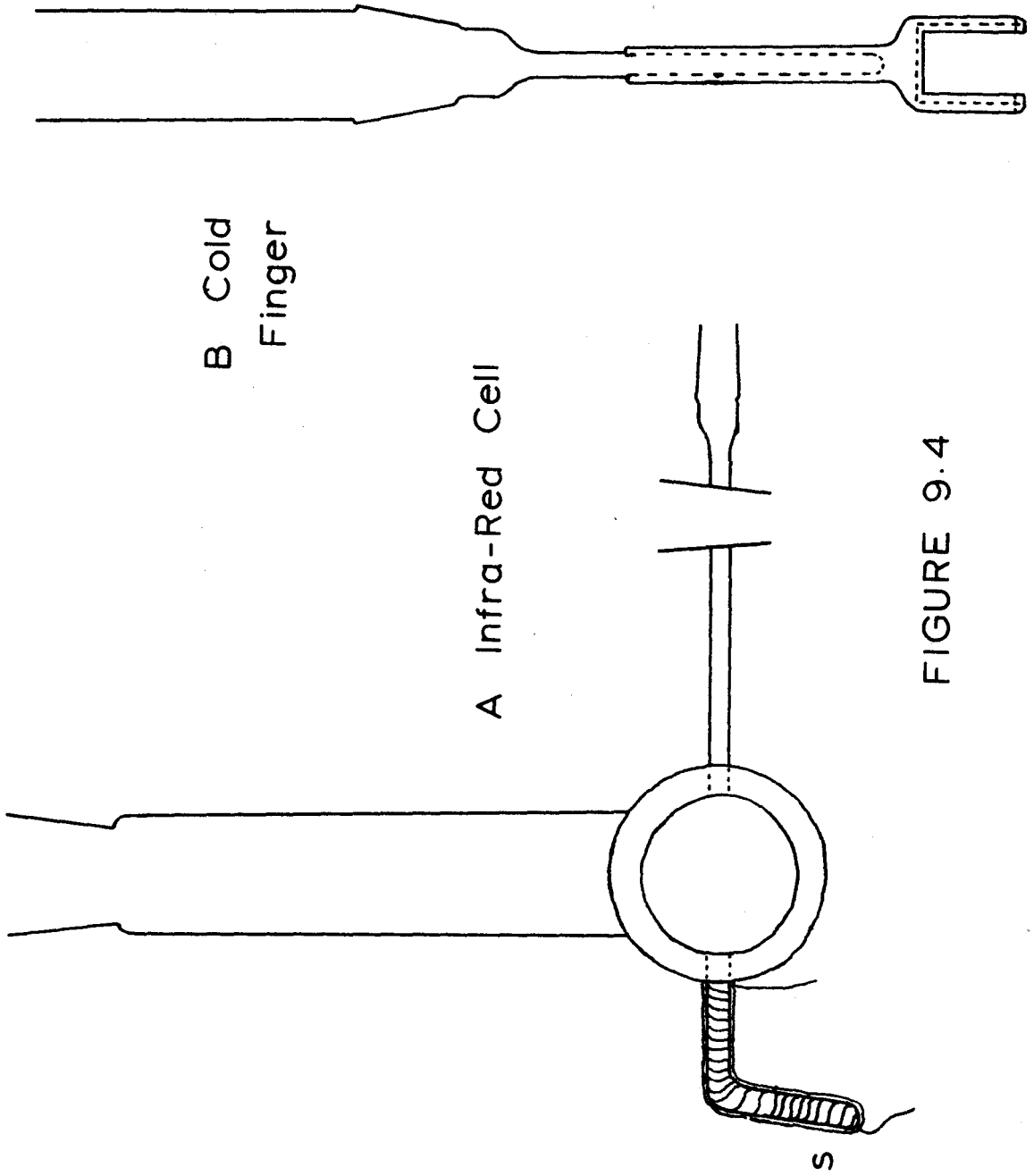


FIGURE 9.4

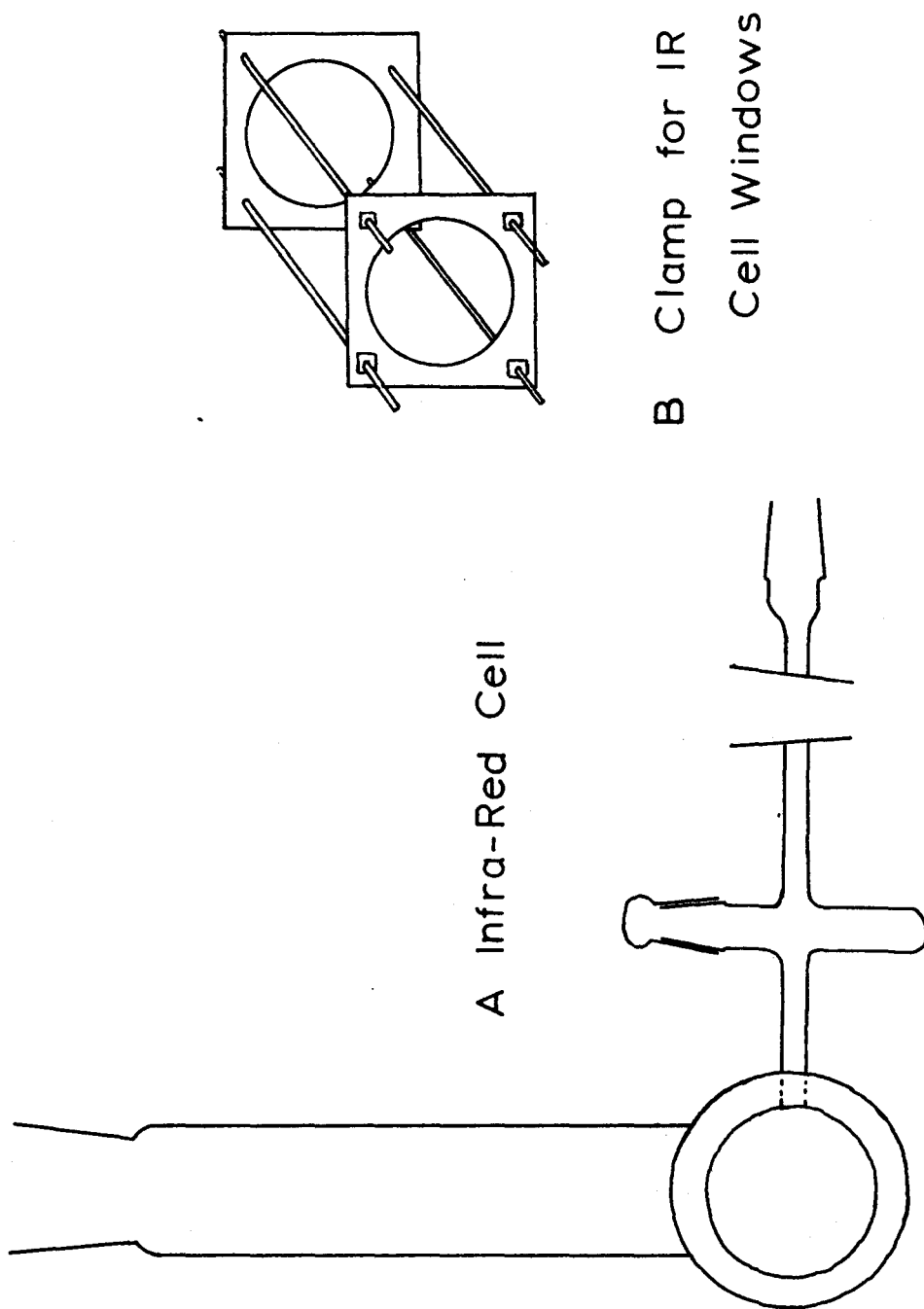


FIGURE 9.5

3. Nuclear Magnetic Resonance Spectroscopy

The nuclear magnetic resonance spectra were obtained using a Varian Associates DP-60 high resolution n.m.r. spectrometer operating at 56.4 Mc./sec. The spectra were calibrated using audio side band techniques, the modulation frequency being obtained from a Muirhead-Wigan, D-890-A, decade oscillator. Referencing of the spectra was carried out by exchanging the sample tube with a tube of fluorosulfuric acid or of trifluoroacetic acid.

The sample tubes of selected 5 mm. tubing were filled in the dry box and sealed off under vacuum.

The high temperatures required to liquefy the samples were obtained by passing heated air through a Varian Associates variable temperature n.m.r. probe accessory, model V-4340. The air heater (Fig. 9.2) described for high temperature Raman spectra was used to provide the hot air necessary to raise the temperature of the probe. Temperatures were measured with a copper-constantan thermocouple connected to a Leeds and Northrup temperature potentiometer.

The spectra at low temperature were obtained by passing air from a liquid air boiler through the variable temperature n.m.r. probe; the temperature was measured in the same manner as above.

4. Conductivity Measurements

The conductivity cell (Fig. 9.6,A), designed to have a cell constant of approximately 1 cm.^{-1} and a sample volume of approximately 3 ml., was used to measure the conductivity of melts. The cell was standardized at 25°C by comparison with a cell of known cell constant using a solution of potassium chloride. The cell used for comparison was standardized at 25°C with sulfuric acid by adjusting its composition to obtain the minimum conductance. The minimum specific conductance of sulfuric acid at 25°C , $1.0432 \times 10^{-2} \text{ ohm}^{-1} \text{ cm.}^{-1}$ (60), was then used to calculate the cell constant. A Wayne Kerr Universal Bridge (Type B-221, No. 599) was used to measure the conductance of all solutions.

The platinum electrodes were coated with platinum black by electrolyzing a solution of chloroplatinic acid. A current of ten milliamperes was passed for twenty minutes with reversal of the current every fifty seconds.

The cell was evacuated, and the cell and the side arm of the adapter (S, Fig. 9.6,B) were dried by heating gently with a bunsen flame. The cell was filled with the compound in the dry box, and evacuated immediately on removal from the dry box. Mercury was placed in the glass tubes to the electrode connections, and copper wires were inserted into the mercury and connected to the conductivity bridge leads. A large dewar flask was placed around the conductivity cell. The temperature inside the dewar was raised above the melting point of the compound by passing a stream of air through a heater (Fig. 9.2) and down a 5 mm. glass tube to

the bottom of the dewar. Turbulence within the dewar was reduced by placing three circles of wire gauze, one at the bottom, one just above the position of the electrodes and one near the top of the dewar. The temperature of the melt in the cell was measured with a copper-constantan thermocouple placed in the air bath adjacent to the electrodes of the cell.

The temperature of the air bath was raised until it was fifteen to twenty degrees above the melting point of the compound. When the temperature was steady, the conductance and the temperature of the melt were recorded. The temperature was reduced slowly two to three degrees at a time, allowing twenty to thirty minutes for the temperature to stabilize before each reading was taken. In this manner, a series of values for the conductance of the melt was obtained for temperatures down to the melting point of the compound. The conductance values were plotted against temperature, and the specific conductance at the melting point determined for each compound. Duplicate determinations were made for each compound on samples of the compound with different histories. Generally, one of the experiments was performed using freshly sublimed product.

Conductivity measurements on solutions were carried out using the cells in Fig. 9.7. These cells were standardized with minimum conducting sulfuric acid at 25°C.

For conductivity measurements in fluorosulfuric acid, the cell (Fig. 9.7,A) was weighed and attached to the outlet from the fluorosulfuric acid still, where it was dried by heating while a slow stream of dry air was passed through it. The acid was distilled into the cell, and

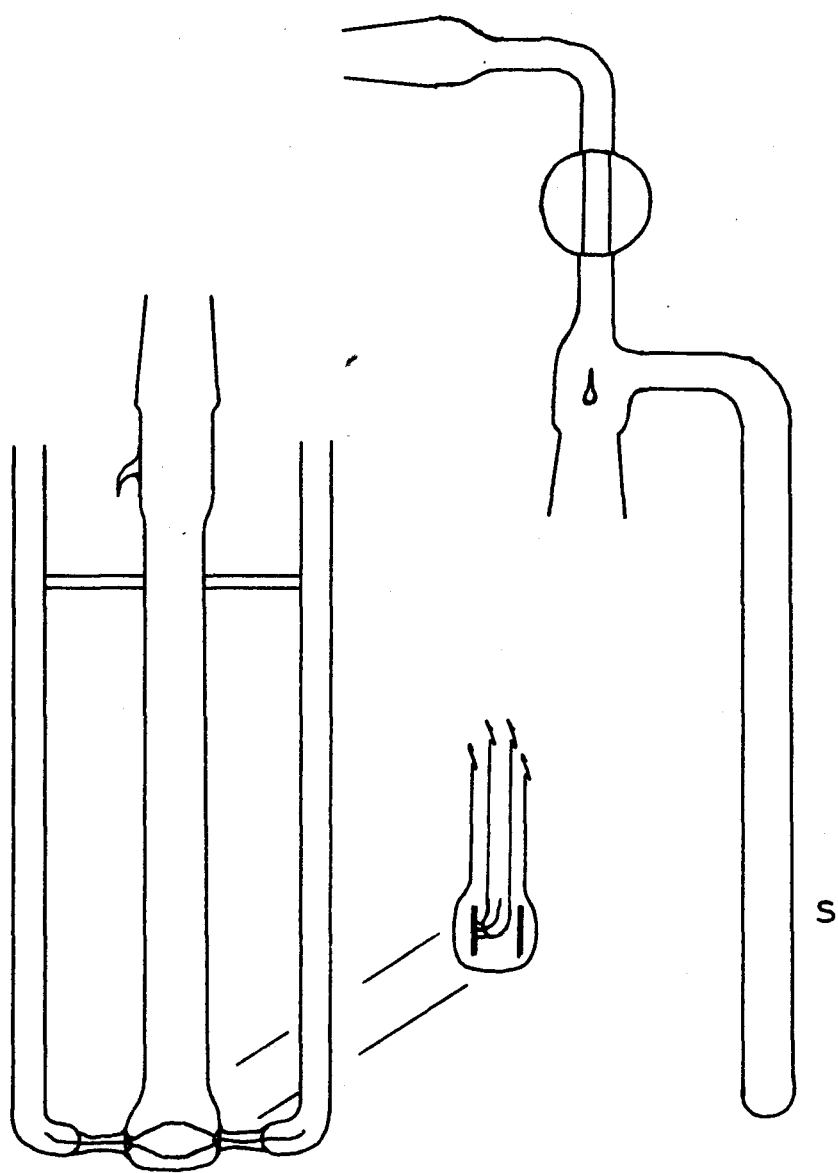
the cell reweighed to determine the amount of acid in the cell. The pure acid has a specific conductance between 1.0×10^{-4} and 2.5×10^{-4} ohm⁻¹ cm.⁻¹. Additions of solute were made to the conductivity cell using the weight dropper in Fig. 9.8A. The cell was placed in an oil thermostat regulated at $25.000 \pm 0.002^\circ\text{C}$.

The conductivity measurements in nitrobenzene were made using the conductivity cell shown in Fig. 9.7,B. The conductivities were measured in a bath regulated at $10.00 \pm 0.005^\circ\text{C}$, the temperature being determined with a platinum resistance thermometer.

The cell was filled with nitrobenzene from a weight dropper (Fig. 9.8,B). Additions to the cell were made with the weight dropper in Fig. 9.8,A, which was filled in the dry box. The solutions were mixed thoroughly after each addition and the conductance read; the solutions were then mixed again and the conductance redetermined until no further change was observed. In this way variations in conductance due to improper mixing were eliminated.

Several of the conductivity experiments in nitrobenzene were obtained by a dilution technique using the conductivity cell shown in Fig. 9.6A. A B24-B19 ring adaptor with a rubber diaphragm over one end was used to close the cell. The clean, dry cell was weighed, a small amount of the compound placed in the cell in the dry box, and the cell reweighed to determine the amount of compound. Using a 5 ml. syringe, 8-10 g. of nitrobenzene was then introduced into the cell through the

rubber diaphragm. The exact weight was determined by weighing the syringe before and after the addition. The compound was dissolved, and the conductance of the solution determined at 10°C as above. Then a portion of the solution was removed by inserting the needle of the syringe into the solution and withdrawing the desired amount of solution. The weight of solution removed was determined by weighing the syringe before and after the removal. Then a second quantity of nitrobenzene was added, the weight being determined as before. The solution was mixed thoroughly, and the conductance measured. Generally, a second addition of nitrobenzene was made before more of the solution was removed. By such alternation of additions of nitrobenzene and removal of solution, the concentration of the solution was gradually reduced to as low a value as desired. The concentration corresponding to the measured conductance was determined from the known weights of solution removed and solvent added. In this manner, the conductivity was determined under anhydrous conditions using a very small quantity of the compound.



B Adaptor for Cell

A Conductivity Cell

FIGURE 9.6

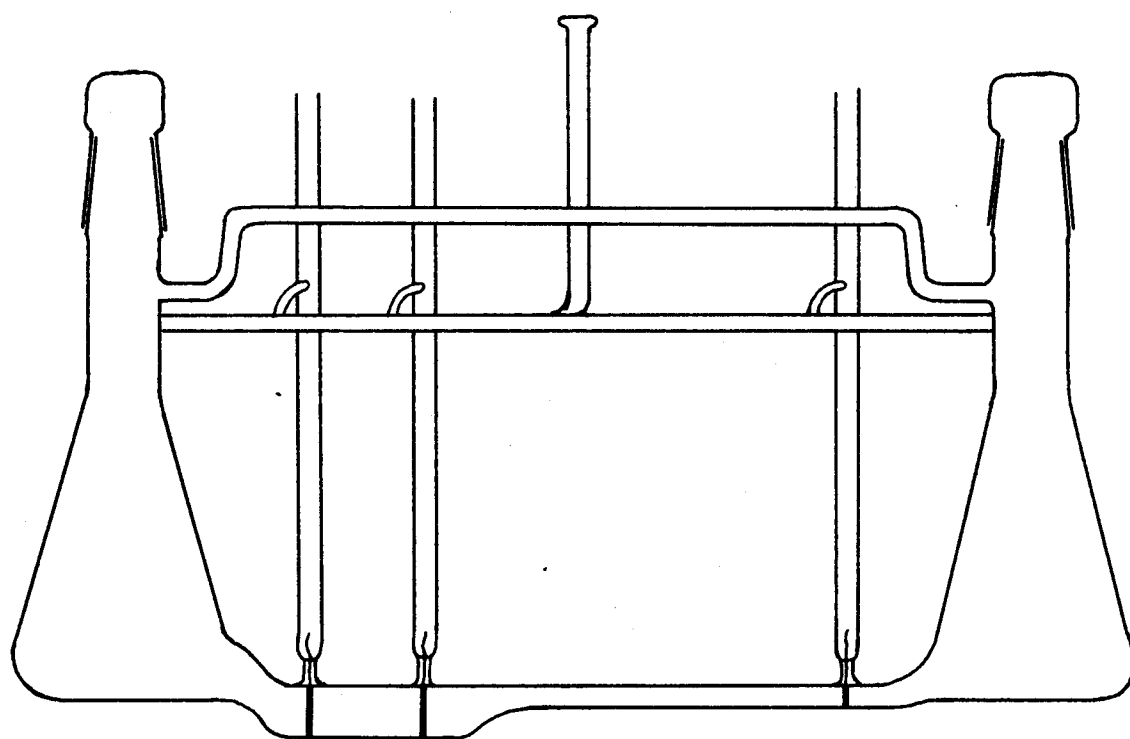
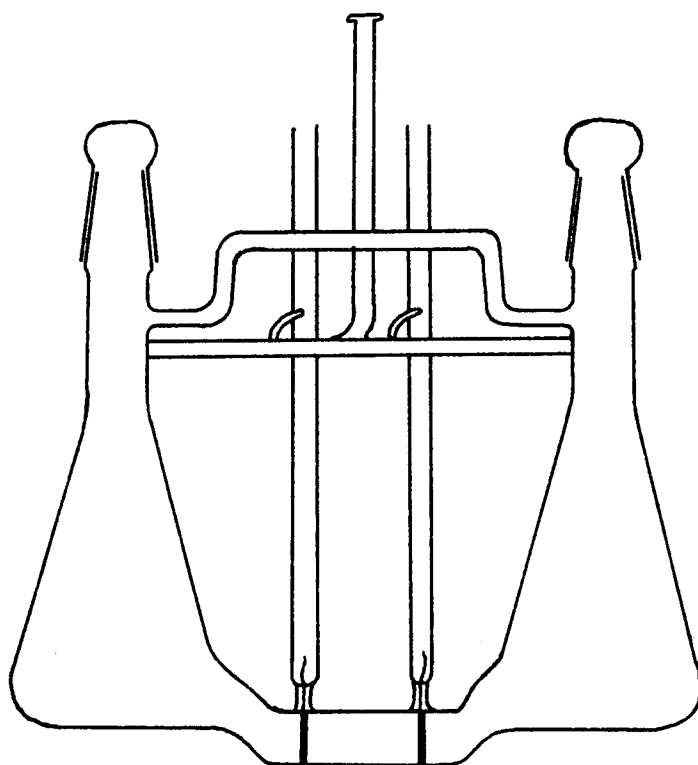
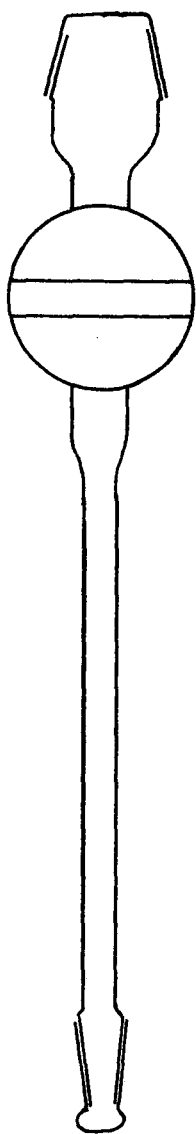


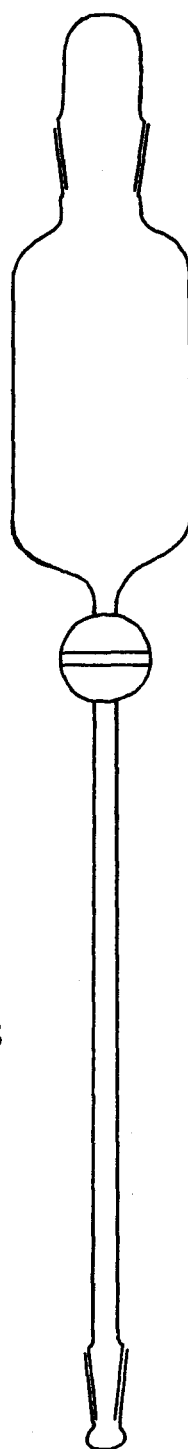
FIGURE 9.7

Conductivity
Cells





A Weight Burette
(solids)



B Weight Burette
(liquids)

FIGURE 9.8

5. Viscosity

The viscosity of trifluoroselenium (IV) hexafluoroantimonate was determined to test the validity of the equations used to interpret the conductivity data.

A modified Ostwald viscometer was used (Fig. 9.9). The viscometer was calibrated with 100% sulfuric acid and with a 40% sucrose solution. The viscometer was calibrated with the same volume of liquid as was used in the measurements (about 5 ml.).

The viscometer was dried by heating on the vacuum line and filled with SeF_4SbF_5 in the dry box. The viscometer was immersed in the air bath used for conductivity measurements of the melts (Section IX, 4). The temperature was measured with a copper-constantan thermocouple. The viscosity was determined at 140°C, 132°C and 126°C. One to two hours were allowed for the system to come to equilibrium between each set of readings.

Dry air was introduced into the viscometer with the ground-glass tap at A, Fig. 9.9, to force the liquid up through the capillary tube. Then the tap was turned to position B, Fig. 9.9, to measure the time for the liquid level to fall. This process was repeated, reevacuating the viscometer as necessary, until sufficient readings were obtained to give a good value for the viscosity.

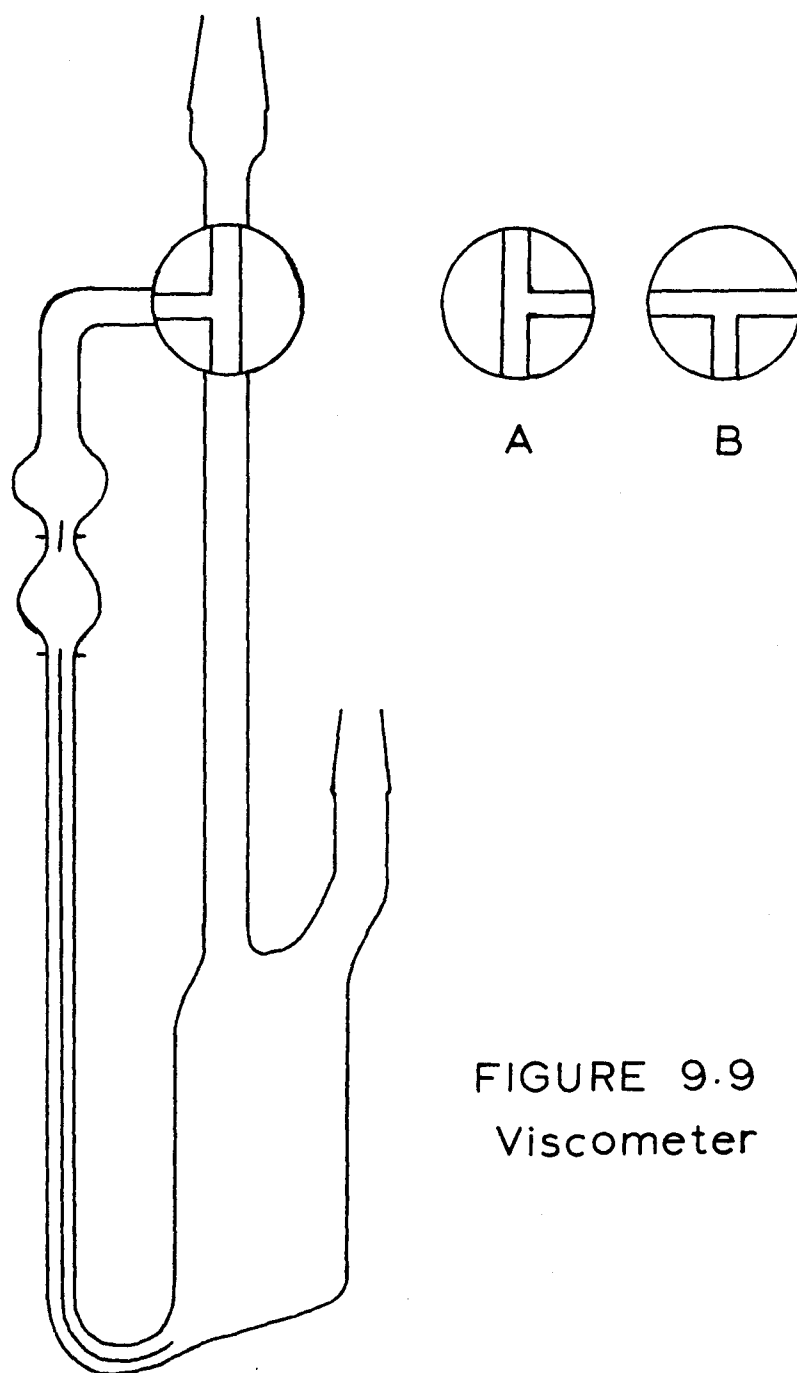


FIGURE 9.9
Viscometer

6. Cryoscopy in Nitrobenzene

A cryoscope (Fig. 9.10), similar to that used previously for sulfuric acid⁽⁶¹⁾, was used for nitrobenzene. The B14 ground glass joint on the thermometer was inserted in an adapter for the B19 joint on the cryoscope, and by rotation of the adapter the thermometer could be centered in the cryoscope. All ground glass joints on the cryoscope, with the exception of A (Fig. 9.10), were greased with a narrow ring of silicone grease (Dow-Corning). Temperatures were measured with a Tinsley platinum resistance thermometer (No. 111712), calibrated by the National Physical Laboratory. The resistance of the thermometer was measured on a Mueller resistance bridge (Leeds and Northrup No. 1338840). The ice point resistance of the thermometer was checked by determining its resistance at the triple point of water using a Trans-sonic Inc. "Equiphase Cell".

The cryoscope was charged with approximately 100 g. nitrobenzene, using the weight dropper shown in Fig. 9.8, B. The nitrobenzene was cooled with an ice bath around the outside of the cryoscope. At temperatures below the freezing point, the contact of the stirrer with the bottom of the cryoscope caused the solvent to seed out; thus it was necessary to discontinue stirring once the contents had cooled to the freezing point. When the solvent had super-cooled 2.5 to 3.0 degrees, the ice bath was removed and replaced with a second bath at $4 - 5^{\circ}\text{C}$, with an air jacket placed around the lower part of the cryoscope (J, Fig. 9.10). The super-cooling temperature was recorded, and the stirrer was started to seed out the solution. As the first crystals appeared in the solution, a stop-watch

was started, and after one minute, readings of the resistance of the thermometer were taken every twenty seconds for the first five minutes, and every thirty seconds thereafter. Readings were continued for fifteen minutes after the solution was seeded out. The C adjust resistance was changed after the determination of the first freezing point, so that the correction for the resistance of the thermometer leads would be as small as possible for the succeeding freezing point determinations.

The freezing point for the solution was calculated from the maximum value observed for the thermometer resistance. This value was attained from three to four minutes after the solution was seeded out, and corresponds to equilibrium between the solid solvent and the solution.

When a reliable value for the freezing point of the pure solvent had been obtained, the first addition of solute was made. The weight dropper (Fig. 9.8,A) was filled in the dry box and all the caps made secure. The weight dropper was weighed quickly after removal from the dry box. After its contents were emptied into the cryoscope through A (Fig. 9.10), the weight dropper was immediately reweighed. The addition was made to nitrobenzene at its freezing point as this was found to slow down darkening of the solutions. During the remainder of the experiment the solution was not allowed to warm above 10°C.

The freezing point of the solution was determined in the same manner as described for the solvent. The super-cooling temperature was noted, the solution seeded out by starting the stirrer, and readings of the thermometer resistance taken with time. The maximum thermometer resistance was used for the resistance at the freezing point.

For each compound, at least three additions were made for each experiment.

A correction was made to the solution concentration for the amount of solvent frozen out when the solution was seeded. The weight of nitrobenzene frozen out, W_n , was given by the expression

$$W_n = \frac{(W_{\text{solv.}})(C_p)(\Delta T)}{(\Delta H_f)}$$

where $W_{\text{solv.}}$ is the weight of solvent in the cryoscope, C_p , the heat capacity of nitrobenzene ($1.52 \text{ J.g.}^{-1} \text{ deg.}^{-1}$ at 5°C)^(62 - by extrapolation) ΔT , the amount of super-cooling, and ΔH , the heat of fusion of nitrobenzene ($94.25 \text{ cal. g.}^{-1}$ ⁽⁶²⁾). Then the concentration of the solution, C , in equilibrium with the solid nitrobenzene was determined by the following:

$$C = \frac{W_s}{(W_{\text{solv.}} - W_n)} \times 1000 \text{ g./kg. nitrobenzene}$$

where W_s is the weight of the solute. Using the formula weight of the adduct, the molality of the solution was given by $C/F.W.$ No correction was made for the heat capacity of the cryoscope.

A value for the molecular weight of the compound was obtained from the slope of the plot of the freezing point depression against concentration. From the value for the heat of fusion given above, the molal freezing point depression constant for nitrobenzene was calculated to be 8.684 deg.^{-1} .

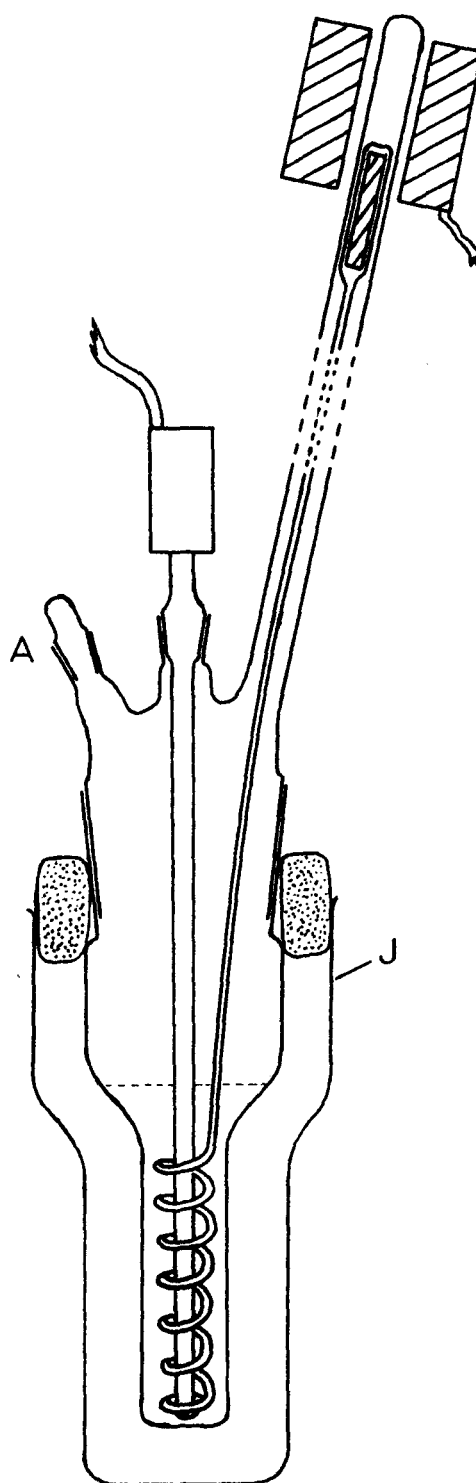


FIGURE 9.10

Cryoscope

7. X-Ray Powder Diffraction

Thin-walled 5 mm. pyrex tubing was drawn down to make thin-walled capillaries of approximately 0.5 mm. diameter. From the capillaries that were drawn down, only those which were cylindrical, of even wall thickness, and of suitable diameter were selected.

These capillaries were charged in the dry box. The compound was ground to a fine powder in an agate mortar, and transferred into the capillary which was sealed off immediately on removal from the dry box.

X-ray powder diffraction patterns were obtained using an 11.46 cm. Debye-Sherrer camera. The radiation was provided by a Phillips (Type PW 101030) X-ray generator using a copper target with a nickel filter.

The films were measured from microphotometer tracings. The conversion factor from inches on the chart paper to mm. on the film was determined by measuring the distance between two scratches on the film using the microphotometer tracing and a travelling microscope. A correction for film shrinkage was applied in the usual manner.

References

1. P. Lebeau. Compt. Rendu. 144, 1042, 1347 (1907).
2. E.B.R. Prideaux and C.B. Cox. J. Chem. Soc. 133, 1603 (1928).
3. E.E. Aynsley, R.D. Peacock and P. L. Robinson. J. Chem. Soc. 1231 (1952).
4. R.E. Dodd and P. L. Robinson. Preparative Inorganic Chemistry. Elsevier Publishing Co., New York. 1957. p.219.
5. H.M.J. Bowen. Nature. 172, 171 (1953).
6. W.M. Tolles and W. D. Gwinn. J. Chem. Phys. 36, 1119 (1962).
7. R. J. Gillespie. Can. J. Chem. 38, 824 (1960).
8. J.A. Rolfe, L.A. Woodward and D.A. Long. Trans. Far. Soc. 49, 1388 (1953).
9. H.C. Clark. Chem. Rev. 58, 882 (1958).
10. M.A. Hepworth, P.L. Robinson and G. Westland. Chem. and Ind. 1516 (1955).
11. R.D. Peacock, J. Chem. Soc. 3617 (1953).
12. N. Bartlett and P.L. Robinson. Chem and Ind. 1351 (1956).
13. F.A. Cotton (ed.). Progress in Inorganic Chemistry, Vol. 2. R.D. Peacock, Some Fluoride Compounds of the Transition Metals. Interscience Publishers Inc., New York. 1960. p.237.
14. N. Bartlett and K.C. Yu. Can. J. Chem. 39, 80 (1961).
15. R. G. Cowell and H.C. Clark. J. Chem. Soc. 2692 (1962).
16. H.C. Clark and Y.N. Sandana. Can. J. Chem. 42, 50 (1964).
17. N. Bartlett and D.H. Lohmann. J. Chem. Soc. 5253 (1962).
18. N. Bartlett and J. W. Quail. J. Chem. Soc. 3728 (1961).
19. N. Bartlett and P.L. Robinson. J. Chem. Soc. 3417 (1961).
20. N. Bartlett and P.L. Robinson. J. Chem. Soc. 3549 (1961).
21. F.A. Cotton and J.W. George. J. Inorg. Nucl. Chem. 2, 397 (1958).

22. Von. F. Seel and O. Detmer. Z. anorg. allg. Chem. 301, 113 (1959).
23. D.W.A. Sharp. J. Chem. Soc. 3761 (1957).
24. D.W.A. Sharp and N. Sheppard. J. Chem. Soc. 674 (1957).
25. R.J. Gillespie and E.A. Robinson. Can. J. Chem. 40, 644 (1962).
26. H. Siebert. Z. anorg. allg. Chem. 289, 15 (1957).
27. H.C. Clark and R.J. O'Brien. Inorg. Chem. 2, 1020 (1963).
28. B.J. Hathaway and D.E. Webster. Proc. Chem. Soc. 14 (1963).
29. C. Dural and J. Lecomte. Bull. Soc. Chim. Fr. 14, 1057 (1947).
30. G.L. Coté and H.W. Thompson. Proc. Roy. Soc. 210 [A], 217 (1951).
31. N. N. Greenwood. J. Chem. Soc. 3811 (1959).
32. D. Cook, S.J. Kuhn and G.A. Olah. J. Chem. Phys. 33, 1669 (1960).
33. R. Paris, G. Tridot and J.F. Laurent. Bull. Soc. Chim. Fr. 142 (1954).
34. B.P. ~~Sauer~~ and J.J. Wahrmann. Helv. Chim. Acta. 40, 722 (1957).
35. R.D. Peacock and D.W.A. Sharp. J. Chem. Soc. 2762 (1959).
36. D.W.A. Sharp and A. G. Sharpe. J. Chem. Soc. 1855 (1956).
37. J.O. Edwards, G.C. Morrison, V.F. Ross and J.W. Schulz. J. Amer. Chem. Soc. 77, 266 (1955).
38. J. Goubeau and W. Bues. Z. anorg. allg. Chem. 268, 221 (1952).
39. H.H. Hyman, L.A. ~~Quarterman~~, M. Kilpatrick and J.J. Katz. J. Phys. Chem. 65, 123 (1961).
40. O.L. Keller. Inorg. Chem. 2, 783 (1963).
41. G.A. Olah, S.J. Kuhn, K.S. Tolgyesi and E. B. Baker. J. Amer. Chem. Soc. 84, 2733 (1962).
42. G.A. Olah, W.S. Tolgyesi, S.J. Kuhn, M.E. Moffatt, I.J. Bastein and E.B. Baker. J. Amer. Chem. Soc. 85, 1328 (1963).

43. D. Cook, Can. J. Chem. 37, 48 (1959).
B.P. Susz and J.J. Wuhrmann. Helv. Chim. Acta. 40, 971 (1957).
44. D. Cassimatis and B.P. Susz. Helv. Chim. Acta. 44, 943 (1961).
45. R.J. Gillespie and E.A. Robinson. Spect. Acta. 19, 741 (1963).
46. E.A. Robinson. Can. J. Chem. 39, 247 (1961).
47. R.J. Gillespie and R.A. Rothenbury. Can. J. Chem. 42, 416 (1964).
48. J. M. Schreeve and G.H. Cady. J. Amer. Chem. Soc. 83, 4521 (1961).
49. R.J. Gillespie and E.A. Robinson. Can. J. Chem. 39, 2171 (1961).
50. Von A. Simon and R.L. Lehmann. Z. anorg. allg. Chem. 311, 224 (1961).
51. R. J. Gillespie and E.A. Robinson. Can. J. Chem. 39, 2179 (1961).
52. F.B. Dudley and G.H. Cady. J. Amer. Chem. Soc. 79, 513 (1957).
53. International Critical Tables, Vol. VI.
McGraw Hill Book Co., Inc. 1929. p.89.
54. N.N. Greenwood and R.L. Martin. J. Chem. Soc. 1427 (1953).
55. N.N. Greenwood and R.L. Martin. Pure Appl. Chem. 6, 85 (1963).
56. H.J. Emeleus and K.J. Packer. J. Chem. Soc. 771 (1962).
57. C.J. Hoffman, B.E. Holder and W.L. Jolly. J. Phys. Chem. 62, 364 (1958).
58. E.E. Aynsley, R.D. Peacock and P.L. Robinson. Chem. and Ind. 1117 (1951).
59. G. Herzberg. Molecular Spectra and Molecular Structure, Vol. II.
D. Van Nostrand Co., Inc., New York. 1945. p.311.
60. R.J. Gillespie, J.V. Oubridge and C. Solomons. J. Chem. Soc. 1804 (1957).
61. R.J. Gillespie, E.W. Hughes and C.K. Ingold. J. Chem Soc. 2473 (1950).
62. International Critical Tables. Vol. V.
McGraw Hill Book Co., Inc. 1929. p.133.
63. B. Monostari and A. Weber. J. Chem. Phys. 33, 1867 (1960).
H.H. Claassen. J. Chem. Phys. 22, 50 (1954).
E.K. Plyler and W.S. Benedict. J. Res. Natl. Bur. Stand. 47, 202 (1951).
D.M. Yost, E.N. Lossette and S.T. Gross. J. Chem. Phys. 4, 325 (1936).

64. J. Gaunt and J. B. Ainscough. Spect. Acta. 10, 57 (1957).
65. R. J. Gillespie and E. A. Robinson, unpublished results.
66. E. B. Wilson, J. C. Decius and P. C. Cross. Molecular Vibrations, Appendix X, Table X-14.
McGraw Hill Book Co., Inc., New York. 1955.
67. F. A. Cotton. Chemical Applications of Group Theory, Appendix IIB.
Interscience Publishers, New York. 1963.
68. N. Bartlett and M. A. Hepworth. Chem. and Ind. 1425 (1956).
69. D. M. Yost and J. E. Scherborne. J. Chem. Phys. 2, 125 (1934).
70. E. E. Aynsley, R. E. Dodd and R. Little. Spect. Acta. 18, 1005 (1962).
71. E. L. Muetterties and W. D. Phillips. J. Amer. Chem. Soc. 79, 3686 (1957).
72. E. L. Muetterties and W. D. Phillips, J. Amer. Chem. Soc. 81, 1084 (1959).
73. E. L. Muetterties and W. D. Phillips. J. Amer. Chem. Soc. 85, 3035 (1963).
74. R. M. Fuoss, J. Amer. Chem. Soc. 57, 488 (1935).
75. R. M. Fuoss and C. A. Kraus. J. Amer. Chem. Soc. 55, 476 (1933).
76. R. E. Van Dyke and H. E. Cramford. J. Amer. Chem. Soc. 73, 2018 (1951).
77. J. Barr, R. J. Gillespie and R. C. Thompson. Inorg. Chem. 3, 1149 (1964).
78. A. J. Edwards, R. D. Peacock and R. W. H. Small. J. Chem. Soc. 4486 (1962).
79. J. H. Holloway, R. D. Peacock and R. W. H. Small. J. Chem. Soc. 644 (1964).
80. SeF_4NbF_5 - G. B. Hargreaves and R. D. Peacock, Unpublished results.
 SeF_4TaF_5 - N. Bartlett, unpublished results.
reported by R. D. Peacock in Progress in Inorganic Chemistry, F. A. Cotton, (ed.), Vol. 2, p. 237.
81. G. Brauer. Handbook of Preparative Inorganic Chemistry, Vol. I.
Academic Press, New York. 1963. p. 201.
82. Ibid., p. 202.
83. N. H. Furman, (ed.). Scott's Standard Methods of Chemical Analysis, Fifth Edition, Vol. I.
D. Van Nostrand Co., Inc., New York. 1939.
84. A. I. Vogel. Quantitative Inorganic Analysis, Third Ed.
John Wiley and Sons, Inc., New York. 1961.